Design and Performance Assessment for a Novel Friction Smoke Generator

A thesis presented in partial fulfilment of the requirements for the degree of

Master of Engineering

in

Chemical and Bioprocessing

At Massey University, Palmerston North

New Zealand

Muhammad Abdulrahman M. Seraj

2018

Abstract

Friction is one of the methods used to generate smoke for food smoking applications. The method involves pressing a plank of wood against a spinning wheel, roughened to provide frictional heating. The heating raises the interface temperature above 240 °C, where smouldering occurs. The primary objective of this project was to understand the dynamics of a novel friction smoke generator, designed in a prior project, but optimised here. Sub-objectives included understanding the frictional system and its thermodynamic behaviour, and preliminary attempts to define the composition of the smoke.

The novel aspect of the design is supplementary heating additional to the heat generated by friction. This means the interface temperature is less dependent on frictional heating. A system control strategy was developed to control temperature and force.

Twenty seven experiments were carried out. Nine of them investigated the smouldering limits without supplementary heating for various pressing forces and sliding speeds. The other twelve runs were conducted with supplementary heating for 100, 150 and 200 ˚C and various forces at constant sliding speed. The last six experiments were selected runs from the previous experiments where smoke was collected for composition analysis.

With no supplementary heating, pyrolysis takes place when the pressing force is ≥49.1 N and the wheel speed is at ≥2500 rpm. These conditions generate interfacial temperatures within the pyrolysis range. When the system was heated, the limit where smouldering starts when 9.81 N and 200 ˚C were applied. Two significant results were obtained. First, the progression of smouldering, resulted in a low and high wear rate of wood. The shift between these is proposed to be an endothermic to exothermic transition. Second, the time to reach this shift is a function of the pressing force and system temperature, becoming instantaneous at 200°C for forces > 29.4 N. These allowed insight to be gained into the dynamics of heat and mass transfer during friction smoking. The smoke composition analysis indicates that controlling the volatiles formation is highly achievable by varying the smoking conditions (i.e. auxiliary heat, pressing force).

The current design has some limitations, which include uncertainties in the conversion of electrical to mechanical power, vibration of the wood plank, conduction along the motor shaft and ingress of air. Recommendations are to address these by placing a thermal break on the shaft, preventing ambient air ingress into the chamber and adding a torque transducer. Further study is also recommended on the roughness and design of the friction wheel, and on scale up.

Acknowledgement

First I would like to thank God for giving me the strength and patience to complete this project. My special thanks to my awesome supervisor Prof Jim R Jones for considerate advice, patience and constructive comments during the course of this work. Also Dr Georg Ripberger and Dr Qun Chen for their contribution and advice. Also, I am grateful to Prof Jim Jones and Food Industrial Enabling Technology (FIET) for providing the financial support to complete this project.

I also would like to thank the following:

Mr Anthony Wade and Dr Morio Fukuoka for their technical support on the system control. Mr Ian Thomas and Mr Clive Bardell for the valuable guidance during the fabrication of the friction smoker. Dr Graham Eyres and Yuanyang Zhang for the help on the smoke analysis and interpretation during the course of this work.

My family, especially my parents Abdulrahman and Sabah for their prayers and love. Also my friends, for the enjoyable times we shared at Massey University.

List of Publications

Conference papers:

Seraj, M. A., Jones, J. R., Ripberger, G. D., and Chen, Q. (2018) *Smouldering Limits in Frictional Heating of Wood – Pilot Study.* In Chemeca 2018: Queenstown, New Zealand. Available in September, 2018

Posters:

Seraj, M. A., Jones, J. R., Ripberger, G. D. (2017, June). *Design of a friction Smoke Generator with Precise Control*. Poster presented at FIET symposium [Presented by Muhammad Seraj].

Seraj, M. A., Jones, J. R., Chen, Q., Eyres, G. (2018, June). *The Smouldering Limits of Mānuka Wood in Friction Smoke Generator*. Poster presented at FIET symposium [Presented by Muhammad Seraj].

Conference and Seminar presentations:

Seraj, M. A., Jones, J. R., Ripberger, G. D. (2016, June). *Friction Smoke Generator*. Oral presentation presented at FIET symposium [Presented by Muhammad Seraj].

Seraj, M. A., Jones, J. R., Ripberger, G. D. (2017, June). *Design of a Friction Smoke Generator with Precise Control*. Oral presentation presented at FIET symposium [Presented by Muhammad Seraj].

Seraj, M. A., Jones, J. R., Chen, Q., Eyres, G. (2018, June). *The Smouldering Limits of Mānuka Wood in Friction Smoke Generator*. Oral presentation presented at FIET symposium [Presented by Muhammad Seraj].

Seraj, M. A., Jones, J. R., Chen, Q., Eyres, G., Zhang, Y. (2018, June). *Frictional Smoking of Food*. Oral presentation presented at NZIFST conference [Presented by Muhammad Seraj].

Thesis Contents

List of Figures

List of Tables

Chapter 1 Introduction

1.1 Background

Over the centuries, mankind has used wood smoke to preserve and add flavour to foodstuff. Preservation occurs chemically due to the antibacterial properties of the deposited smoke and by drying. The inhibitory chemicals from smoke contribute to extend the shelf life while affecting the sensory properties (Smith *et al.*, 2007). These days, the preservation aspect is generally not a factor, as modern food storage practises have made traditional preservation unnecessary. Therefore, smoking is primarily used for enhancing the flavour and colour of food items.

Smoked food adds significant value to New Zealand exports. In 2012, New Zealand had a turnover value of USD$1,238M of seafood exports, which represent 6% of the total (Coriolis, 2014). According to Coriolis (2013), smoked salmon was ranked 6th of the top 30 seafood exports with USD$22.11 per kg and annual growth of 26% recorded in 2012. On average, smoking doubles the value of salmon.

When making smoked food commercially, wood is pyrolysed using a smoke generator and the conveyed to a separate chamber that contains the food. Smoking technologies have gone through several advancements to be cost effective and minimise environmental emissions (Maga, 1988). One of these is the friction-type smoke generator, where a plank of wood is forced against a spinning wheel; the friction generates heat and causes smouldering. Other forms of smoking are the hot plate or element, and steam or air injection. Operation and control of all smoke generators is difficult, often relying on artisanal techniques rather than scientific method. Such artisanal techniques involve peering into the smoke generation chamber to assess smoke density and colour, and opening the smokehouse door to check on the colour progression of the food being smoked. This raises the issue of how to generate consistent smoke. In part, this is due to the difficulty of controlling the smoking temperature and the environment. Typically, hot plate or element smoke generation will have wood particles at all stages of heating depending on their proximity to the heating element and residence time near it. The smoke generated will also depend on whether they are in an environment rich or starved in oxygen. Potentially, the temperature range of the smouldering particles is several hundred degrees. The problem in friction smokers is the balance between frictional heating, temperature achieved, and the smoke generation rate; generally, these type of smokers are intermittently operated to avoid excessive temperature gain. Poor control of the smoking temperature can cause formation of undesirable compounds such as polycyclic aromatic hydrocarbons (PAHs). PAHs have carcinogenic

properties and so must be minimized to as low as reasonably achievable (ALARA). Regulatory limits for PAHs in food have been set by the European Union (Commission, 2011), but not by New Zealand or Australia. The mechanistic understanding of the dynamics of friction-type smoking is not well-established which makes any control challenging. Nevertheless, friction smokers both represented most of the more recent patent activities (section 2.11), and have been shown to produce the least PAHs (Pöhlmann *et al.*, 2013a). Therefore, friction smoking is a good system to study.

Here, a lab-scale design for friction smoke generator has been developed and adapted to study the dynamics and controllability of the smoking environment. Mānuka is the wood of choice, because it is the most favoured smoking wood in New Zealand.

1.2 Project objectives

This project aims to build the knowledge needed to operate and control friction smokers in order to generate smoke with good sensory properties. Specific targets are:

- Continue prior design work to develop a smoke generator with tight control over the chamber set-point temperature to ± 2 °C. The prior work developed good control of the load and wheel speed.
- By conducting experiments, determine the relationship between the smoking generation, imposed set-point temperature, load and wheel speed.
- Interpret the experimental results to understand the kinetics of wood decomposition during frictional heating.
- Devise a system for smoke sampling.
- Analyse the chemical composition of smoke produced at various conditions.
- Conduct proximate analysis on the char residue to infer the interface temperature and thus the temperature of smoke formation.
- Out of these objectives, the project hopes to propose guiding principles for the design and operation of friction smokers to deliver consistent smoke quality.

The project links to others with the FIET: Smoke Generator project. Other sub-projects investigate other smoke generator technologies and aspects of kinetics.

Chapter 2 Literature Review

2.1 Introduction

Smoke is a complex material, made of char particles, soot particles, oily and watery aerosols, volatiles and simple gases. It is no surprise that the formation chemistry and thermodynamics are not well understood, as will be highlighted within the review.

This research is on friction-type smoke generators, selected as discussed in Chapter 1, and so the literature review presented here will focus on the influential factors to smoke generation caused by the heat generated during friction. Because wood thermally decomposes whatever the heat source, this review includes is a brief summary of the chemistry of wood decomposition, and a discussion of the parameters are that most likely to have a significant effect on the smoke quality during the pyrolytic reaction. Comparison to other smoke generation methods is discussed relative to the production of phenolic compounds and PAHs in section 2.4.1. The methods of smoke analysis are also presented. Following this is a short review of patented designs.

2.2 Review of wood degradation chemistry

Wood smoking is a complex system where volatile and particulate phases are adsorbed by foodstuff to give the properties of smoked food, such as colour, flavour, and preservation (Gilbert *et al.*, 1975). When wood undergoes pyrolysis it produces volatiles, liquid and char in different proportions across a temperature range and over time. Understanding some the chemical properties of wood will be useful in linking the knowledge behind wood smoking.

Wood comprises three major constituents: cellulose, hemicellulose, and lignin. Schematic structures are shown in Figure 2.1. The pyrolytic reactions in lignin are most likely to have the significant contribution to the smoke flavour, which plainly appears by the number of different chemical groups it holds (Gilbert *et al.*, 1975). Under the thermal reaction, fission of the aromatic rings in lignin will be more likely to occur at the heterocyclic furan (1) and pyran (2) shown in Figure 2.1. The linkage breaks at (3) will presumably yield guaiacol and homologs, where at (4) it is assumed to yield phenol and cresols. The breakdown mechanism is similar for hard and softwood types, yet the yield will differ; guaiacol yield dominates softwood, and hardwood will have a mixture of guaiacols and syringols.

Initiation Temperature [°C] **Chemical Structure**

Figure 2.1: The primary chemical constituents in woods:
25% hemicellulose (a), 50% cellulose (b) and 25% lignin (c) retrieved from (Ahmad, 2003; Basu, P., 2013)

2.2.1 Contribution of various volatiles to the overall aromatic flavours

Several chemical groups have been identified that make up the characteristics of smoke flavour. There are 48 volatiles that contribute to the aromatic flavours present in Chinese traditional smoke-cured bacon (CSCB) (Yu *et al.*, 2008). Those compounds have been classified into these chemical groups: aldehydes, ketones, alcohols, thioesters and thiols, furans, and phenols. Maga (1987) identified over 400 volatiles estimated to be responsible for smoke flavours in which they were categorised into their chemical groups. Most agree with the previous findings from the (CSCB) study, adding following groups: esters, lactones and other miscellaneous compounds. Both references agree that the phenol group significantly affects the smoke flavours, adding other carbonyl groups.

Colour is also an important feature of smoked foods. Quoting Coggins (2012),"*Smoked meats develop surface colours due to the interaction of phenols, aldehydes, and acids*". It is the aldehydes that are widely acknowledged as important to colour development. He also suggests that sulphurous and carbonyl groups are predominant contributors to muscle food aroma. A study by Guillén *et al.* (2005) using dissimilar oak species showed that the main components for flavouring were aldehydes, ketones, diketones, acids, esters, furan and pyran derivatives, alkyl aryl ethers, and phenol, guaiacol, pyrocatechol, syringol and their alkyl derivatives and some anhydro-sugars. They also showed that the fraction of phenols and ethers presence in smoke were correlated to different aromatic flavours.

While none of the previous studies used Manuka wood for analysing volatiles characteristics, it is interesting to note that many wood species have been used, and all yielded similar results. It therefore remains to determine what, if at all, makes a particular wood species distinctive (Ahmad, 2003).

2.2.2 Major compounds that contribute to aromatic flavours

Several research articles agree on the significant contribution of phenol group to the aromatic flavour in smoked food (Ahmad, 2003; Coggins, 2012; Maga, 1987; Yu *et al.*, 2008). Within the phenol group, some specific compounds were repeatedly mentioned in (Ahmad, 2003; Kostyra *et al.*, 2006; Maga, 1987) that have a strong influence on the smoke flavour; those compounds are guaiacols, syringols, and carbonyls derivatives (4-methylguaiacol). Table 2.1 describes some major components/derivatives attributed in relation to the sensory flavours.

Table 2.1: Sensorial judgment of few phenols adapted from (Ahmad, 2003).

Substance	BJC* [mg/100 ml]	Smell	Taste
Guaiacol	3.75	Phenolish, smoky, aromatic, sharp, sweet	Phenolish, sharp, spicy, smoked-sausage aromatic, sweet, dry
Syringols	7.5	Smoky, spicy, aromatic, smoked-sausage-toned, Phenolish, sharp, sweet	Phenolish, smoky, like freshly charred wood, like whiskey, dry, sharp
4-methyl-guaiacol	1.9	Sweet, like vanilla, fruity, like cinnamon, somewhat smoky, pleasantly sharp, phenol tones	Sweet, like vanilla, caramel-like, aromatic, pleasant, smoke tones, burning
i-Eugenol	9.8	Sweet-fruity, like vanilla, like rhubarb, phenol tones	Sweet-fruity, mild smoke tones, dry, sharp
o-Cresol	7.5	Phenolish, sweet-fruity, aromatic, like caramel, smoked-sausage-tones	Sweet-fruity, mild smoke tones, dry, sharp
Dimethyl-phenol	0.9	Phenolish, like ink, aromatic, sweet	Phenolish, sharp, somewhat charred, sweet, dry

**Best Judged Concentration*

Phenols have an aromatic hydrocarbon structure comprising benzene with different hydroxyl groups. Phenols can also carry other functional groups, such as aldehydes, ketones, acids, and esters (Maga, 1987). Maga also stated the yield of the phenolic compounds varies depending on the type of wood; for instance, oak releases twice the

amount of phenolic compounds as cherry. Another study concluded that hardwoods and softwoods differ in their partial release of some phenolic compounds, such that syringols, which is 12% relatively higher in hardwood compared to softwood (Baltes, 1985).

According to Pearson *et al.* (1996), the importance of individual phenolic compounds from within the group is still unknown. Tóth *et al.* (1984), suggest that the number of different phenols is more important than the impact of an individual phenol. To study this, an investigation by Sérot *et al.* (2004).has been done on the effect of 10 major phenolic compounds from five different smoking process. The 10 compounds (phenol, *p*-cresol, *o*-cresol, guaiacol, 4-methyl guaiacol, 4-ethyl guaiacol, syringol, eugenol, 4-propyl guaiacol, and isoeugenol) were analysed, and concluded that phenol, guaiacols, syringols and 4-methylguaiacol, are the major contributors to the smoke flavour and sensory

2.2.3 PAHs formation and transportation to foodstuff

Polycyclic aromatic hydrocarbons are condensed aromatic rings fused together from different sides. According to (Ahmad, 2003), PAHs are formed through the condensation of naphthalene where concentration increases by adding other organic materials during combustion. (Ledesma *et al.*, 2016) mentioned that PAHs can be found in tertiary tar products formed during pyrolysis at about 750˚C, where condensed tertiary aromatics are formed from tertiary tar.

PAHs, once formed, are carried to the smokehouse in the smoke aerosol and deposit onto the food products (Ledesma *et al.*, 2016). Because PAHs are variously toxic, the European Union have placed limits on the concentration of four indicator PAHs (PAH4) as suitable indicators of the total level of PAHs presence in foodstuff. Those PAHs are benzo[a]pyrene (BaP), chrysene (CHR), benzo[a]anthracene (BaA), and benzo[b]fluoranthene (BbF), which is a suitable indicator to the sum (Pöhlmann *et al.*, 2013a). Therefore, effort is needed to identify how they form and how to minimise their production in order to future proof New Zealand smoked foods exports, not only to Europe, but to other markets that may adopt similar levels of consumer protection.

2.3 Influences of smoking conditions on the flavouring and PAH compounds

Various conditions are assumed to affect the aromatic flavours and the PAHs content. Previous studies have shown that manipulating certain variables, such as temperature, moisture, and smoking technique, can lead to significant change in the composition of the produced smoke (Gilbert *et al.*, 1975). These are discussed below.

2.3.1 The effect of temperature

The temperature and flavour are strongly correlated (Maga, 1987). Increasing smoking temperature increases the released flavouring compounds as seen in Tables 2.2 and 2.3.

Table 2.2: The effect temperature on aromatic volatiles in wood smoke. Adapted from (Maga, 1987).

Smouldering temperature (˚C)	Phenols (g phenol/ml)	Carbonyls (mg acetaldehyde/ml)	Acids (Meq acid/ml)
252	88	20.0	0.082
287	91	20.2	0.077
322	153	27.3	0.121
355	197	31.2	0.104
386	165	37.2	0.112

Table 2.3: Influence of the glowing temperature on the phenol, carbonyl and acid yields in smoke in [mg/100 g of sawdust]. Adapted from (Ahmad, 2003)

Temperature (˚C)	Total phenols	Total carbonyls	Total acids
380	998	9,998	2,506
600	4,858	14,952	6,370
760	2,632	7,574	2,996

Table 2.3, which covers the range over which Lignin pyrolyses from 380˚C to 760˚C; this is where the secondary reaction mostly takes place, and most of the aromatic components are formed. Maga (1987), found that the maximum yields for phenol, carbonyl, and acids occurred at about 600˚C based on what has been reported from Tóth *et al.* (1984). Tóth *et al.* also stated that double-valanced phenols are stable at high temperatures at the expense of thermally less stable compounds. Figure 2.2, from Ledesma *et al.* (2016) confirms the high starting temperature of 500˚C for the formation of the flavouring compounds peaking at 750°C, and for the PAHs, forming from 750˚C and thereafter continuing to increase with temperature. Tóth *et al*. (1984) found the maximum release of phenolic compounds occurs at a slightly lower temperature, about 650 ˚C in Figure 2.3, which might be caused by experimenting with different wood species and possibly the operating conditions.

Figure 2.2: Formation of primary, secondary and tertiary volatiles during biomass conversion. Reproduced from (Ledesma *et al.*, 2016)

Figure 2.3: Influence of smouldering temperature on the amount of phenolic constituents in beech wood. Reproduced from (Tóth *et al.*, 1984)

Ledesma *et al.* (2016) and Sérot *et al.* (2008) agreed that the level of PAH formation increases with the increase of temperature and residence time. McGrath, T. *et al.* (2001) stated based on experimentation that PHAs formation increases with the increase of temperature and residence time during smouldering. In Figure 2.4, Sharma *et al.* (2003), showed from experiment the temperature influence on PAH yield from pyrolysing lignin.

Figure 2.4: The PAH yield from lignin at various temperatures. Reproduced from (Sharma *et al.*, 2003)

The low tar final temperature (LTFT) PAH formation route was done in a reactor consisted of a quartz tube with two zones. The first zone was used to pyrolyse the material at 250 – 400 ˚C and then goes through the second zone for post-treatment at 700 – 920 ˚C. On the other setup, the high tar final temperature (HTFT) was done by pyrolysing the material at 625 ˚C which then goes to the second zone with the same temperature as above.

Both experiments were conducted under inert atmosphere with residence time of 1.4 seconds for each zone. The author concluded that the formation of most PAH increases as the pyrolysing temperature increase except for the cases with (HTFT), which resulted in lower yield of PAH. This was probably due to the low reactivity of the volatiles products and condensed structure of the lignin.

2.3.2 The effect of oxygen level

The significance of oxygen concentration can strongly affect the combustion rate, which will influence the rate of reaction. The variation of oxygen present during wood combustion has shown significant effects on aromatic flavours. According to Maga (1987), Wasserman and Fiddler experimented with the variation of oxygen concentration during combustion from 0% to 59% which caused noticeable differences in the volatile composition. The phenolic compounds guaiacol and cyclotene increased by almost double at 10% OC (oxygen concentration); however, it dropped by almost the same amount at 20%OC. They concluded that the sensory smoke properties are derived from 0% to 10% OC, yet the rest of the OC has shown no significant changes in the volatile composition. Table 2.4 lists the findings from the experiment.

Table 2.4: Influence of OC used in smouldering on volatile component composition (Maga, 1987).

	% Peak area/g sawdust consumed		
% Oxygen in gas	Furfuryl alcohol	Cyclotene	Guaiacol
0	100	55	55
10	75	100	100
20	44	45	55
30	40	43	50
40	38	46	55
50	36	45	48

The yield of PAHs formation from cellulose char was determined at different oxygen concentration by McGrath, T. E. *et al.* (2003). The results showed that adding 5% and 10 % of oxygen to the carrier gas stream reduced the yield of PAHs formed. However, the reduction in yield was varying, depending on the PAH constituent, where BbF was the only detectable compound from the PAH4 with the oxygen trials at 600˚C.

2.3.3 The effect of moisture content

The moisture content (MC) in wood smoke influences the overall sensory properties of the volatiles. Data were published by Grobatov *et al*. claiming that lowering the wood moisture content will yield higher amounts of phenols, acids, and carbonyls "cited in (Maga, 1987)". However, Maga suggested that more research needed to be conducted to conform Grobatov's findings. Other research has shown evidence that the formation of PAHs is related to the amount of moisture content in wood. Chomanee *et al.* (2009), experimented with rubberwood at different moisture contents, starting from 37.4% up to 73.6%. Thus, he concluded that the PAHs emissions decrease as MC% decrease.

2.4 Synopsis of friction smoke generator

Friction smoking is the process of generating smoke by pressing a log of wood against a rapidly rotating rough wheel, where the heat of friction causes the wood to pyrolyse thus volatiles are released. Friction smoking offers instantaneous production of smoke, with low consumption of timber and a low level of maintenance required (Toldrá, 2010, p. 241; Tóth *et al.*, 1984, p. 96).

In a friction smoke generator, the smoking temperature is maintained by periodic withdrawal of the plank from the friction surface to prevent burning of the wood by frictional heat (Tóth *et al.*, 1984). Another technique for controlling temperature is by adjusting the disc rotational speed and the applied load on the wooden plank as mentioned by Sikorski *et al.* (2010). The usual temperature at the friction zone tends to be in the range of 300 to 350 ˚C depending on the control of the applied pressure and wheel speed (Pöhlmann *et al.*, 2013a; Sikorski *et al.*, 2010). According to the review of Tóth *et al.* (1984), a temperature of 380 ˚C ±20 ˚C at the contact area was recorded using IR equipment during 5 to 25 seconds of friction contact time. Khavan *et al* (1971) "cited in (Maga, 1988)", mentioned the actual smouldering temperature at the friction zone could reach 450 to 560 ˚C, however the smoke temperature is much lower due to rapid cooling induced by turbulence from the friction wheel. Maga (1988, p. 40) stated that different smoking practices can affect the temperature of the smoke released, for instance, discontinuous operation of the friction wheel (i.e. spinning for 10 seconds and then rested for several minutes) resulted in smoke temperature a few degrees above ambient. Conversely, continuous operation of the friction wheel produced smoke temperature within 140 to 160 ˚C. The author also mentioned that several factors that influence the smoke temperature, such as the applied force on the wood plank, wheel speed and the shape of the friction side of the wheel.

On the sensory properties side, a comparison between smouldering and friction smoke generators was made to evaluate volatiles release. The friction smoker yielded lower phenolic, guaiacol and syringol volatiles and higher amount of allyl- and propenyl syringol with only 10% of higher molecular weight compounds compared to smouldering. This result is most likely due to the rapid cooling of the volatiles immediately after escape from the frictional contact with the wheel, which limits both the time and temperature for the primary compounds to undergo secondary reactions, thus restricting the number of compounds formed (Maga, 1988, p. 40). In this work, the compounds formed are highlighted in section 5.6.

2.4.1 Friction-type smoker comparison to other smoke generators

Earlier studies have shown the influence of using different smoking techniques in the production of aromatic compounds. Pöhlmann *et al.* (2013a), has investigated the effect of various smoking techniques (smouldering[1], friction[2], steam[3], and touch[4]) on the production of some major phenolic and PAH substances under similar conditions. The results were profoundly affected by smoking technique. The PAHs content was highest for smouldering and lowest for the friction method. Similarly phenolic constituents were highest from smouldering and lowest from the friction method. Figure 2.5 shows the phenolic and PAH compounds that were obtained.

Pöhlmann *et al.* (2013a) justified, "due to a large amount of phenolic compounds transferred to sausages, a large PAH content was associated. However, in terms of phenolic content, steam smoking was the highest by 45 mg/kg, and friction was the lowest by 15 mg/kg".

Another study by Sérot *et al.* (2004), investigated the effect of smoking methods on 10 major phenolic compounds and similarly found that different smoking technique varied in the production of phenolic compounds. However, nothing was declared about the PAHs level in this study. While Cardinal *et al.* (2006) stated that friction smoke generator has lower total production of the phenolic compounds than auto-combustions[5] generator.

It is possible that different smoke generation methods are more suitable for different foods. However, this has not been well studied see for example (Pöhlmann *et al.*, 2013b).

[1] *The use of hot plate in contact with wood chips to generate smoke.*
[2] *The use of wood logs forced against spinning wheel to generate smoke.*
[3] *The use of superheated steam through wood chips usually between 450 and 650˚C for smoking.*
[4] *A new technology in which wood planks are pyrolysed by direct contact to a heating plate, the smoke intensity is controlled by varying the contact time. The following website show a picture of the smoker: (www.touchsmoke.com/fleischerhandwerk/touch-smoke/weltpremiere.html).*
[5] *Pyrolysing of sustained sawdust by air circulation.*

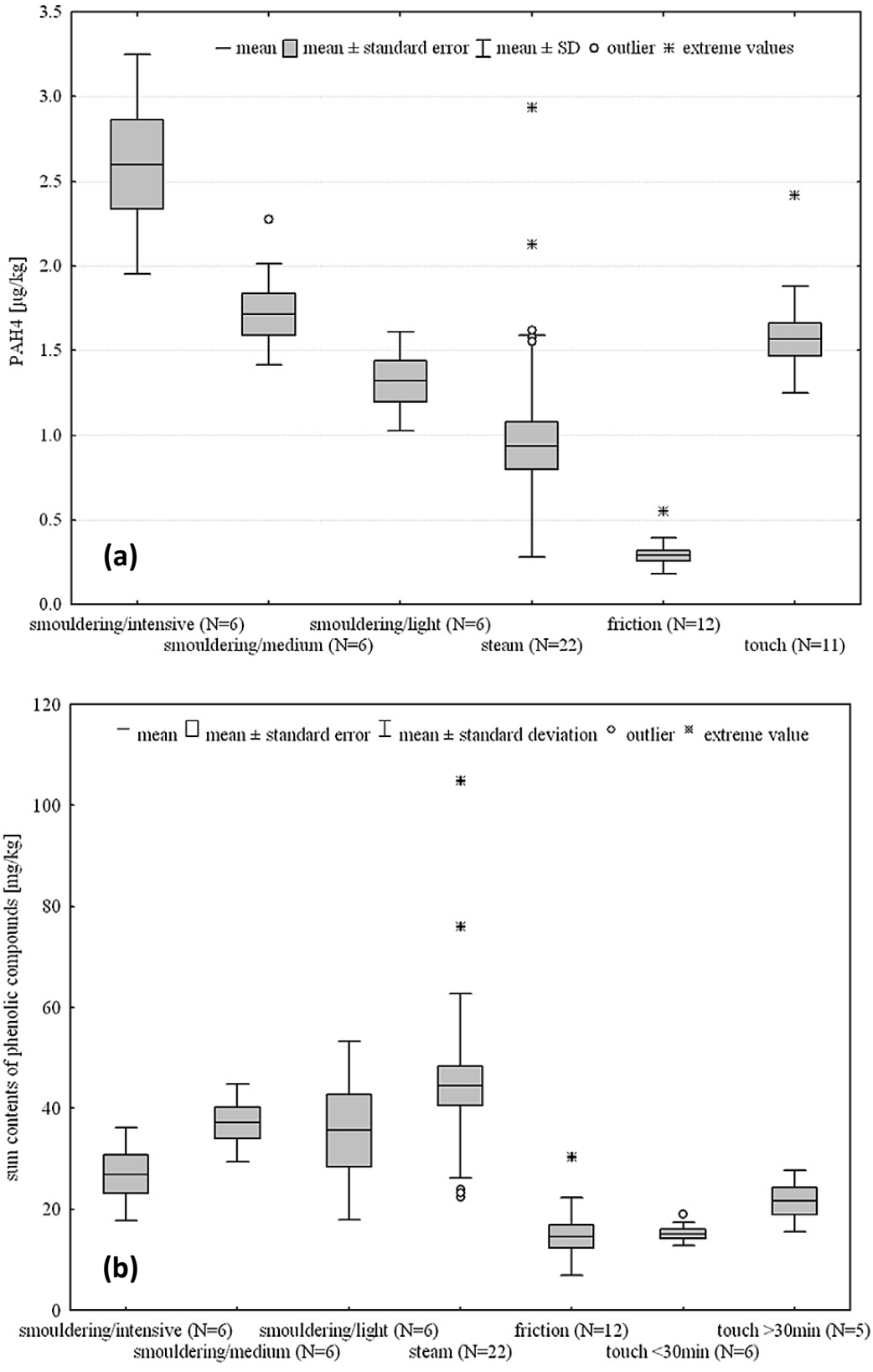

Figure 2.5: Content of (a) PAHs and (b) some major phenolic compounds in [µg/kg] using different smoking techniques. Adapted from (Pöhlmann *et al.*, 2013a)

2.5 Frictional properties of wood

Friction and wear between two bodies in contact during sliding result in energy dissipation in the form of heat. The rate of heat transfer can highly depend on the tribological properties of materials and operating conditions. Thus, understanding of the mechanism of friction and wearing is crucial for predicting heat transfer in a frictional system.

2.5.1 Friction and wear of wood

Friction is the resisting force parallel to the tangential motion of when two bodies are in contact under nonzero normal force. The ratio between the resisting force to the tangential motion defined as the frictional force (F_τ) in [N] and the normal force (F_N) in [N]is known as the coefficient of friction (CoF) (μ) in [-] (Blau, 2009), expressed as.

$$\mu = \frac{F_\tau}{F_N} \tag{2.1}$$

The CoF in this context will be referring to the kinetic CoF when the two surfaces are in relative motion. The static CoF is not relevant here. As stated by Svensson, B. (2007), it is important to remember that the CoF is not a property of the material but a system property concerning experimental condition.

Wear or ablation of material is another crucial factor between dissimilar materials. The mechanical action between surfaces results in the removal of the softer material. The common wearing mechanisms are adhesive, abrasive, corrosive and fugitive wear (Rabinowicz, 1995). Wood rubbing against metal follows the adhesive and abrasive wear mechanisms, where adhesive wear is the loss of material to viscous shear of the wood against the sliding metal surface and abrasive wear is the loss of material due to mechanical failure within the substance. Abrasive wear occurs when the adhesive force is higher than the tensile strength of the wood. Therefore, when considering the friction, adhesive failure contributes to the adhesion term of friction and cohesive failure to the deformation term (Svensson, B., 2007). Atack *et al.* (1958) wrote:

$$\mu = \mu_D + \mu_A \tag{2.2}$$

where (μ_D) is linked to the deformation and internal friction effects in the bulk material and (μ_A) is related to the interfacial adhesion (Svensson, B., 2007).

In polymeric materials, the tribological[6] properties are governed by various parameters such as Young's modulus, creep resistance, hysteresis, damping properties and crystallisation ability. Since these properties highly depend on temperature and sliding velocity, wood can exhibit viscoelastic behaviours which cannot be explained by the classical law of friction (Svensson, B., 2007).

2.6 Influential factors on friction mechanisms

2.6.1 Effect of moisture content

Guan *et al.* (1983) conducted a study on friction for various Swedish wood species rubbed against steel, applied to the pulping industry. They showed an increase in CoF with the increase in moisture content of woods regardless of the fibre orientation against the rubbing surface (Figure 2.6). A trend which was similarly found by Svensson, B. (2007) (Figure 2.7) where he used blocks of woods pressed against a smooth steel surface and the fibres orientation were parallel to the sliding direction. One explanation is that the wood fibres yield elastically, which leads to greater contact area as the moisture content increases. This is tested in Figure 2.8, where the elastic recovery from deformation after unloading the samples is plotted, which is measured using a dial gauge, noting that even dry wood has some elastic recovery.

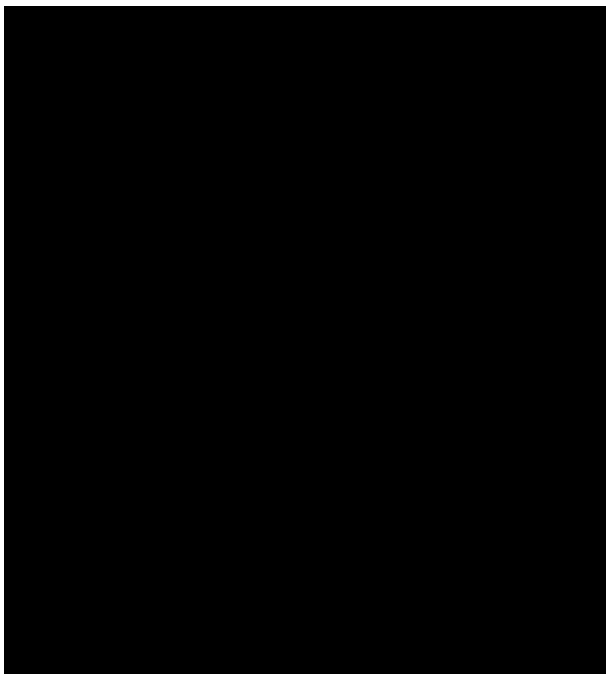

Figure 2.6: The influence of MC on CoF for different wood species. Reproduced from (Guan *et al.*, 1983)

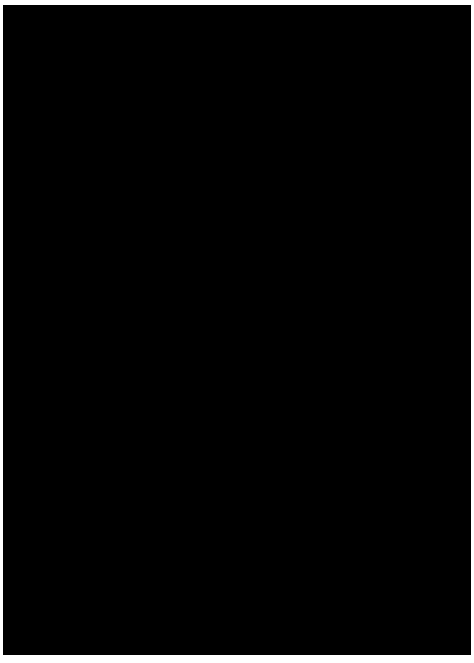

Figure 2.7: Effect of MC on CoF from wood on steel. Reproduced from (Svensson, B., 2007)

[6] *Is the science of friction, wear and lubrication of interacting surfaces in relative motion (Bhushan, 2013).*

Figure 2.8: The influence of MC on fibre recovery from the surface softness measurement. Reproduced from (Guan *et al.*, 1983)

2.6.2 Effect of temperature

The temperature rise due to friction is a significant factor that affects the tribological properties of a polymer, in some cases if the temperature is high enough phase shift occurs causing thermal degradation (Blau, 2009). Svensson, B. A. *et al.* (2007) have studied different wood species sliding on smooth steel under environment temperatures between 100˚C to 170˚C, where the temperature is achieved using saturated steam; again the application is wood pulping. They showed that temperature has a significant influence on the CoF, as presented in Figure 2.9. At temperatures between 100 to 130 ˚C, the softwood species had noticeably lower CoF due to their higher extractives which the act as a lubricant layer. Conversely, as the temperature increases beyond 130 ˚C, the lubrication layer decreased. Also, fibre debris started to appear between 150 – 165 ˚C, indicating a transition to cohesive failure.

Figure 2.9: The influence of saturated steam on the CoF for various wood species. Retrieved from (Svensson, B. A. *et al.*, 2007)

2.6.3 Effect of surface roughness and contact area

Surface roughness (R_a) and the contact area (A_c) have a significant influence on the CoF which reflect to the temperature rise at the contact interface. McKenzie *et al.* (1968), conducted an experiments that highlights the variation of CoF in relation to the surface roughness of the rubbing surface against different wood species. The results, according to the authors in Figure 2.10, were obtained based on various fibre orientations, normal loads and moisture contents. Hence, they concluded that roughness of the steel has a significant effect on the CoF.

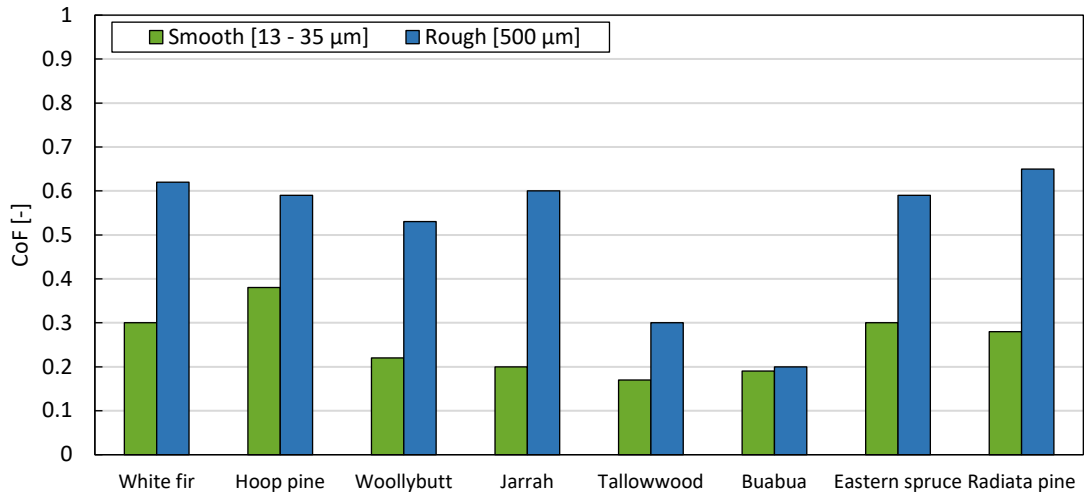

Figure 2.10: The variation of CoF for various wood species and steel roughness at sliding speeds [55 mm/s] and MC [10 – 14%] for various fibre orientations and applied loads. Reproduced from (McKenzie *et al.*, 1968)

Surface roughness is manifested by asperities, which have height and a number density. These factors were explored by Havimo *et al.* (2010) in a mathematical model for temperature gradient in wood pressed against a grinding stone. The model showed a temperature increase with the increase of the grit size (a) whereas increasing the distance between grits resulted in a lower temperature (b) as presented in Figure 2.11.

Figure 2.11: Simulated temperature distribution in wood with respect to (a) grit size and (b) distance. Reproduced from (Havimo *et al.*, 2010)

2.7 Temperature rise at the friction zone

When two bodies are in contact with a specific load and sliding velocity relative to one another, the temperature will rise from the dissipated energy during friction. The increase in temperature at the friction zone can subsequently affect the deformation, cracking and tribochemical[7] reactions. The dissipated energy can be quantified by equation (2.3):

$$q = \mu \frac{F_N}{A_c} U \tag{2.3}$$

Where (q) is the total heat flux in [Wm^{-2}], (μ) the kinetic friction coefficient [-], (F_N/A_c) is the applied pressure over the contact area [Pa] and (U) is the relative sliding velocity $|v_{12} - v_{21}|$ between objects 1 and 2 in [ms^{-1}] (Basu, B. *et al.*, 2011).

The temperature at the interfacial contact, denoted by (T_c) [˚C] in equation (2.4), can be regarded as having three contributions. The flash temperature (ΔT_f) [˚C], is a very high temperature rise at an instant, usually less than 10 μs, in the interface between asperities. The nominal temperature (ΔT_{nom}) [˚C], is the average temperature dissipated between surfaces and it is usually lower than the flash temperature. As the nominal temperature propagates, heat transfer occurs from the friction zone through the bodies in contact to increase their bulk volumetric temperatures (T_b) [˚C]. This temperature is lower than the others (Kennedy, 2001). Figure 2.12 shows the temperatures positions in the context of friction-type smoke generator.

$$T_c = \Delta T_f + \Delta T_{nom} + T_b \tag{2.4}$$

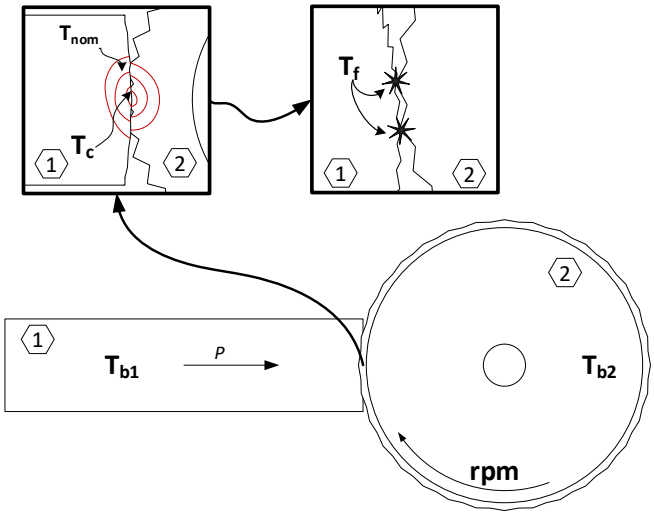

Figure 2.12: Interface temperature between (1) stationary wood log and (2) rotating steel disc at high speed.

[7] *The occurrence of chemical reaction between surfaces in contact under lubricated environment during friction (Hsu et al., 2002).*

2.7.1 Friction welding of wood

Friction welding is application technology used to create strong bonds between wood surfaces which was first attempted by Sutthoff *et al* (1996) "cited in (Stamm *et al.*, 2005)". The welding mechanism occurs by high frequency rubbing between stationary and moving pieces of wood (~100 – 200 Hz) under high pressure (>1 MPa), where the relative motion depends on the application examples shown in Figure 2.13. The heat due to friction creates a high temperature interface >200 ˚C which forces decomposition at the interface which creates new joining layer mostly made of molten lignin that welds the pieces together (Gfeller *et al.*, 2003).

Stamm *et al.* (2005), studied the possibility of joining wood without any additional matter using friction welding for various pressures (0.31 – 0.94 MPa) and vibration frequencies (80 – 150 Hz). The study followed configuration (c) in Figure 2.13, using Norway spruce and beech with MC of ~12.5%. Four thermocouples were inserted from the bottom all the way through the stationary wood block to measure the interface temperature.

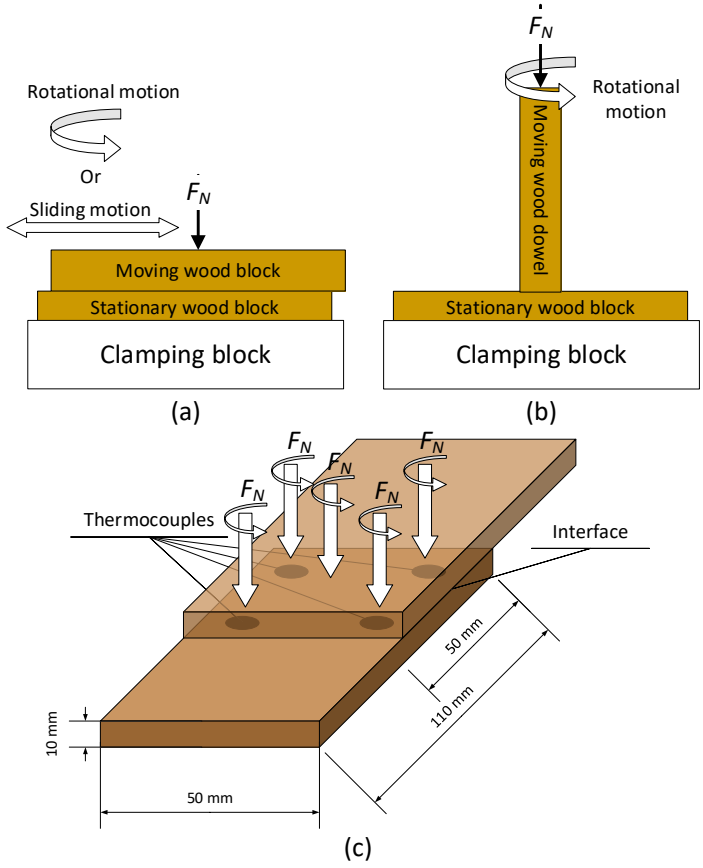

Figure 2.13: Schematic of various configurations of friction welding of wood.

Although the study aimed to investigate the strength properties of the weld, what is of interest to this project is the interface temperature and CoF profiles during the welding process shown in Figure 2.14.

Figure 2.14: Temperature and CoF profile at the interface during friction welding at 0.78 MPa and 130 Hz. Reproduced from (Stamm *et al.*, 2005)

According to Stamm *et al.* (2005), phase (I), shows ramping of temperature where softening and smoothing of surface asperities occurs. Phase (II) shows a constant CoF and a linear increase in temperature due to heat accumulation (see Eq.(2.3)). Later in phase (II), a sudden ramp of temperature and CoF occur and volatilisation is observed. CoF reaches a peak point at the end of the phase (~0.25) while the temperature kept on rising. In phase (IV), the CoF drops due to the change in surface lubrication, this caused by the presence of thermally decomposed products at the interface. Here the temperature reaches a peak point of ~420 - 440 °C which was relatively steady for the rest of the vibration time. In phase (V) both temperature and CoF reach a steady state, as the heat is dissipated by the smoke released and into the decomposed cell wall. This phenomena is indicative of pyrolysis and it is highly endothermic it takes place in the temperature range between 300 - 500 °C according to Shafizadeh and Rowell (1984) "cited in (Stamm *et al.*, 2005)".

Stamm's work assessed the progression of temperature at different distances from the interface, which are presented in Table 2.5. In addition, his work showed that increasing the pressure and frequency reduces the welding time. This also indicates that these two factors can escalate the smouldering rate (see Section.2.8.4).

Table 2.5: The peak recorded temperature as a function of the thermocouple distance from the interface.

Distance from interface [mm]	0	2.2	4.3	8.3
Peak interface temperature [°C]	680	380	345	325

The steep temperature gradient away from the interface is expected as wood is known to have good insulating properties. It demonstrates that heating is local to the friction zone where pyrolysis takes place.

2.8 Evaluation of the contact temperature

While the division of the temperature in the frictional interface into T_c, ΔT_f and ΔT_{nom} is hypothetical, the three contributing factors from which these temperatures arise are not easily dissociated experimentally. Nevertheless, for smoke generation, it is important to understand how friction causes a temperature rise because pyrolysis is highly temperature dependent. Therefore, this section will highlight the measuring and estimating techniques of the contact temperature during friction.

2.8.1 Measuring techniques

Here some measuring techniques were gathered to decide what approach could be adapted for experimental use.

1. **Thermocouple sensors**

With thermocouples, there are two commonly used methods to indicate the contact temperature, embedded and dynamic thermocouples. An embedded thermocouple is one implanted into either body close to the friction surface (Figure 2.15), connected by slip rings or similar if the thermocouple is embedded into a rotating element. This approach will give a good estimate of the bulk temperature change, however it cannot indicate the flash temperature due to the finite thermal mass between the sensor and the contact interface (Kennedy, 2001).

A dynamic thermocouple is also referred to as the Herbert-Gottwein technique (Figure 2.15). This technique relies on the electromotive force (emf) property of the material, where the two parts in contact are used to form a junction where the change in temperature translates into voltage difference. The advantage of this approach is that it has a fast response, but it cannot be used with material that has poor emf potential such as wood.

Figure 2.15: Schematic diagram for (left) embedded and (right) dynamic thermocouples set-up (Kennedy, 2001)

2. Thermal camera and Infrared (IR) sensors

Thermal photographic techniques have been broadly used for temperature detection in different applications. The working concept is based on detecting the emitted thermal energy from an object, as confirmed by Stefan-Boltzmann law which states that an object at high temperature emits higher power than when it is at low temperature. Boothroyd (1961) developed a technique which utilises infrared sensitive film to study the temperature distribution in metal cutting in 1961. Since then, the method has been used to measure frictional heat in tribological systems. The accuracy of this method depends on the calibration and particular procedure. Because of the long exposure time (~5s or more) relative to the duration of flash temperature, it gives an average, or nominal, surface temperature distribution(Kennedy, 2001). Infrared thermometers are similar to a thermal camera. However, they display a digital outputs rather than visual image.

The measurement of average surface temperature can be compared to theory, adapted to the classic 'pin-on-disc' problem which is typical of tribology experiments and also representative of friction smoking. Here, the average interfacial temperature depends on the ease with which heat flows away from the contact surface where it is generated into the pin (wood) and disc (wheel). Wood has very low thermal diffusivity compared to steel, and so the heat transfer is mostly into the wheel. The following three sections review the theoretical basis for the partitioning of heat between the steel wheel and the wood, and the theoretical expressions for the average (nominal) temperature rise and the flash temperature rise at the frictional interface.

The assumptions were set for 1D heat transfer for a moving heat source due to frictional heat generated at the contact area:

- The thermophysical properties of the bodies in contact are independent of temperature.
- The plane source of heat is generated from the contact area (i.e. square $A_c = 4b^2$) illustrated in Figure 2.16.
- Uniform generation of frictional heat across the contact area.
- Negligible heat loss where all the produced heat dissipates into the contacting bodies.
- CoF is constant during friction and steady-state conditions are attained ($\frac{\partial T}{\partial t} = 0$)

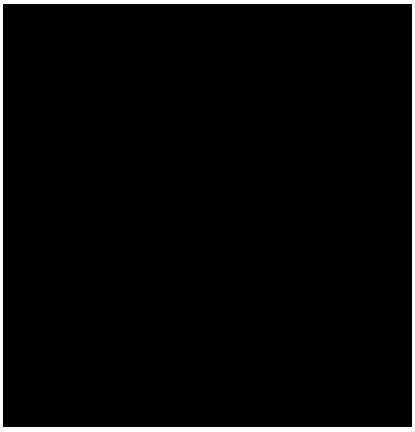

Figure 2.16: Geometrical contact areas (Stachowiak *et al.*, 2014)

2.8.2 Estimating the partition of frictional heat

Understanding the partitioning of frictional heat is crucial to predict the temperature distribution at the surface accurately. Partitioning plays a significant role in cases where friction occurs between bodies with different compositional nature, geometrical shape and working conditions. From Kennedy (2001) and Straffelini (2015), the total heat flux generated at the surface conducts between two bodies in contact. The ratio of heat flow describes the partitioning, where the following schematic (Figure 2.17) illustrates a common friction situation in the tribology field know as pin-on-disc contact.

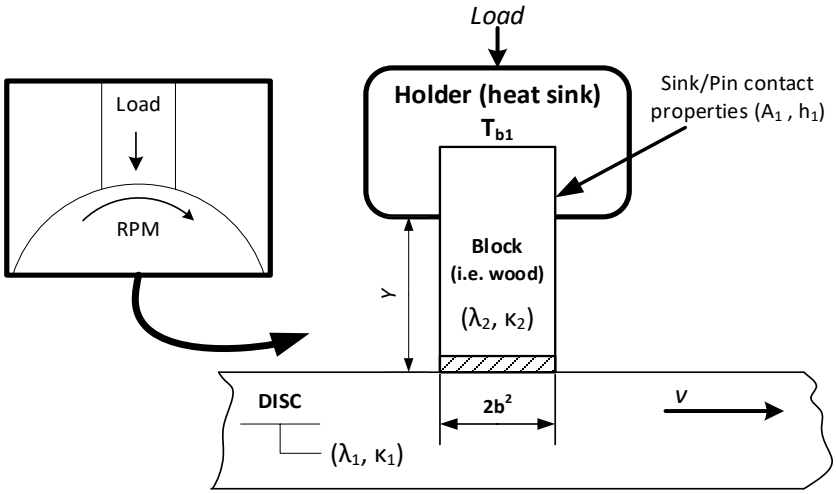

Figure 2.17: Schematic diagram of Pin-on-Disc contact. Reproduced based on (Kennedy, 2001)

The concept of frictional heat partitioning can be added to the general equation (2.3) then expressed as follow:

$$q_1 + q_2 = q_{tot} = \mu \frac{F_N}{A_c} U$$

where q_1 = the portion of heat flux entering the stationary body [Wm^{-2}] and q_2 = the portion of heat flux entering the moving body [Wm^{-2}]. The frame of reference to analysing these problems is to regard the pin (wood) as the moving body and the disc (wheel) as the stationary body. Replacing the subscripts to reflect this, the partitioning factor (γ) in [-] is expressed as such:

$$\gamma_{disc} = \frac{q_1}{q_{tot}} \quad \text{and} \quad \gamma_{wood} = 1 - \gamma_{disc} = \frac{q_2}{q_{tot}} \tag{2.5}$$

Therefore;

$$q_1 = \gamma_{disc}\, \mu\, \frac{F_N}{A_c}\, U \quad \text{and} \quad q_2 = \gamma_{wood}\, \mu\, \frac{F_N}{A_c}\, U \tag{2.6}$$

Later work by Tian and Kennedy have found that the heat transfer is enhanced by the sliding, defined by the Peclet number. They made the following modification:

$$\gamma_{disc} = \frac{1}{1 + \frac{\lambda_{disc}}{\lambda_{wood}}\sqrt{1 + Pe}}: \quad [Pe > 0.1] \tag{2.7}$$

$$Pe = \frac{v\, b}{2\, \kappa_{disc}} \tag{2.8}$$

$$\kappa_{disc} = \frac{\lambda}{\rho\, C_p} \tag{2.9}$$

where (λ) the thermal conductivity [W m^{-1} K^{-1}], (Pe) Peclet number of the moving body (the disc), (v) rubbing speed [m s^{-1}], (κ_{disc}) is the thermal diffusivity of the moving body [m^2 s^{-1}] and (ρ, C_p) are density [kg m^{-3}] and specific heat capacity respectively [J kg^{-1} K^{-1}].

Assuming the thermal conductivities are constant, equation (2.7) is governed by the Peclet number as its raises the value of the denominator. Therefore, at high sliding speed, more of the heat generated flows to the moving body (the disc) as more new material is introduced continuously to reach the maximum temperature equivalent to the heat been generated. The stationary face (the wood) temperature is always assumed at its maximum (Kennedy, 2001).

In case of low sliding speed ($Pe < 0.1$), Kennedy (2001) stated that the partitioning factor will be mostly influenced by the thermal conductivities of the two bodies. Where the majority of heat will favour the higher conductive material. Therefore, equation (2.7) can be simplified by excluding the Pe term.

The friction smoke generator is a classic pin-on-disc problem, but where wood has a very low diffusivity compared to the steel. The problem is complicated because the disc is turning and so accumulates heat until its external heat loss equals the heat gained from friction.

2.8.3 Estimating the nominal temperature

The nominal or (bulk surface) temperature can depend on some factors described by Kennedy (2001):

$$\Delta T_{nom} = f\left(Q, A_c, h, t_f, G\right)$$

Where (h, t_f, G) respectively are the convective heat transfer coefficient at the contact boundaries [$Wm^{-2}K^{-1}$] (discussed in section 2.10.3), the friction time [s] and geometrical and material factor [-] that describes the finite shape of the body at contact and its thermal properties.

Ashby and co-workers have investigated nominal surface temperature. As previously noted Eq.(2.17) is useful where considering a first approximation of the flash temperature. Where Ashby has proposed a simple configuration to determine the thermal length (l_1) moving and (l_2) stationary bodies in [m] for pin-on-disc test approach at low sliding speed (Straffelini, 2015):

$$l_1 = Y + \frac{A_{nom}\,\lambda_1}{A_Y\,h_Y} \tag{2.10}$$

$$l_2 = \frac{r_0}{\sqrt{\pi}}\tan^{-1}\left[\frac{2\,\pi\,\kappa_2}{r_0 v}\right]^{\frac{1}{2}} \approx 2\sqrt{\frac{\kappa_2\,r_0}{v}} \tag{2.11}$$

Where (Y) is the distance between the contact surface and the holder [m], $(A_Y\,, h_Y)$ are the area [m^2] and the conductive heat transfer coefficient between [$Wm^{-2}K^{-1}$] the block and the holder respectively. (κ) is the thermal diffusivity in [m^2s^{-1}], (r_0) is the contact radius [m] and (v) is the sliding speed in [ms^{-1}].

Rowe *et al.* (2013) examined the temperature rise at contact from natural rubber against an optical smooth CaF_2 surface during sliding. The investigation also included assessing some of the commonly used models for average surface temperature prediction with experimental results. Thus, Rowe and co-workers have settled that Jaeger and Archard model's Eq.(2.12) and (2.13), were the closest approximation to the measured nominal temperature as presented in Figure 2.18. Here the normalised temperature rise was expressed as a function of the Peclet number with respect to the change in sliding speed.

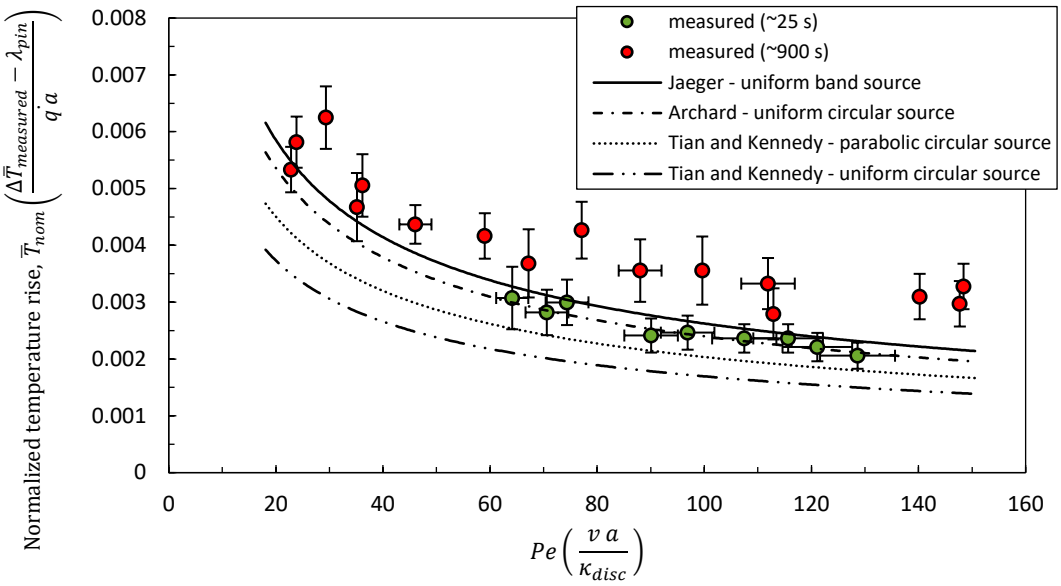

Figure 2.18: Non-dimensional contact temperature rise comparison between measurement and models prediction. Reproduced from (Rowe *et al.*, 2013)

Jaeger's model

$$\Delta T_{nom} = \frac{0.903\ q\ a}{0.849\ \lambda_{disc}\ \sqrt{Pe} + 1.064\ \lambda_{wood}} \tag{2.12}$$

Archard's model

$$\Delta T_{nom} = \frac{0.765\ q\ a}{0.785\ \lambda_{disc}\ \sqrt{Pe} + 0.974\ \lambda_{wood}} \tag{2.13}$$

Where (a) is the wood radius in [m]. Both models here can be used for square contact as well. Rowe has also investigated the difference in temperature rise under forced and natural convection under constant load and speed shown in Figure 2.19. The results show that forced convection caused a drop in the contact temperature for short period where time is a factor to reach a steady state.

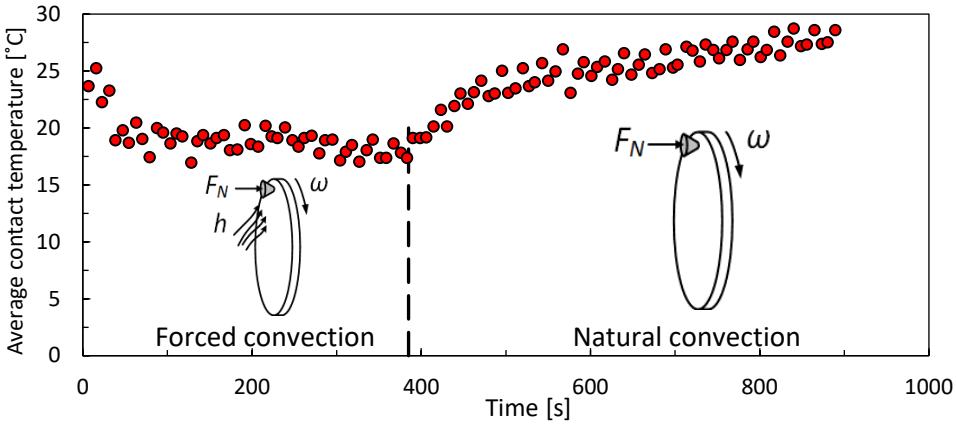

Figure 2.19: The effect of forced and natural conviction on contact temperature rise (Rowe *et al.*, 2013)

2.8.4 Estimating the flash temperature rise

Several mathematical models have been developed to predict the peak temperature at contact. The following model in Eq.(2.14) was developed by Blok and Jaeger to estimate the maximum flash temperature arising from frictional heat (Stachowiak *et al.*, 2014).

Blok, Kennedy and Jaeger model:

$$\Delta T_f = \frac{2\ q\ b}{\lambda\sqrt{\pi\ Pe}} : [Pe > 10] \quad \text{and} \quad \Delta T_f = \frac{2\ q\ b}{\lambda\sqrt{\pi}} : [Pe < 10] \tag{2.14}$$

Where (b) is the contact width [m], for a constant (q), the change in flash temperature decreases as the sliding velocity increases as shown in Figures 2.20 and 2.21. Also, a faster turning wheel will have a shorter time interval between exposures to the contact friction. Therefore, there is a balance between the frictional heating and dissipation through thermal diffusivity and surface convection as shown in Figure 2.21.

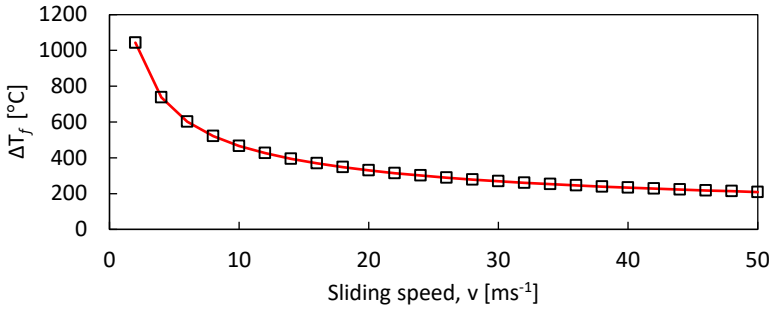

Figure 2.20: The influence of the sliding speed on the flash temperature rise over time.

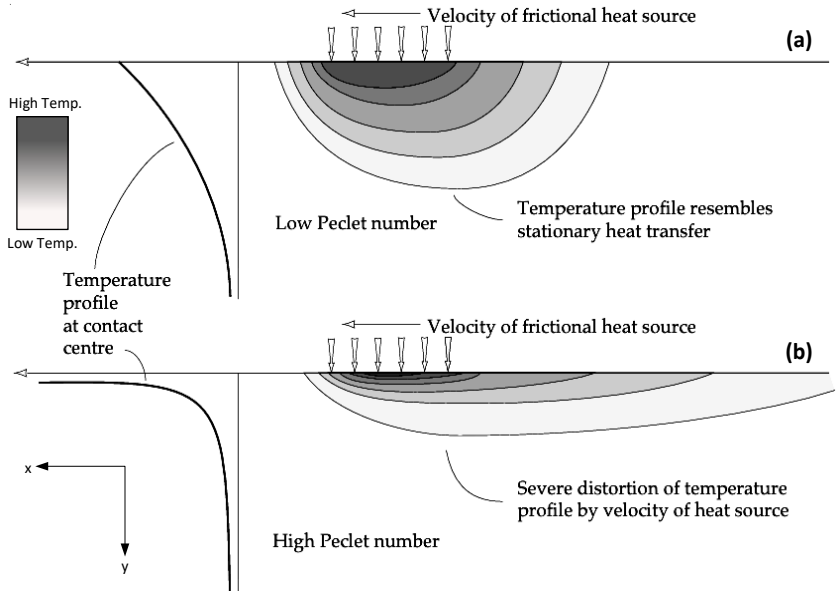

Figure 2.21: Frictional temperature profiles for low and high Peclet numbers. Enhanced from (Stachowiak *et al.*, 2014).

Figure 2.21 shows the temperature profile at the contact between two bodies for low (a) and high (b) Peclet number. The heat source is stationary in contact with a sliding body beneath it moves along an infinite path on one direction (x-direction) and heat flows on the y-direction. At low velocity (case – a), the frictional heat penetration has enough time to build a temperature gradient to raise the bulk temperature of the sliding body. Conversely, at high velocity the heat penetration is localised on the layer close near the surface at which it dissipates faster.

Another model was developed by Kong and Ashby (1991) based on the previous assumption to predict the flash temperature. The authors stated that at high sliding speed, the flash temperature would increase which often induces oxidation reactions between (polymer-to-metal or metal-to-metal) in contact to take place at contact (Basu, B. *et al.*, 2011). The flash temperature for this model is:

Kong–Ashby model:

$$T_f - T_b' = \frac{\mu\, F_N\, v}{A_r}\left[\frac{1}{\frac{\lambda_{wood}}{x_{wood\,(f)}} + \frac{\lambda_{disc}}{x_{disc\,(f)}}}\right] \tag{2.15}$$

where,

$$T_b' = T_b - \frac{A_r}{A_{nom}}(T_b - T_o) \tag{2.16}$$

$$T_b = T_o + \frac{\mu\, F_N\, v}{A_{nom}}\left[\frac{1}{\frac{\lambda_{wood}}{x_{wood\,(b)}} + \frac{\lambda_{disc}}{x_{disc\,(b)}}}\right] \tag{2.17}$$

$$l_{f,b} = \frac{r_j}{\sqrt{\pi}}\tan^{-1}\sqrt{\frac{\chi\, 2\,\pi\,\kappa}{r_j\, v}} \tag{2.18}$$

(κ, r_j) are with respect to each body

$$r_j = r_0\left[\left(1 - \frac{P}{P_s}\right)\left(\frac{r_0}{r_a}\right)^2 + 1\right]^{-\frac{1}{2}} \tag{2.19}$$

$$\frac{A_r}{A_{nom}} = \frac{P}{P_s} \tag{2.20}$$

$$P_s = \frac{A_{nom}\, Hr_0}{\sqrt{1 + 12\,\mu^2}} \tag{2.21}$$

The terms are: (T_b' is the effective bulk temperature [K]), (T_o [K]) is the reference temperature at the contact surface, (A_r, A_{nom} $[m^2]$) are the nominal and real contact area respectively, (P_s) is the seizure load[8], (x_f, x_b $[m]$) are the equivalent linear heat diffusion distance for flash and bulk heating respectively, where $x_f \ll x_b$. (Hr $[J\,m^{-3}]$) is the hardness of material where Hr_0 is the lesser of (Hr_1, Hr_2), (χ $[s^{-1}]$) is the measure of lifetime of a contacting asperity, and (r_a, r_j and r_0 $[m]$) are the radius of a single asperity junction, a contact junction and nominal contact area, respectively.

The model expresses the flash temperature proportionally to (load) $^{0.5}$, yet the model is only accurate for low sliding speed based on Kong and Ashby findings.

2.9 Reaction kinetics during friction

When wood is pressed against a spinning wheel, the close contact minimises the presence of air to that which occupies the pore volume of the wood. Frictional heating will first cause water evaporation because air-dried wood is *ca*. 10 – 15% moisture. Further heating results in sensible heat gain of the wood until the volatilisation temperature of extractives is reached. Extractives, however, are generally insignificant in smoking woods which are hardwood, unlike softwoods like pine. At higher temperatures, the wood begins to decompose. In the oxygen-lean environment, this process is pyrolysis. Because the friction causes simultaneous heating and removal of wood, this action is known as an ablative process. It occurs rapidly and is classified as fast pyrolysis ($Time_{heating} \gg Time_{reaction}$) with heating rate normally of (100 – 1000 ˚C/s). The process is advantageous for maximum production of gas or liquid yields at minimal char formation, because of the high heating rate with low residence time (Di Blasi, 1996).

It is well known that pyrolysis of wood undergoes a number of complex chemical and physical changes. Thus, to achieve tunable smoke an understanding of the reaction pathways is important. Figure 2.22 shows the reviewed mechanisms of wood thermal degradation.

[8] *Defined as the highest load at which elasto-hydrodynamic lubrication exists before boundary lubrication occurs (Fastexlubes).*

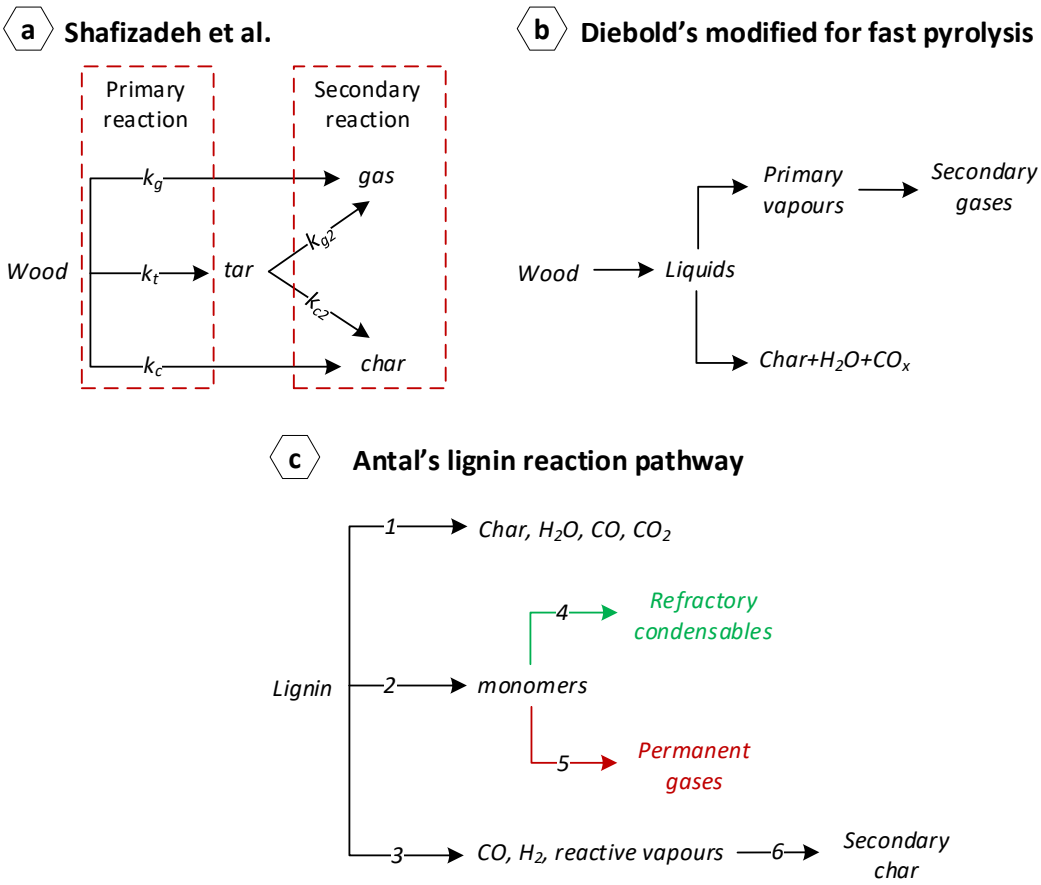

Figure 2.22: Kinetic mechanisms of wood and lignin decomposition (Park *et al.*, 2010; Peacocke, 1994)

Shafizadeh *et al*. (1979) proposed a mechanism (a) that wood decompose into three major products: tar, gas and char in a primary reaction followed by partial decomposition of tar in a secondary reaction, where $(k_g, k_{g2}, k_t, k_c, k_{c2})$ are the reaction rate constants for gas, tar and char respectively for primary and secondary reactions. This pathway is the simplest and most used in modelling the of the reaction kinetics of slow pyrolysis (Di Blasi, 1996; Park *et al.*, 2010).

In 1985, Diebold "cited in (Peacocke, 1994, pp. 78-79)" proposed a modified mechanism for ablative pyrolysis (b) from a comprehensive reaction scheme prepared by a number of specialists in pyrolysis in 1980, that focused on the production hydrocarbon gases. The pathway considers the influences of heating rate, temperature and pressure on biomass. The primary interest of this model at that time was for the production of olefins in the chemical industry. The reaction does not account for secondary char formation based on conditions of the process. The author stated that primary liquid vaporises to primary vapours.

The breakdown of lignin is particularly important to the aromatic flavours of the smoke. .Antal (1985) proposed reaction pathway (c), where the monomer degradation pathway (2) is favoured by high heating rate and low pressure. Antal (1985) also proposed pathway (5)

occurs at temperatures above 500 °C, leading to monomer cracking to form CO, CH_4 and higher hydrocarbons. Conversely, pathway (4) is favoured at low temperatures (not defined) to produce refractory condensables. Jeger and Klein (1985), in work on lignin decomposition at temperatures between 300 – 500 °C, found evidence of a high content of aromatic compounds. Another study, by Iatridis and Gavalas (1979) on lignin pyrolysed between 400 – 700 °C, obtained 60 wt% yield of the total volatiles. Nunn *et al.* (1985) "cited in (Peacocke, 1994, pp. 75-77)" stated that across the temperature range, 330 – 1100 °C, lignin yields a significant amount of char due to the stability of the aromatic hydrocarbons (Peacocke, 1994, pp. 75-77).

The findings in the previous paragraph and Figure 2.22 agree with the work done by Ledesma *et al.* (2016) concerning the regional temperatures for the formation of aromatic volatiles and PAHs.

2.10 Estimating the influential parameters on heat and mass transfer

A study by Lede *et al.* (1985) was conducted to measure the ablation rate of a wood surface undergoing fast pyrolysis by using a heated spinning stainless steel disc. In this approach, the sliding speed was set to 1 ms^{-1} to eliminate the role of local frictional heat generation. They concluded that fast pyrolysis of wood in the ablation regime with a maximum yield of gas is most likely to be achieved under two conditions: the availability of high heat flux and by efficient removal of the primary decomposed layer from the surface of the wood. These two conditions are crucial because the accumulation of primary products from wood ablation forms a layer which reduces the magnitude of thermal heat flux able to penetrate to the fresh wood surface, and the heat absorbed by this layer then drives further secondary reactions, including char gasification. While Lede et al.'s (1983) work was not aimed at food smoke production, it is likely that these secondary reactions, which favour more char formation, are also not likely to be favourable for smoke flavour.

The knowledge for this section was based on Lede *et al.*'s (1985) and Peacocke's (1997) experiments on ablative fast pyrolysis of wood rods. The experimental setups used by both researcher groups are illustrated in Figure 2.23 and their results are discussed below. In both cases the disc speed was kept relatively low to avoid localised frictional heating: the purpose of the disc being to remove ablated material.

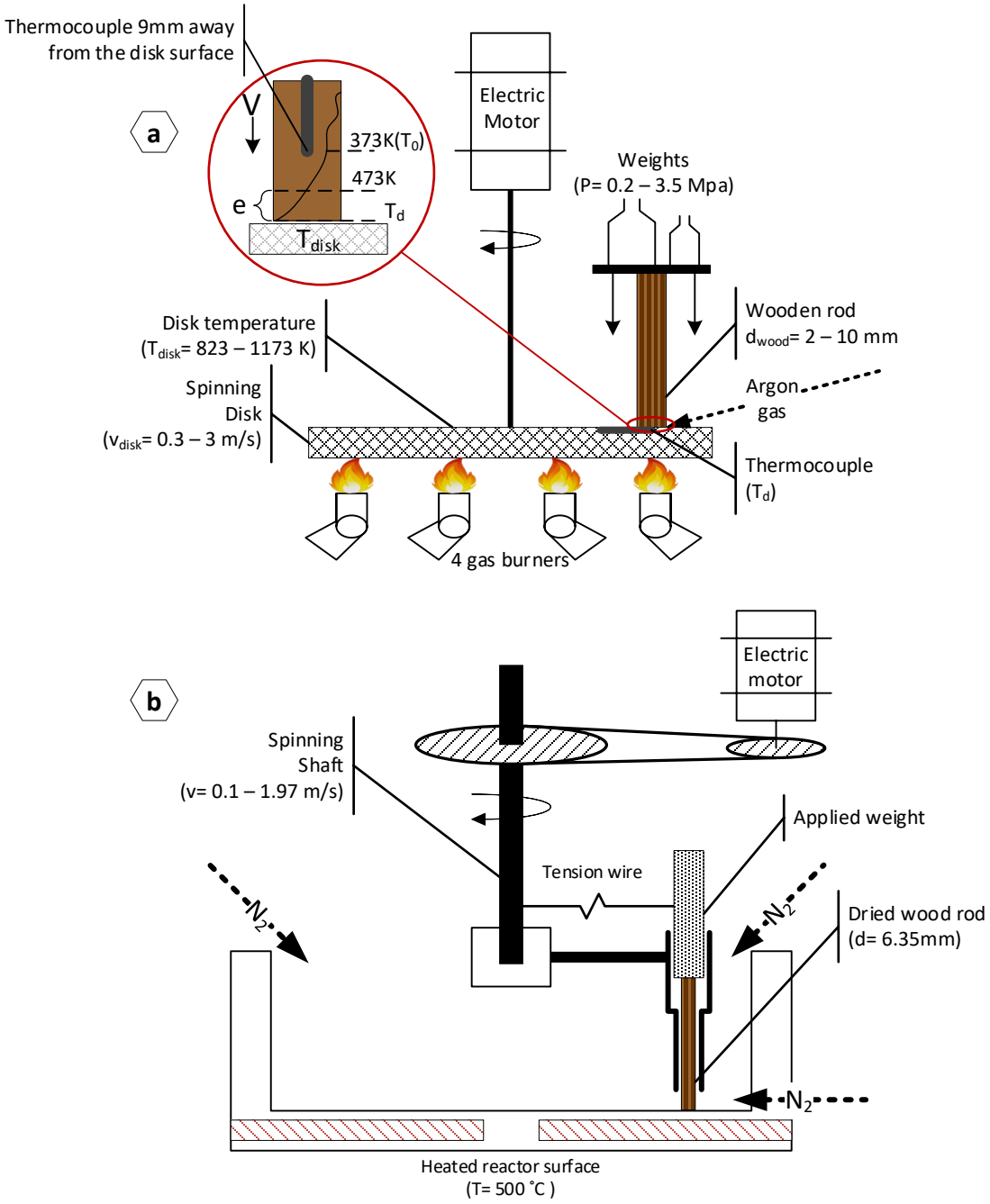

Figure 2.23: Experimental setup from (a) Lede *et al.* (1985) and (b) Peacocke (1994)

2.10.1 Ablation rate

Lede *et al.* (1985) found that the ablation rate (V) in [ms^{-1}] increases with the increase of disc speed (v_{disc}) [ms^{-1}], pressing pressure (P) [Pa] and disc temperature (T_{disc}) [˚C] using different diameter sizes (d) [m] of wooden rod, as shown in Figures 2.24 to 2.27.

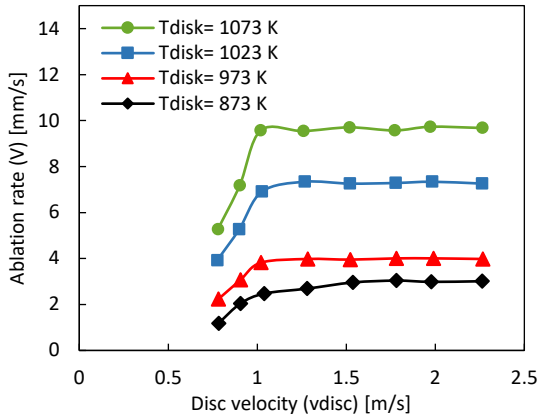

Figure 2.24: The effect of disc velocity on ablation rate at d=5 mm, P=0.5 MPa and different T_{disc}. Reproduced from (Lede *et al.*, 1985)

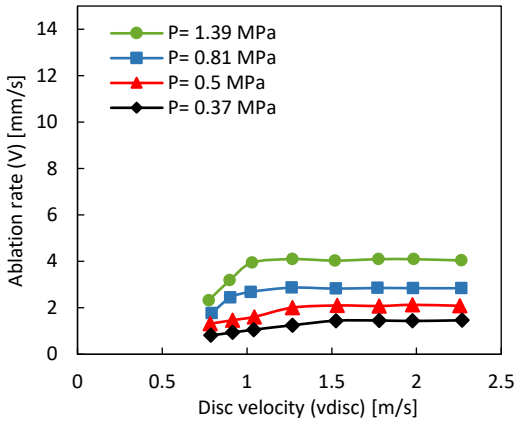

Figure 2.25: The effect of disc velocity on ablation rate at d=5 mm, T_{disc} =1073 K and different P. Reproduced from (Lede *et al.*, 1985)

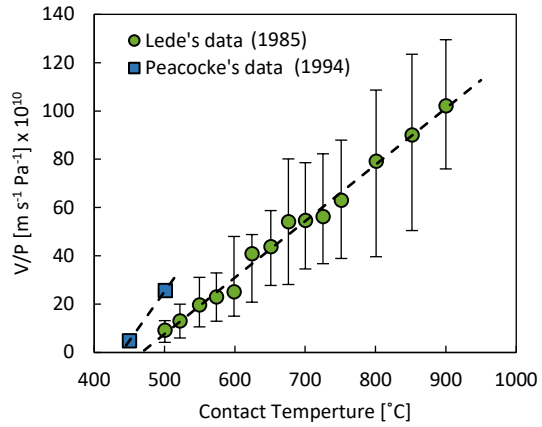

Figure 2.26: Comparison of Lede's and Peacocke's work on the variation of V/P with heating temperature. Reproduced from (Peacocke, 1994)

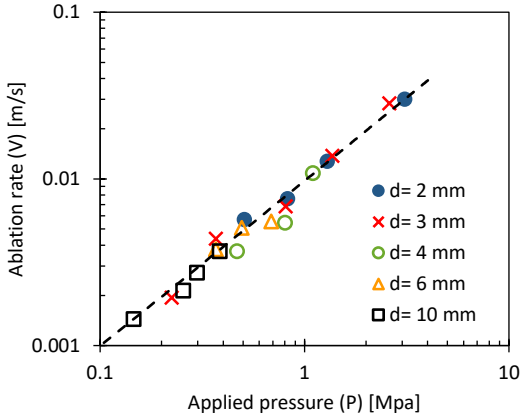

Figure 2.27: The effect of pressure on ablation rate at (T_{disc}=1173K) relative to different rod diameters. Reproduced from (Lede *et al.*, 1985)

It is clear that the ablation rate, V, is directly proportional to both the disc temperature ,T_{disc} , and the applied pressure, P, but that it is insensitive to disc speeds except at low values where, according to Lede *et al.* (1985), the speed is insufficient to completely remove the ablation layer of liquid which reduces the heat penetration through wood.

Figure 2.26 shows that the ratio of the ablation rate to the applied pressure V/P is a linear function of temperature. Hence, the following expression was derived to estimate the ablation rate as a function of pressure (Lede *et al.*, 1985):

$$V = \Gamma P^{\zeta} \approx \Gamma P \qquad (2.22)$$

Where (Γ) is an experimental constant [m s^{-1} Pa^{-1}] as a function of heating temperature Eq.(2.23) and (ζ) is an exponent of (P); the value of (ζ) is very close to 1, which indicates the adequate quality of the fitting line. The equation can be used to estimate (V) regardless of the wood contact area as Lede claimed.

$$\Gamma = 4.7317 \times 10^{-11} \times 10^{0.0020438\,(T_{disc})}, \qquad T_{disc} \text{ in [K]} \qquad (2.23)$$

Later work done by Peacocke (1994) from preliminary data at 450 and 500 ˚C in Figure 2.26 agreed on the linearity of (V/P) [m s^{-1} Pa^{-1}] with Lede's data. However, Lede's results had a lower ratio of V/P due to the variation of the experimental constant. Thus, Peacocke has developed a 2nd order polynomial Eq.(2.24) for estimating (Γ) as a function of (T_{disc}) [˚C] (Peacocke *et al.*, 1993):

$$\Gamma = 2 \times 10^{-14}(T_{disc})^2 + 1.57 \times 10^{-11}(T_{disc}) - 5.86 \times 10^{-9}, \qquad T_{disc} \text{ in [°C]} \qquad (2.24)$$

There is the diameter factor (i.e. contact area), which probably explain the difference between the models in both works. Where the relative error between equations.(2.23) and (2.24) was calculated to be 36% and 8% respectively, relative to the measured ablation rate (0.51 mm s^{-1}) by Peacocke (1994).

2.10.2 Thickness of the lubricant layer

The lubricant layer of ablated material affects the heat transfer. Despite the poor accuracy of the technique, Lede *et al.* (1983) showed that the lubricant layer thickness, *e*, decreases as *V* increases. From this result, Lede *et al.* (1983) approximated that the product *Ve* is constant. The author also noted that for a very high ablation rate (i.e. extreme grinding) $e \approx 0$.

Peacocke (1994) also measured the thickness of the lubricant layer using a single particle (5×5 mm) pressed by an angled rotating blade (10°) on the heated reactor surface (450 – 600 ˚C) and relative velocity > 1.2 m/s as shown in Figure 2.28.

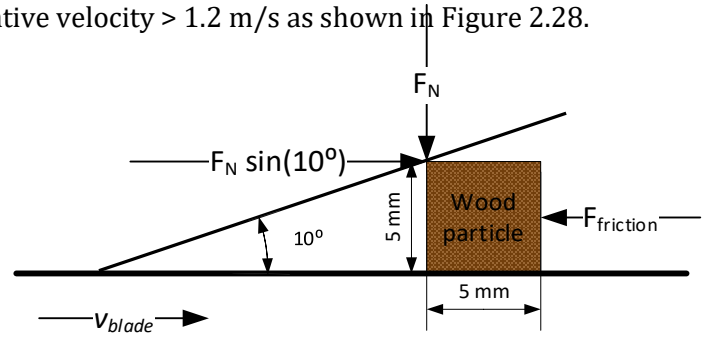

Figure 2.28: Force diagram for wood particle ablation experiment (Peacocke, 1994)

The thickness of the liquid layer was calculated by mass balance using Eq. (2.25) and by assuming the liquid film viscosity to be 0.07245 Ns/m^2

$$e = \frac{A_{pa}\,\mu_l\,v_b}{F_\tau} \qquad (2.25)$$

where (A_{pa}) is the particle contact area [m^2], (μ_l) is the liquid film viscosity [Ns m^{-2}], (v_b) is the blade velocity in [m s^{-1}]. The results are presented in Table 2.6.

Table 2.6: The estimated thickness of liquid layer with variation of friction force (Peacocke, 1994, p. 197)

F_τ	$[N]$	3.5	1.0	0.8	0.6
e	$[m]$	6×10^{-7}	2×10^{-6}	3×10^{-6}	4×10^{-6}

The viscosity of the liquid layer changes with temperature. Peacocke (1994) found that at temperatures above 500 °C sufficient lubrication occurs with reduced pressure applied on the particle. He related the increase in the ablation rate with increasing temperature to the increase in reaction rate. To do this, the volatiles formed are assumed to be in the vapour phase and the rate can be estimated by the Arrhenius model Eq. (2.26)

$$k = A \exp\left(\frac{-E_a}{R\,T}\right) \tag{2.26}$$

where (k) is the rate constant [s^{-1}] (A) is pre-exponential factor [s^{-1}], (E_a) is the activation energy for reaction [J mol^{-1}], (T) is the absolute reaction temperature [K] and (R) is the universal gas constant[J mol^{-1} K^{-1}]. The values for (E_a) and (A) are generally determined experimentally by Thermogravimetric Analysis (TGA)[9].

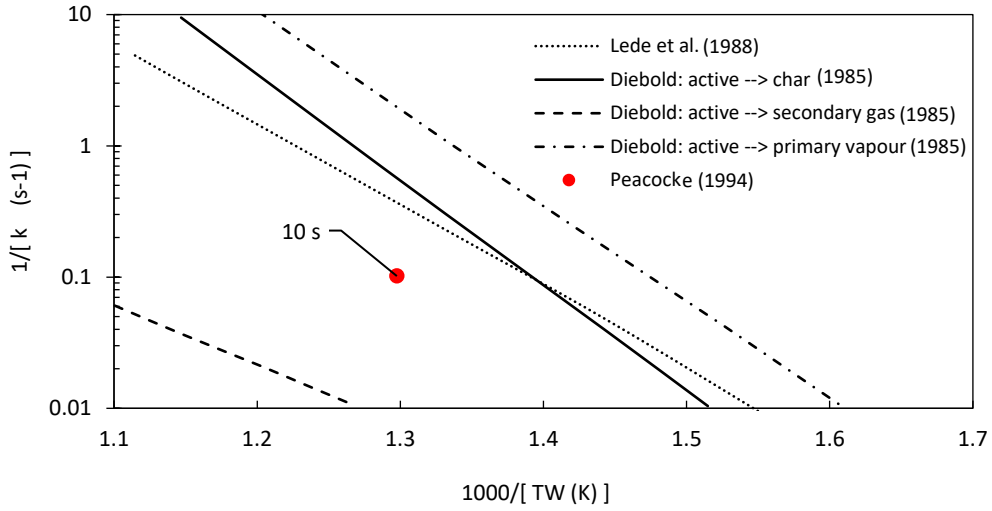

Figure 2.29: Estimation of liquids devolatilization times with reactor temperature. Reproduced from (Peacocke, 1994)

[9] *TGA is an instrument that continuously measure the weight change of a sample heated at either constant temperature or at a fixed eating rate, the result is represented graphically as weight change over time (Peacocke, 1994).*

Thus, he found by using Eq.(2.25) and $E_a = 11600\ J\ mol^{-1}$ and $A = 2.7 \times 10^7\ s^{-1}$ from Lede, J. *et al.* (1988) devolatilization time of 2.55 seconds compared to 10 seconds from his work in comparison with Lede (1988) and Diebold (1985) shown in Figure 2.29. Peacocke concluded that the difference in parameters is due to:

- Lede's parameters were obtained for 600 ˚C and above.
- The nature of the biomass could affect the chemical composition of liquids.

Another factor could be the ineffective removal of the char layer is reducing the amount of heat to be conducted to the fresh wood face. Whereas the layer builds up the conductive heat transfer coefficient will reduce due to the low thermal conductivity of char compared to wood. This reasoning was based on the study by Gupta *et al.* (2003), where he experimentally showed that the thermal conductivity of softwood ($0.2050\ W\ m^{-1}K^{-1}$) is higher than its derived char ($0.0946\ Wm^{-1}K^{-1}$).

2.10.3 The conductive heat transfer coefficient

When designing ablative systems, the heat transfer is best encapsulated by a heat transfer coefficient (h). The relationship between heat transfer coefficient and pressure has been developed by Lede *et al.* (1985) as follows, Eq.(2.27)

$$h = \Psi\ P \tag{2.27}$$

The proportionality term ($\Psi = 0.017$) in $[Wm^{-2}\ K^{-1}\ Pa^{-1}]$ assumes that the solid will directly convert to gas/vapours during pyrolysis y for temperatures between 773 – 1173 K,

$$q = \overbrace{h(T_{disk} - T_d)}^{\text{supplied heat}} \approx \overbrace{V\rho_w cp_w(T_d - T_0)}^{\text{sensible heating}} + \overbrace{V\ \rho_w\ \Delta H}^{\text{heat of reaction}} \tag{2.28}$$

where (q) is the heat flux $[Wm^{-2}]$, (h) is the heat transfer coefficient between the wood and the heated disc [$Wm^{-2}K^{-1}$], (T_{disc}, T_d, T_0) are the disc, decomposition of wood and the initial wood temperatures [K] respectively. (V) the ablation rate [ms^{-1}], (ρ_w) the density [$kg\ m^{-3}$], (cp_w) the specific heat capacity [$J\ kg^{-1}\ K^{-1}$] of wood and (ΔH) the heat of pyrolysis [$J\ kg^{-1}$].

The heat of pyrolysis was neglected by Lede, in Eq. (2.28) stating that the value of the heat of pyrolysis can be difficult to be accurately estimated for fast pyrolysis of wood as he measured a value of $\approx$ 40 kJ kg^{-1} at 773K which account only for 3.6% of the heat required to heat the wood from 373 to 773K. Thus, Lede has suggested Reed's *et al*. (1980) proposed model which assumes that the wood is heated first without any reaction up to the reaction temperature. Then depolymerisation occurs to yield solid that rapidly melts before vaporisation (Lede *et al.*, 1985).

In correlation to Lede's work, Peacocke (1994) developed an expression Eq.(2.29) for estimating the (Ψ) based on the thermophysical properties of wood and process parameters and known pressure where he accounts the effect of pyrolysis heat from equation (2.28). Two sets of temperatures 450 and 600 °C were used to derive the average line equation as a function of pressure. Then he compared his equation with Lede's Ψ value on the effect of predicting the heat transfer coefficient as presented in Figure 2.30.

$$\Psi = 2.058 \times 10^{-3} + 7.111 \times 10^{-9}\, P \qquad (2.29)$$

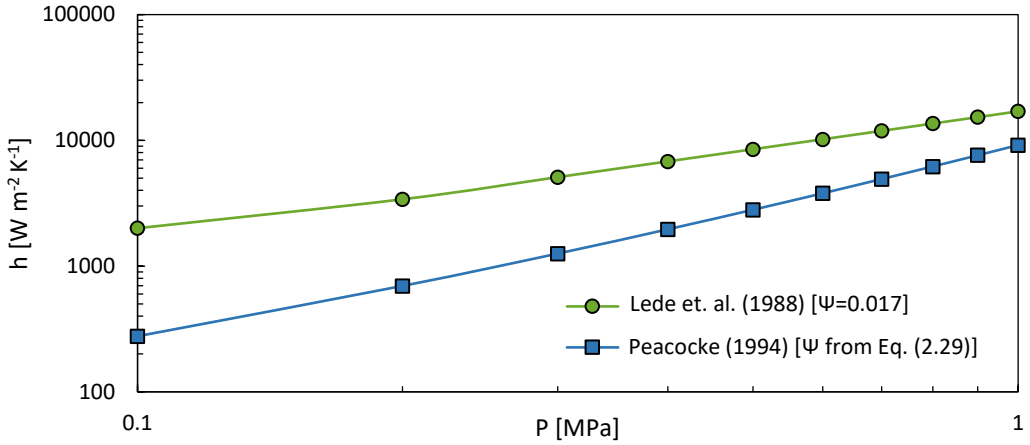

Figure 2.30: Variation of heat transfer coefficient with contact pressure.
Produced from Lede and Peacocke equations.

The variation is evident as shown in Figure 2.30, where Lede's (1988) constant resulted in higher predicted heat transfer coefficient in comparison to Peacocke (1994). Both models were established with different wood densities, where Peacocke's and Lede's density values are 396 and 700 kg m^{-3} respectively. The difference between the models is likely to be due to this difference.

2.10.4 Effect of grain direction

Several workers have studied the effect of grain direction of wood on heat and mass transfer. It was found that the heat transfer rate was doubled if the thermal penetration is parallel to the grain. Similarly, the permeability along the grains is 10^4 higher than when it is across the grain (Roberts, 1971).

In a study conducted by TenWolde *et al.* (1988) on thermal properties across the fibre direction of soft and hard American woods, they showed that the increase in wood density linearly increases the thermal conductivity (λ) in [W m^{-1} K^{-1}]. Figure 2.31 shows the wood species used in their work. The authors stated that the heat conductivity along fibers is 1.5 – 2.8 times the conductivity across the grain.

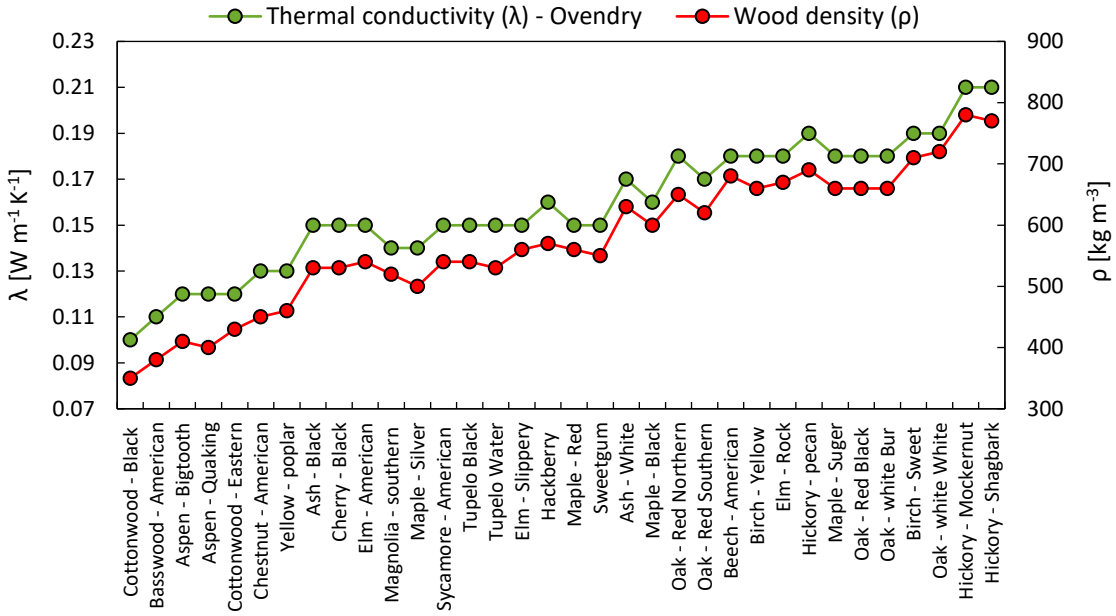

Figure 2.31: The change in (λ) as a function (ρ) for various American hard wood species, estimated across the grains. Reproduced from (TenWolde *et al.*, 1988)

The conductivity of the American woods were computed using eq.(2.30) that was validated with experimental data. The equation is reliable for densities > 300 kg m^{-3} and MC < 25%.

$$\lambda = \left(\frac{\rho}{1000}\right)(0.1941 + 0.004064\,MC) + 0.01864 \qquad (2.30)$$

Another study on African woods by Jankowska *et al.* (2013) measured values for the conductivity of wood as shown in Figure 2.32. They similarly concluded that higher wood density exhibits higher thermal conductivity.

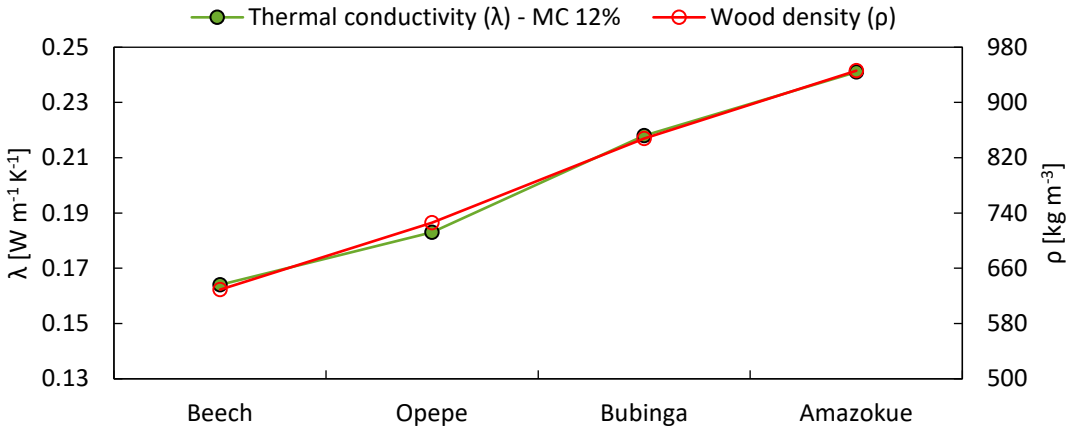

Figure 2.32: The change in (λ) as a function (ρ) for various African hard wood species, measured along the grains. The measurements for (λ) was obtained using ISOMET 2104.
Reproduced from (Jankowska *et al.*, 2013)

For both studies, the change in heat conductivity is a function of wood density has been represented in Figure 2.33. This shows geographic and wood species has negligible effect

on the thermal conductivity compared to the density. If this is true, then the thermal conductivity for Manuka wood, the subject of this work, can be estimated with reasonable accuracy.

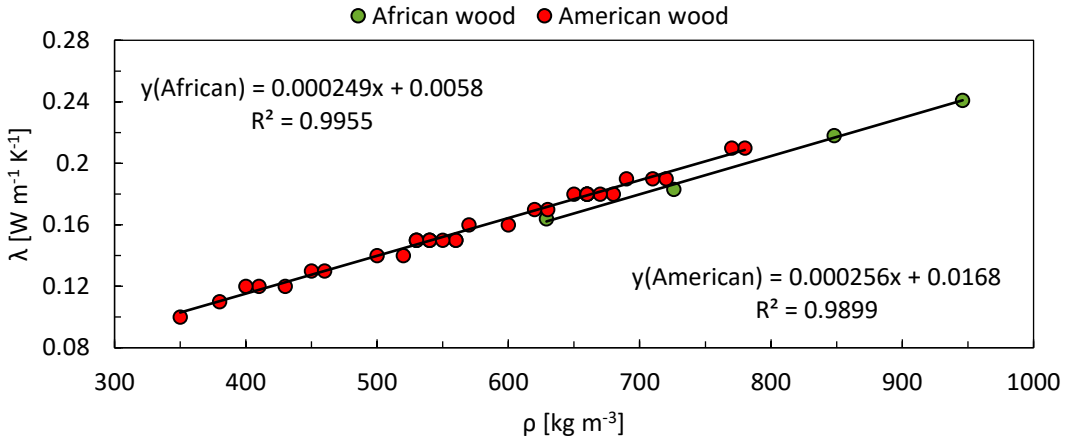

Figure 2.33: Thermal conductivity of wood as a function of density for American and African wood species.

2.11 Review of friction smoke patents

During the research process, it was important to investigate other patent designs around the same area. Several designs were found, using the principle of using a log of wood pushed against a rotating wheel for generating smoke by friction. The purpose of this research around patent designs is to know what has already been registered as a patent to both understand the design parameters used and the copyright boundaries. The review is not exhaustive, but is aimed at discovering the unique techniques that have been used.

Friction smoking designs employ different mechanisms to generate the frictional heating necessary to produce smoke. Patent number (EP 1258199 A1, 2002) is a design of a food smoking chamber using wood blocks pressed vertically on motor-powered friction wheel which runs at 3000 rpm. The wheel has a concave conical surface with three symmetrical friction ridges equidistance apart. The designer claims that using a conical-shape wheel will help to centre the wood rods in place. Other designs have a flat friction wheel with a rough surface. The reason behind adding the protrusions in Figure 2.34 is to remove the charred layer during smoking, which also drives out the desired components in the smoke and to present a fresh face of wood for smoking (3 245 394, 1961) this idea was implemented in several wheel design with different configurations. In the above two designs, the wood log is pressed by a pneumatic actuator. The smoke generator has a smoke filter to purify the produced smoke be removing fine sawdust particles before it goes to the smokehouse.

Figure 2.34: Top and side views of a flat friction wheel with grits (J *et al.*, 1961)

In patent number (EP 2340716 B1, 2009), the designer uses the side of the wheel to generate friction. The side of the wheel has flanges mounted which rotate at 3000 rpm. The wood log is fed in a vertical manner against the friction wheel. There was no information on how the system controlled the smoking temperature.

In an attempt to control smoke generation parameters, in patent number (3 573 223, 1971) has developed a friction smoker which can be controlled by maintaining a constant CoF during operation and thus the heat flux is constant based on equation (2.3). The control principle is based on the relationship between motor current and load as illustrated in Figure 2.35.

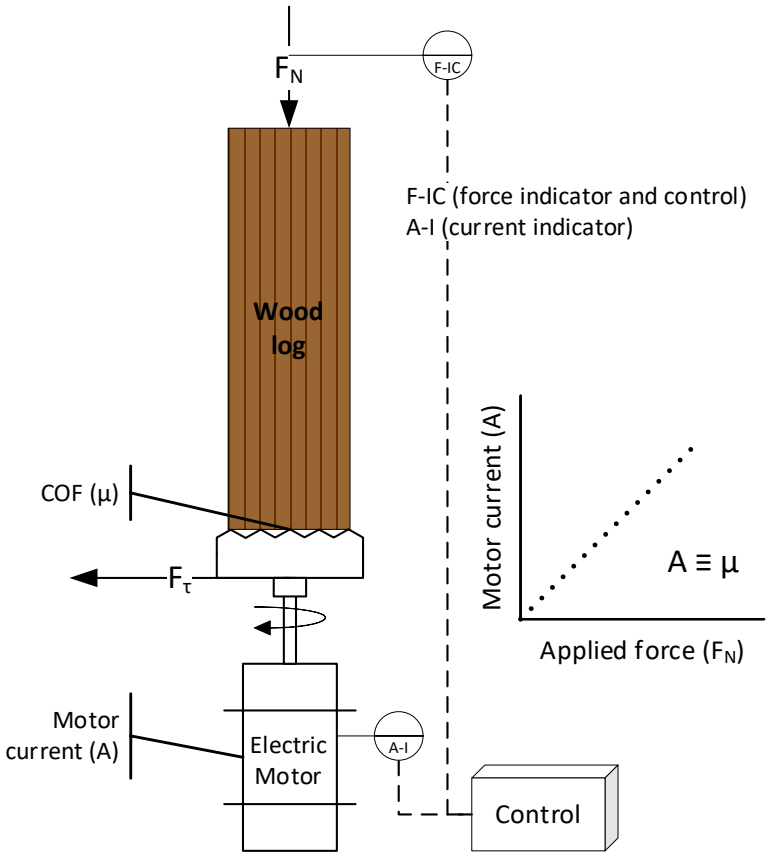

Figure 2.35: Control scheme produced based on Anderson *et al.* (1971) design.

Based on Anderson's (1968) design, in the case when the electric motor runs at constant speed unloaded the current supply will be constant. Once a load is being exerted on the motor (i.e. the applied force on the abrasive wheel as shown in Figure 2.35), the current supply will increase to maintain its constant speed. As the wheel's speed is constant the frictional force also will be. Hence, the change of the motor current is dictated by the change in applied force (i.e. .the frictional force is proportional to current flow). Therefore, the variation in CoF can be equated to the change in current flow. It is this principle that is used in the work presented in this thesis. It is further developed in the next section.

2.12 Torque estimation in an induction motor

In this section, understanding how an induction motor and variable speed drive (VSD) work together will be used to develop a model for estimating the CoF in this project.

Figure 2.36 shows a 3-phase induction motor controlled by a variable speed drive (VSD). It works by responding to the change in the electromagnetic field between the stator and rotor, as induced by a voltage change from the VSD. As voltage changes, different pols in the stator become magnetized which causes the rotor to rotate. The plot in Figure 2.36, shows the phase switch between the three voltage lines, and the rate of one oscillating cycle in milliseconds is a function of frequency which is proportional to the rotation speed of the rotor. Slip is necessary to impose a relative motion between the stator's magnetic field and the rotor. The slip is directly proportional to the load, where a slip value of 1.9% is standard for electrical motor manufacturer at free load conditions "cited in (Gottlieb, 1997)".

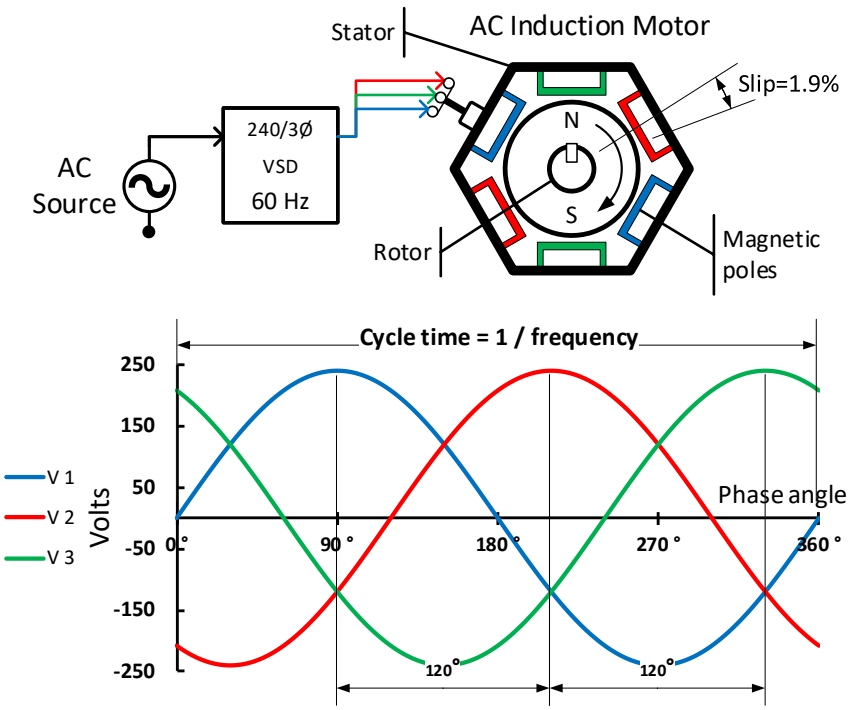

Figure 2.36: Schematic of the voltage envelop for an AC induction motor at free load

The function of the VSD is to vary the output voltage to the motor by altering its frequency while maintaining a constant current by using PWM[10] between input and output voltage as shown in Figure 2.37. When a load is being applied to a motor, the current will vary to maintain the rotor speed running as close as possible to the set point speed. The VSD always maintains the voltage to frequency ratio to run at a particular speed. This ratio is independent of the load added to the motor; thus, as load increases, the current increases. This principle of work has the advantage of sustaining efficiency between the input and output power (Spitzer, 2012).

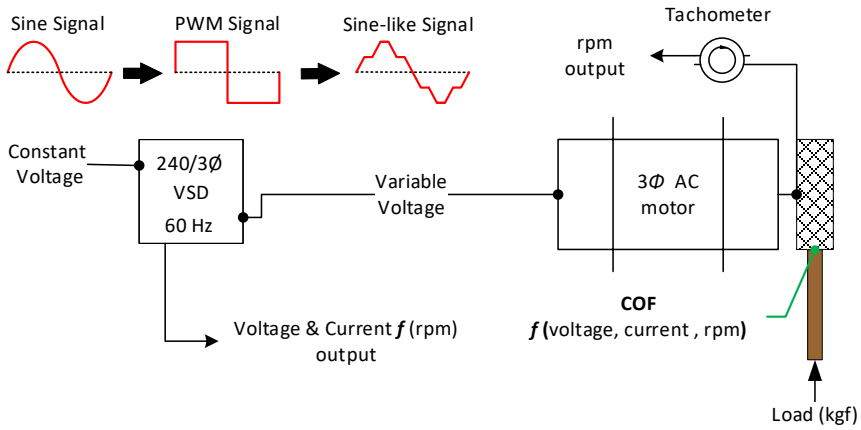

Figure 2.37: Schematic of the AC motor and VSD working principle under load conditions.

While the VSD delivers the synchronous speed to the stator, if a load introduced the slip between the stator and rotor is measured as the change between the measured speed, n, the synchronous speed, n_s shown as follows.

$$s = \frac{n_s - n}{n_s} \tag{2.31}$$

This slip develops the torque. The simplified circuit model for an induction motor is shown in Figure 2.38.

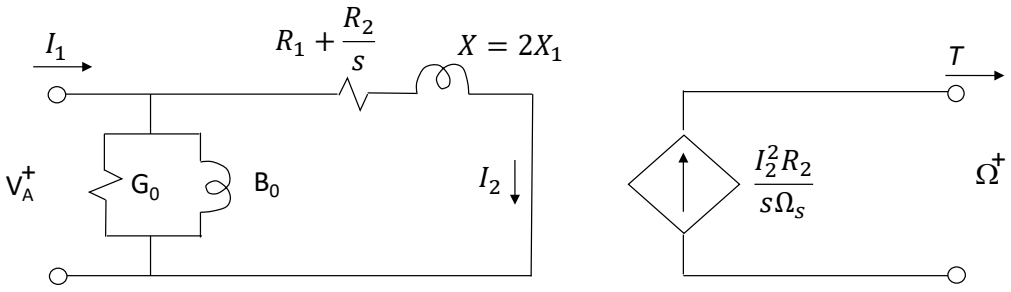

Figure 2.38: Simplified circuit model for an induction motor. R_2 is the resistance in the rotor winding. The reactance $X_2=2\pi f L_2$ and is the product of the stator frequency f [Hz] multiplied by 2π (to convert to radians per second) and the inductance, L_2, of the rotor windings. Adapted from (Gottlieb, 1997)

[10] *Pulse Width Modulation: Is a technique allows for controlling the input power supplied to electrical device.*

A motor running at synchronous speed with no load develops no torque and, in this definition, has no incremental power. The torque developed for non-zero slip is

$$T_d \approx \frac{I_2^2 R_2 s}{\Omega_s} = \frac{V_A^2 s}{\Omega_s R_2} \tag{2.32}$$

where the experimental set-points are the synchronous speed, Ω_s [radians/s] and the supplied voltage, V_1, from which the adjusted voltage is determined, is

$$V_A = V_1 - I_1\sqrt{R_1^2 + X_1^2} \tag{2.33}$$

The magnitude of the second term is unknown, but will probably be less than 10% of V_1. The resistance of the rotor windings, R_2, is also unknown. Thus, the mechanical power is

$$P_{mech} = T_d \Omega_s \approx I_2^2 R_2 s = \frac{V_A^2 s}{R_2} \tag{2.34}$$

As neither I_2 or R_2 are known, I_2 being the current in the rotor, this equation cannot be used. However, it is clear that the power and torque are proportional to the slip, s. If V_A/R_2 is relatively invariant for one synchronous speed, then $T_d \propto s$, as is typically plotted in specification charts by motor manufacturers. If a similar assumption applies, that the VSD voltage output multiplied by the power factor is relatively invariant for one synchronous speed then $T_d \propto I_1$ (I_1 being the stator current supplied by the VSD, which is higher than I_2 due to the losses by the air gap between the stator and the rotor). If so, then for a given synchronous speed, $s \propto I_1$. This is illustrated in Figure 2.39 below for the possible outcomes. These assumptions underline the later work presented in this thesis.

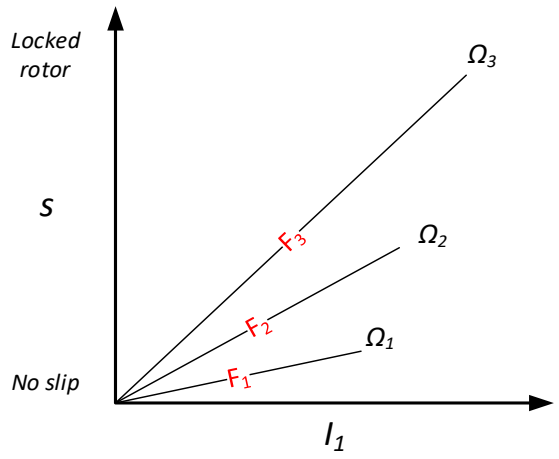

Figure 2.39: The effect of load (F) on current consumption (I_1) and rotor slip at one set point speed. Here $F_3 > F_2 > F_1$, to represent the change in rotor actual speed donated by (Ω).

2.13 Smoke analysis methodology

Smoke analysis is performed by collecting smoke samples on adsorbent material, which is then removed using a solvent (Details in GERSTEL (2017)). This solution is then injected into a gas chromatography-mass spectrometry (GC-MS) technique to identify flavouring compounds. The GC-MS (Figure 2.40) works by first separating the volatile compounds as they transport through a packed capillary column, the GC. Once the separation is done, the MS ionises the compounds and detects the identities of chemical groups. In this way, by matching to standards, the compounds can be identified (McNair *et al.*, 2009). Another method involves using a Pyro-GC-MS, that is, the above instrument with a pyrolysis furnace attached to the front end. Its advantage is that smoke can be directly injected for analysis. In case of analysing liquid or solid samples a micro-Pyrolysing unit that connected to GC-MS is commonly used.

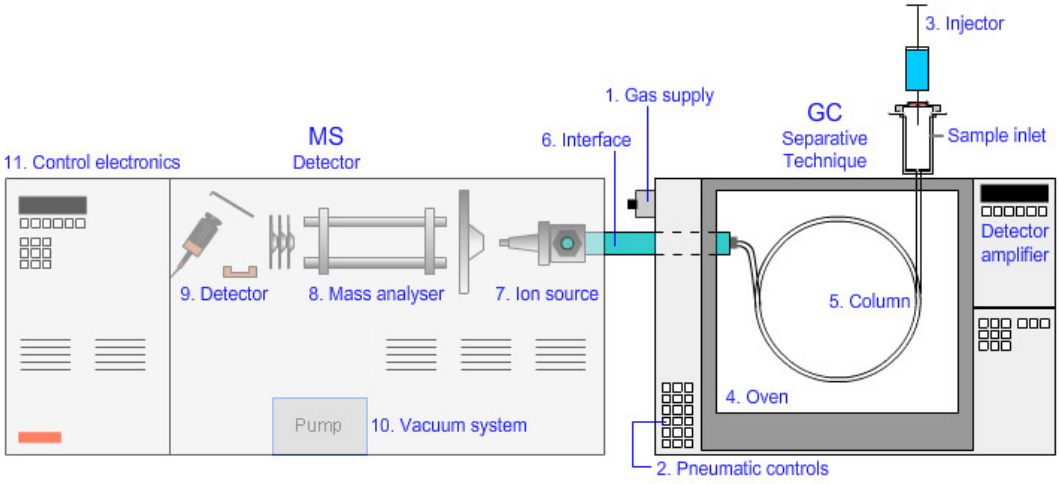

Figure 2.40: Schematic of GC-MS devise. Retrieved from google image.

2.14 Closure

This literature highlights a number of important considerations when generating wood smoke. The major classes responsible for the aromatic flavours of smoke are guaiacol, syringol, phenol, and 4-methylguaiacol, but how these relate to smoke quality as defined by a pleasant aroma profile is not well understood. Smoking conditions (i.e. temperature, moisture content, oxygen concentration, and smoking method) affect not only the proportions of aroma compounds but also the formation of aromatic and PAH compound, which become more prevalent at higher temperatures and longer residence times. In a friction-type smoker, several factors (i.e. the pushing force and friction plate temperature) affect the rate of heat and mass transfer at the wood surface and thus the ablation

rate. Compared to other smoke generation methods, the uniqueness of friction smoking is that it has low PAH yields, which is likely because of the close proximity of the wood to the wheel surface excludes air. However, the effect of these factors on smoke quality has not been explicitly addressed in the literature. Thus, based on the reviewed literature an experimental study has been planned, where the objective is to precisely control the smoking conditions and thereby deliver a tunable smoke. The following sections detail the experimental apparatus, the experimental design and the results directed to this objective.

Chapter 3 Design and Control Strategy

3.1 Introduction

This chapter covers the improvements on design and control for the friction smoke generator.

3.2 Friction smoke generator design novelty

The main objective of the design is to deliver precise control over the smoking temperature by manipulating the pressing force, wheel speed and wheel temperature. The novelty in this design is a heating element to control the wheel temperature and therefore the frictional interface temperature between the spinning wheel and the wood. It must be noted that while control of the wheel or disc temperature is a feature of tribology experiments reported in chapter 2, it has not been a feature in the patent literature for wood smoke generators. This may be because those tribology experiments also used slow disc speeds to avoid the frictional heating that higher speeds cause, but which confound the results of such experiments. Here, in this design both high speed and temperature control are used.

As discussed in section 2.7 (Figure 2.12), the frictional temperature rise has two components, the nominal rise and the flash rise. The nominal rise is proportional to sliding speed, but the flash rise which occurs at the contacts between asperities of the wood and wheel decreases non-linearly with increasing wheel speed. The frictional heat generated will dissipate in both directions, but this is dependent on the thermal conductivities of wood and steel, the latter of which has a greater tendency to conduct heat as shown in Figure 3.1 (left), and expressed mathematically in sections 2.8.2 and 2.10.4. Therefore, the advantage of adding external heating is to maintain the frictional zone near the wood decomposition temperature so that the increment provided by frictional heating is not significant and therefore can be dissociated largely from needing high pressing forces where grinding[11] competes with thermal decomposition.

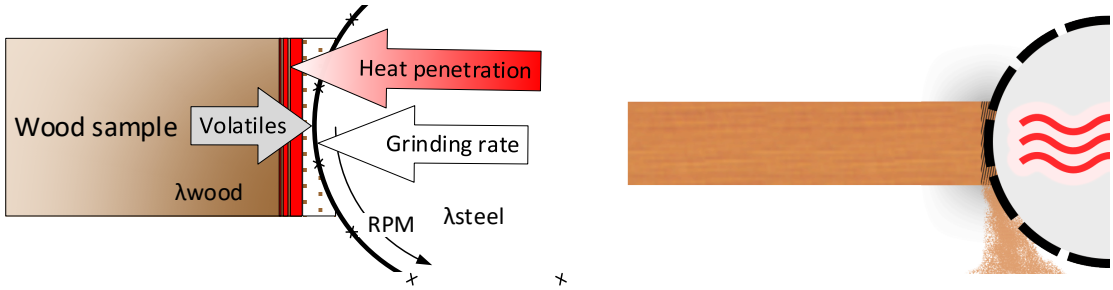

Figure 3.1: Conceptual schematic (left) smouldering vs (right) grinding of wood plank during friction.

[11] *Grinding: Is the sanding effect which contribute to the amount of wasted wood before pyrolysis.*

3.3 P&ID and CAD design

Figure 3.2, shows the improved friction smoke generator P&ID as follows. The chamber and chimney were improved by adding a thermal insulation wool to maintain accurate control over temperature. A heating element (HE-3) was embedded inside the chamber to control the temperature of the smoking environment. The mechanical actuator (A) was used for more solid pressing force control compared to the pneumatic actuator that was used at the early stages of the project. A smoke sampling kit was added to allow for smoke collecting in either volatile or liquid phase. More instrumentation was also added to measure and log the wheel speed (RI) and motor current (CI).

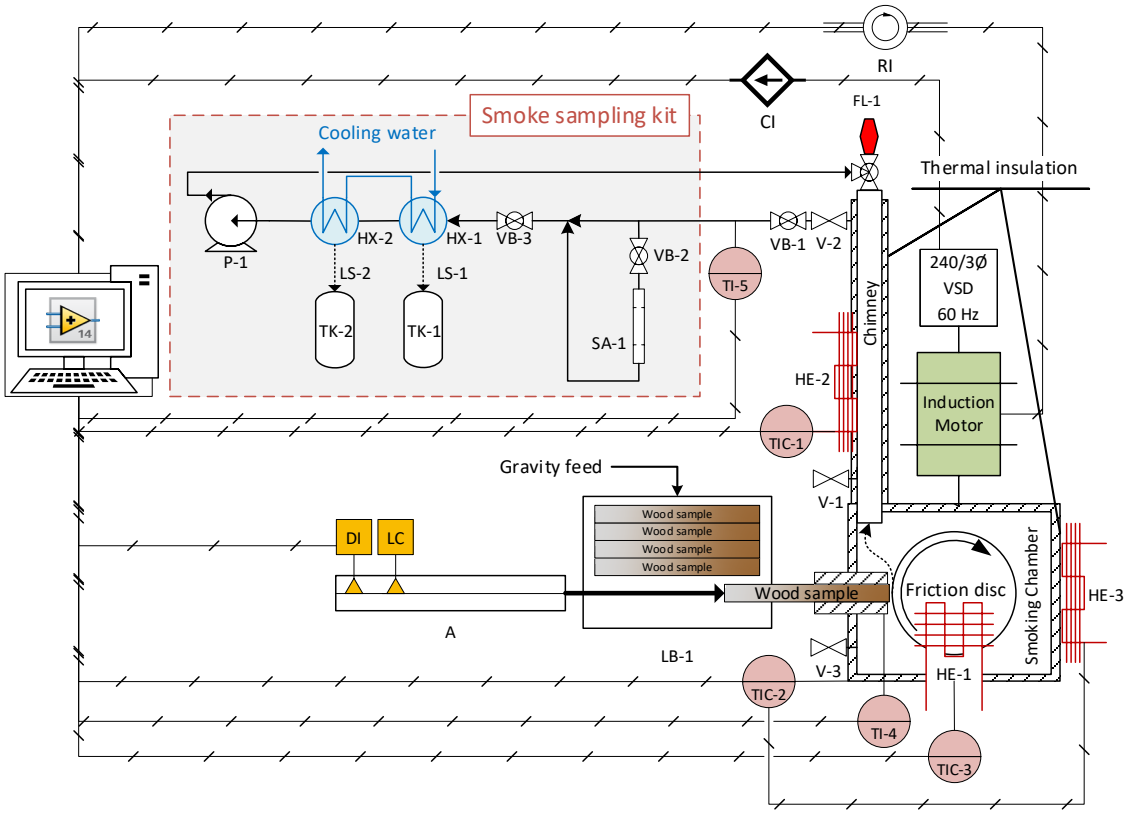

Figure 3.2: Friction smoke generator P&ID schematic

Table 3.1: List of items in friction smoke generator P&ID

Symbol	Description	Symbol	Description
A	Linear actuator	P	Air venturi
LB	Sample loader box	DI	Displacement indicator
LC	Load cell	LS	Liquid smoke line
HE	Heating element	TK	LS collecting tank
HX	Heat exchanger	TIC	Temp. indicator and control
VB	Ball valve	TI	Temp. indicator
V	Sampling valves	SA	Smoke absorbent
V-3	Inert gas inlet	FL	Gas flare
RI	Tachometer indicator	CI	Current meter indicator

The Piping and Instrumentation Diagram (PI&D) and the CAD design encapsulate the modifications to the friction smoker carried out in this project. These represent the

improvement since the project completed as part of the author's Honours research project (Seraj, 2016)

The integration of the friction smoke generator system was presented in Figure 3.3.

ITEM NO.	PART NAME
1	Induction Motor (750 W)
2	Chimney
3	Smoke Trap
4	Air Venturi
5	Air Inlet
6	Cooling Water Inlet
7	Smoke Condenser (x 2)
8	Cooling Water Outlet
9	Heating Element (200 W)
10	Friction Disc (Rs = 0.2 mm)
11	Smoking Chamber
12	Wood Sample Holder
13	Mechanical Actuator
14	Load Cell (Max. 100 kg)
15	Control Box
16	VFD (60 Hz)

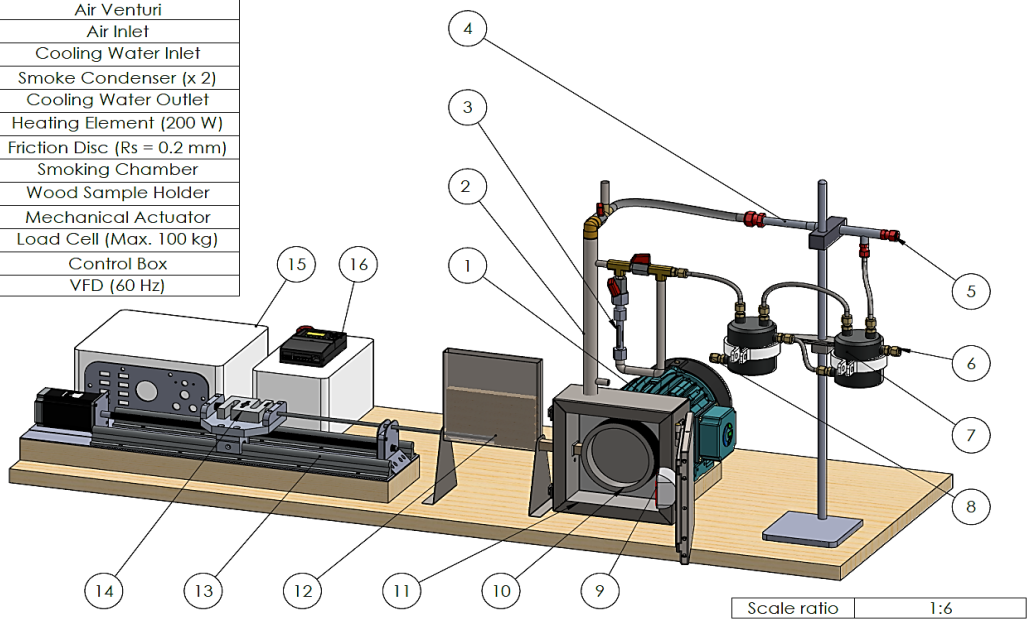

Figure 3.3: Friction smoke generator CAD design.

3.4 Control strategy

The controlling schema of the friction smoke generator was programmed using LabVIEW integrated with Compact DAQ module. The next sections details its components.

3.4.1 Temperature

From Figure 3.2, HE-1 and HE-3 are set to the same set-point within ± 2 ˚C. HE-1 is a planar heating element which has a surface rating of 51.2 kW m^{-2} at 810 ˚C. It is placed inside the friction wheel cavity to ensure the inner surface temperature of the wheel reaches the set point. HE-3 is a flexible heat tape that has been wrapped around the chamber to control the inner wall temperature surrounding the friction wheel. The heating tape is rated at 750 ˚C and has been covered with insulation to mitigate heat lost.

3.4.2 Pressing force and wear rate

The set-point pressing force is maintained with a feedback loop between the load cell and a stepper motor shown in Figure 3.2. When converted to Newtons accuracy is approximately ± 1.2 N. This is somewhat dependent on vibration, which is worse at low pushing forces.

Please refer to Appendix B.4 for load cell and the actuator displacement calibration plots.

3.4.3 Wheel speed

The rotational speed of the friction wheel in [rpm] is controlled via a 60 Hz VSD module which has an embedded PID-controller. The outputs from the VSD are linked with LabVIEW to measure the electrical power change as a function of current and voltage. The wheel speed is measured using a digital tachometer mounted at the back of the motor shaft. Thirty readings were taken for each of three wheel speeds. The standard deviations were found to be ±1.01 rpm at 1000 rpm, ±1.85 rpm at 2000 rpm, and ±2.63 rpm at 3000 rpm. Thus, speed readings are reliable.

3.5 Friction wheel characteristic

From the discussion in section 2.11, a smooth wheel and the two wheel designs shown in Figure 3.4 were tested. When wood was pressed against the smooth wheel, and thin char layer formed and no wear occurred. Wheel (a) was knurled and produced smoke, whereas wheel (b) produced sawdust with smoke formation. Of these, wheel (a) had less grinding and had a more continuous surface contact with the wood. Clearly, the characteristics of the wheel surface are important to smoke generation. Here, the objective was to find a satisfactory wheel for smoke generation, rather than to optimise the surface characteristics. This is an area requiring further study.

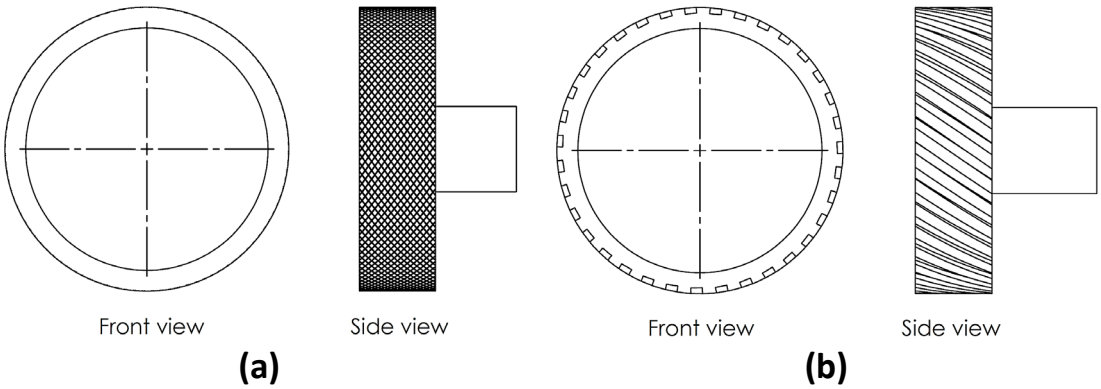

Figure 3.4: Friction wheel design patterns: (a) cross-knurling (R_s=200 µm), (b) grooved (60° slot angle).

3.6 Closure

This section details the design concepts and working principles of the lab-scale friction smoke generator where it has been advanced on that previously reported. It then discusses on the system control and measurement. Chapter 4 goes on to discuss the experimental design.

Chapter 4 Experimental Approach

4.1 Introduction

The research was divided into two phases to compare smoke generation from pure frictional heating versus using an external heating aid and frictional heating. The mechanical power input at the frictional interface was used to determine the coefficient of friction (CoF) which was related to the manipulated variables of wheel speed, pushing force and chamber set-point temperature, and the smoke produced was collected onto an absorbent for analysis in the GC-MS. This section details these experiments.

4.2 Coefficient of friction experiment

The coefficient of friction is the ratio between the shear force and the normal pushing force of the wood against the spinning wheel. It is a good indicator of the change in material properties of the wood.

The CoF is determined from change in mechanical power from the free load condition which, in turn, is determined from the change in input power as a function of current and voltage of 3-phase balanced motor (3Ø), using general assumptions about the conversion between electrical and mechanical power. This is detailed in the remainder of this section.

The electrical power supplied to the motor, measured after the VSD (see Figure 3.2), is the product of current, voltage and power factor. Both current and voltage depend on the onset frequency which controls the set point speed, n_S [rpm] as shown in Figure 4.1. In the operating range, > 2500 rpm, the current for the no-load condition is constant. The voltage is a power function of set point speed. When load is applied, the voltage to frequency ratio (i.e. 240 V/60 Hz) is independent of the motor load. With increasing load, the current draw then increases to provide the required torque to overcome the load (Spitzer, 2012). Electrical power supplied in excess of the no-load condition is converted to mechanical power to overcome the load, with an efficiency loss, typically 80.5% for this size of induction motor at rated conditions (CGGlobal, 2018).

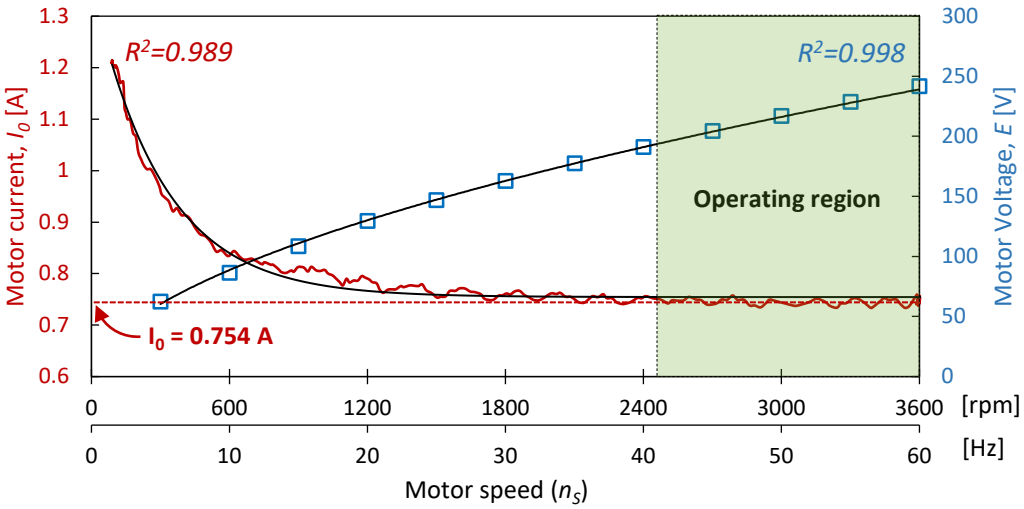

Figure 4.1: The change in VSD voltage and current as a function of the motor speed at free load. Here the axis in [Hz] is suitable for setting the motor speed using a VSD module.

At no-load conditions, the mathematical expressions for voltage and current are given as a function of n_S in [rpm] by equations (4.1) and (4.2):

$$E = 2.5659\, {n_S}^{0.5538} \tag{4.1}$$

$$I_0 = 0.606 \exp(-0.003\, n_S) + 0.754 \tag{4.2}$$

Equation (4.2) reduces to I_0 = 0.754 [A] when the motor speed is within the operating range, 2500 – 3500 [rpm]. In order to accurately estimate the real power consumption by the motor, the effects of capacitance and inductance on current need to be considered. These result in a phase shift between current and voltage, which is accounted for by the power factor which is plotted in Figure 4.2 as a function of the motor load capacity, determined from a standardised datasheet for a 750 [W] motor (CGGlobal, 2018).

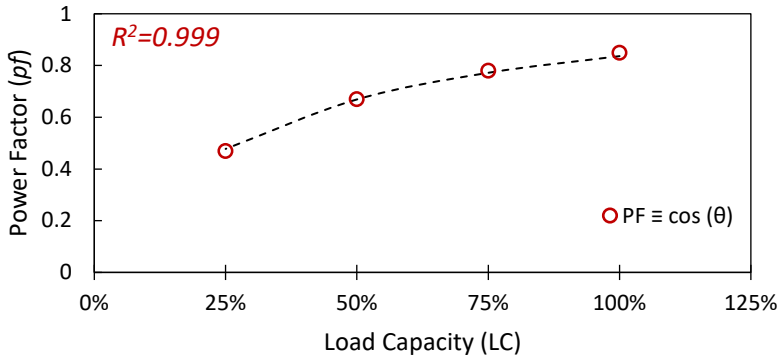

Figure 4.2: Power factor as a function load for 750 W - 3ϕ induction motor (CGGlobal, 2018)

The load capacity is the ratio of the consumed power to the rated power of the motor shown in Eq. (4.3). The relationship between the load capacity and power factor is then given by Eq. (4.4).

$$LC = \frac{E\ I}{E_r\ I_r} \tag{4.3}$$

$$p_f = 1.12\left(\frac{LC}{LC + 0.334}\right) \tag{4.4}$$

At no load, the motor runs at approximately synchronous speed and generates no mechanical power. When load is applied, the excess electrical power, $P_{excess\ elec}$, is converted to mechanical power to overcome friction, with losses which are accounted for by the efficiency, η.

$$P_{mech} = \eta\ P_{excess\ elec} = \eta\ E(I - I_0)p_f \tag{4.5}$$

Without more accurate data, the abovementioned typical motor efficiency is assumed, 80.5%. The mechanical power is assumed to be the brake friction heat loss.

$$P_{mech} = \tau\omega = F_\tau\ r_{wheel}\ n\left(\frac{2\pi}{60}\right) \tag{4.6}$$

The coefficient of friction relates the pressing (normal) force to the resisting shear force F_τ at the sliding interface.

$$\mu = \frac{F_\tau}{F_N} \tag{4.7}$$

Substituting terms gives the coefficient of friction, μ as a function of the excess power draw,

$$\mu(t) = \frac{60\ \eta\ E\ (I - I_0)\ p_f}{F_N\ r_{wheel}\ 2\ \pi\ n} \tag{4.8}$$

where the term, $I - I_0$, represents the power draw excess to the no-load condition.

The CoF is determined with time for all experiments.

4.3 Smouldering limits without supplementary heating experiments

When wood is pressed against the spinning wheel, shown in Figure 3.1, friction alone can generate enough heat to start smouldering. This was investigated for the following wheel speeds, n (2500, 3000 and 3500 rpm) and applied forces, F_N (29.4, 49.1 and 68.7 N). The range of forces selected was based on screening experiments to determine the conditions where smouldering will occur (see Appendix A.2). The speeds were chosen to be in the operating range shown in Figure 4.1 which are close to the rated speed of the motor where speed does not influence the current draw at no load. Practically, this is also the zone which

maintains the motor lifespan. Experiments were conducted with the chamber door open in order to record the apparent interface temperature, T_f between the wood and the frictional wheel, as shown in Figure 4.3:

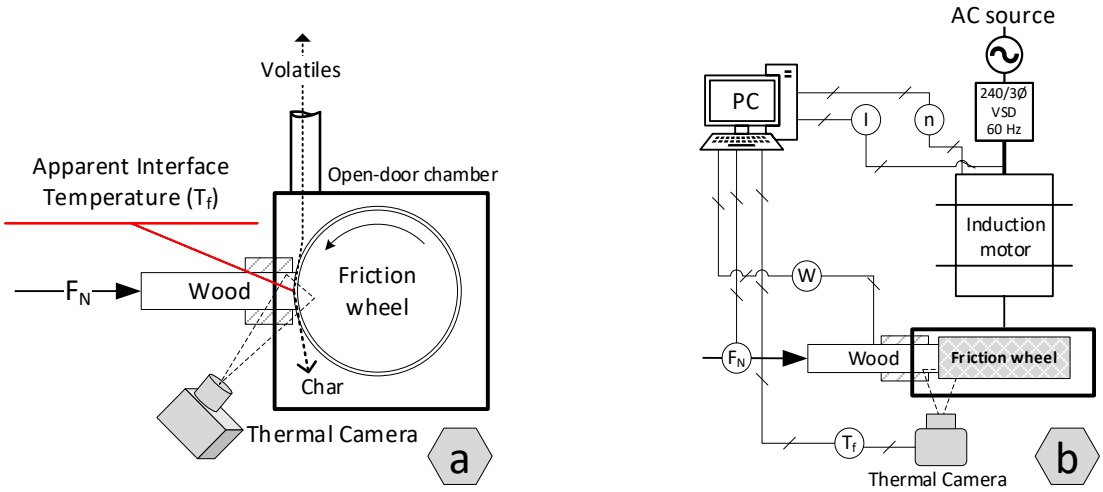

Figure 4.3: Frictional heating experiment set up (a) front view, (b) instrumentation setup, where I is the measured current drawn by the motor (A) and w, is the measured wear of wood (mm), subject to a set-point speed, n (rpm) and pushing force F_N (N).

The temperature measured by the thermal camera is an apparent value and may not be the real interface temperature; instead, it measures the edge of the wood in contact with the wheel, which gives a close estimate to the real interface temperature.

The wood planks were checked for any surface cracks or lateral bends. Nevertheless, sample-to-sample variation was inevitable. Between runs, the wheel surface was cleaned by placing it in a muffle furnace at 600°C for 5 minutes to remove solidified tar residue. This temperature was found effective based on practice, to burn the tar layer without causing excessive thermal expansion to the wheel. This practice ensured each trial began with the same starting conditions.

The following materials were used:

1. Manuka wood (12×12×150 mm ±0.23 mm) air dried, MC ~11%
2. Carbon steel wheel (R_s=200 µm)
3. Thermal camera, T_f (FLIR – E60)
4. 750 W 3-phase (3Φ) induction motor

(Brand: Global Green, Frame: G-GA80ME, 2-poles, rated voltage (E_r): 240 V, rated current (I_r): 2.67 A)

4.4 Smouldering limits with supplementary heating

The second phase of experimentation used a heating element to maintain the rotating wheel at the following temperatures (100, 150, 200 ˚C). Experiments were then carried out varying the force at a constant wheel speed of 3000 rpm.

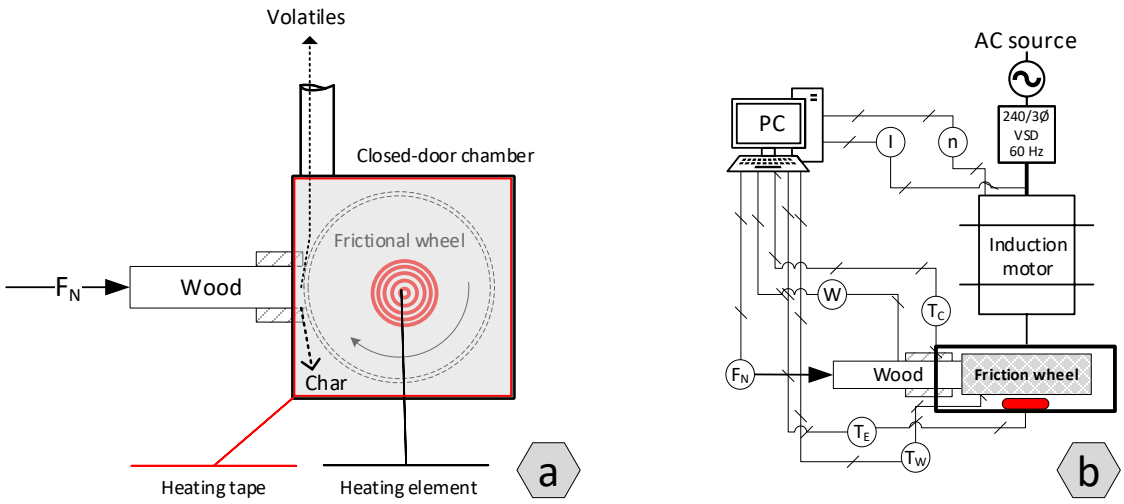

Figure 4.4: Frictional heating with external heating aid experiment set up (a) front view, (b) instrumentation setup, where thermocouples record the heating element temperature, T_E, the chamber temperature, T_C, and the wood temperature 5 mm from the contact, T_W.

Three thermocouples were used. The heating element had a thermocouple mounted nearby within the cylindrical core of the wheel, T_E. The chamber had a thermocouple mounted away from the frictional contact zone, T_C. A third thermocouple was situated in a groove machined into the bottom face of the mānuka plank, which was positioned so that it was 5 mm from the frictional contact, T_W. The thermocouples were all type-K.

4.5 Smoke collection – preliminary experimental design

Smoke was collected from the two phases of the experiment, without and with supplementary heating. Each was a simple factorial design of low-mid-high as shown in Figure 4.5. However, some experiments have two collections, which was carried out because these experiments exhibited two distinctive wear rates. Experiments were not repeated because the twister bars are relatively expensive and required extensive cleaning between uses. Therefore, statistics on the factorial results were not able to be carried out. The work was also carried out right at the end of the project.

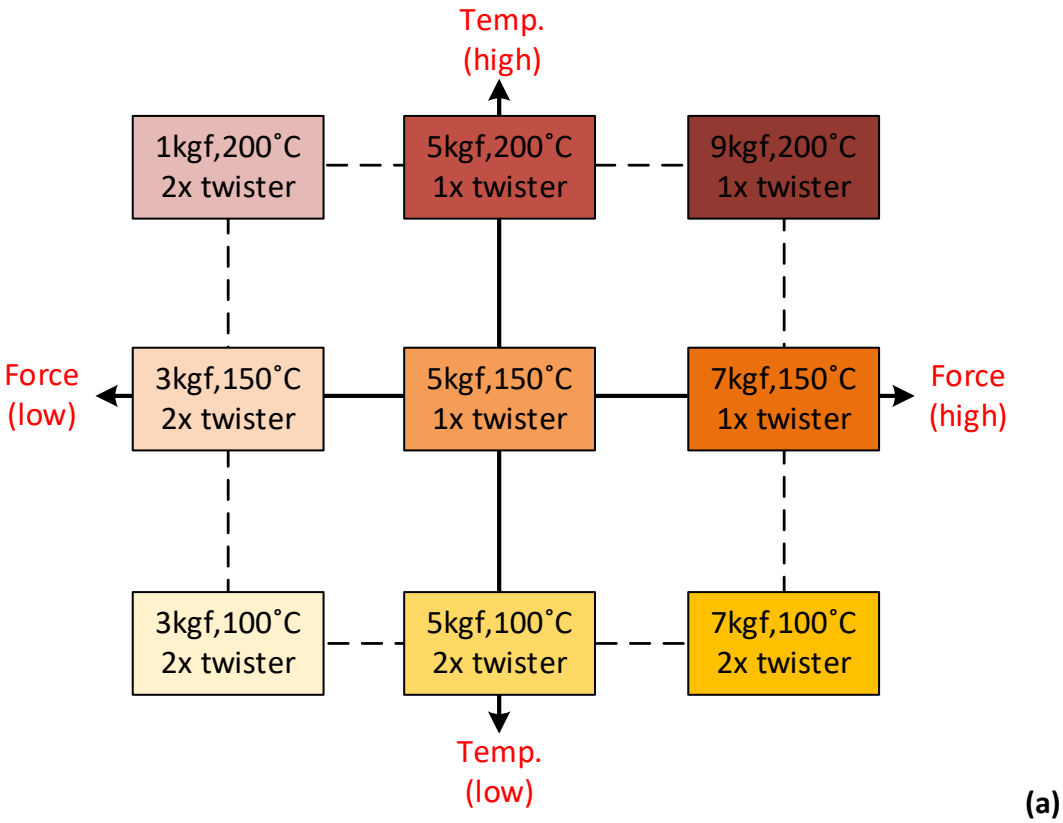

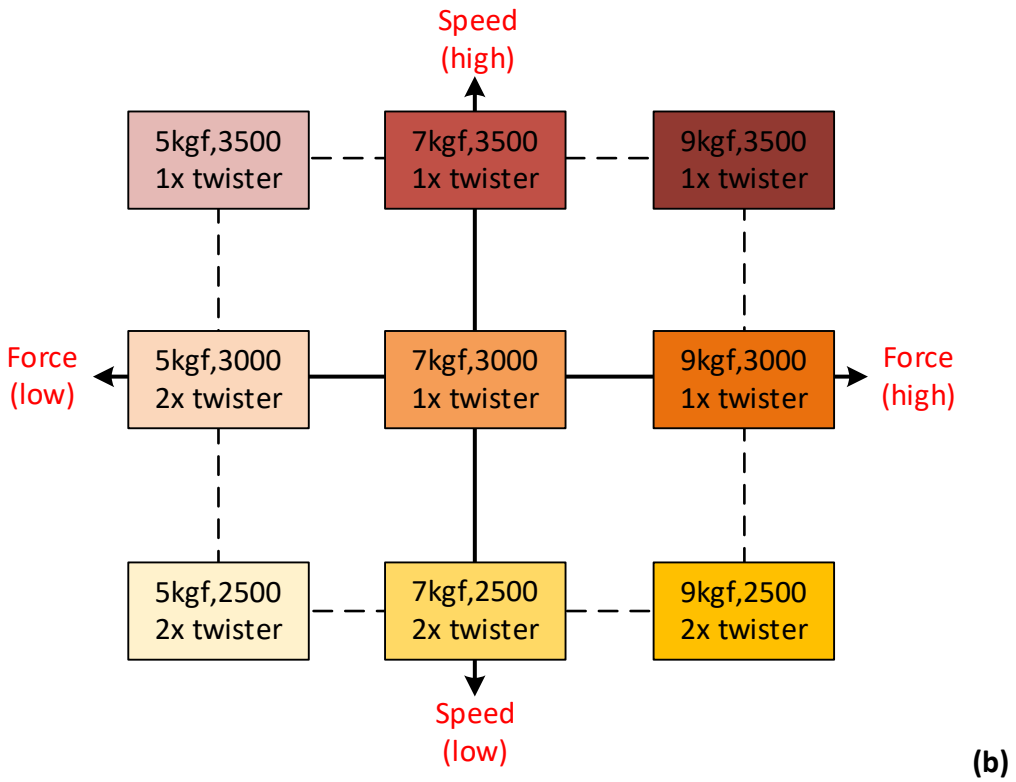

Figure 4.5: Smoke collecting strategy, (a) temperature vs force @ 3000 rpm (b) speed vs force @ ambient temperature.

The smoke was collected on a twister bar (aka magnetic stir bar) (GERSTEL, 2017) encased in glass coated with polydimethylsiloxane (PDMS) as an adsorbent. Figure 4.6 shows the experimental setup. Each PDMS stir bar requires careful handling to prevent it from damage and contamination. The handling procedure is provided in Appendix B.1. The collected smoke was sent to the University of Otago for GC analysis which requires sophisticated technical expertise. This analysis was conducted by Yuanyang Zhang, Dr Graham Eyres and Dr Pat Silcock.

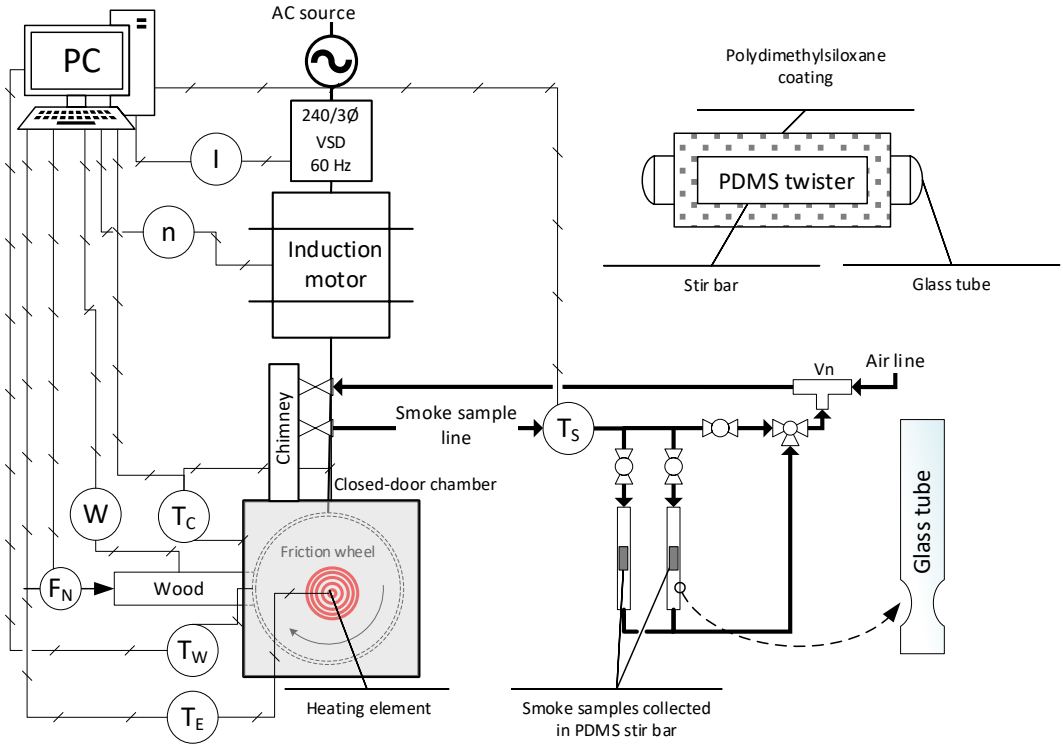

Figure 4.6: Experimental setup and instrumentation for smoke sampling.

4.6 Closure

The experimental details in this section were designed to investigate smoking with and without external heating, followed by a preliminary experimental design to collect smoke samples for composition analysis. The results of the presented experiments are discussed in Chapter 5.

Chapter 5 Results and Discussion

5.1 Introduction

This chapter presents the results of the frictional experiments, examining the onset of smouldering and the transition between steady state behaviours as the pushing force is sustained. It also presents a preliminary investigation of the smoke composition at different smoke generation conditions. A total mass balance on the system was attempted but proved elusive. This was because the friction wheel both heats and causes ablation. Thus, some char gather as particulates in the bottom of the chamber. Then, because the rotation of the wheel effectively pumps air out of the chamber, it also draws air in around the small gap between the housing and the wood plank. The char then oxidises. Therefore, it is difficult to account for the char. Furthermore, decomposition produces tar, some of which bakes onto the wheel, some condenses into the ablated char and the remainder either fouls the walls of the chamber and chimney or leaves the system as a part of the smoke. Some char may also leave this way. Therefore, a mass balance was not obtained. Indeed, proximate analysis of the char residue in the smoking chamber clearly showed secondary oxidation. Therefore, results are discussed in terms of the dynamics and kinetics of pyrolysis rather than mass balance. Several insights are obtained. To begin, however, the limitations of the system to the friction study are discussed.

5.2 System limitations

The power used to overcome friction is assumed to dissipate as heat during pyrolysis. The other mechanism, of softening and grinding, which creates new surface area, is more applicable to wood pulping refining at lower temperatures than pyrolysis. Thus, in a heat flow balance, the mechanical power supplied by the motor is converted to heat at the interface, which goes to both heat the wood and drive endothermic reactions. A complicating factor is whether or not exothermic reactions occur, in which case heat is also generated at the frictional interface. Further complicating things is the dissipation beyond the frictional interface. Understanding this is important, because the measured variable of chamber temperature is an average, reflecting the dynamic response of the system to the overall heat flow.

It is reasonable to assume that all heat, additional to the environmental conditions within the chamber, must be generated at the interface, including heat absorbed by endothermic reactions or generated by exothermic reactions. Subsequent heat flows from the frictional interface in three directions, into the steel wheel, into the wood, and tangentially away with

the wear residue (char, tar, tarry volatiles and gases). Of interest to the system limitations, is the heat that flows into the steel wheel. It conducts from the outer rim into the central disc and along the shaft, following the thermal gradient. Simultaneously, some of this heat is dissipated by convection into the cooler surroundings of the chamber, or to the air that surrounds the shaft. The heat that traverses the shaft will dissipate into the electrical rotor windings of the motor. A schematic is shown in Figure 5.1. Therefore, an important factor that could alter the current measurements is the operating temperature of the motor, which is rated at ≤45 ˚C. In general, induction motors are designed with built-in fans to prevent the stator from overheating. The question then is 'Does the heat flow cause a change in motor performance?' A thermal effect would increase the temperature of the rotor coils which would increase their electrical resistance, and so manifest itself as an increase in motor current to deliver the same mechanical power (per Section 2.12).

Figure 5.2 addresses this for a light pressing force of 9.81 N when the chamber set-point temperature is either ambient, 100, 150 or 200°C; experiments were heated for ~10 min to stabilise at the set points. All trials begin with the same current flow, which indicates that none of the set-point temperatures electrically affect the motor to this point. After the wood was pressed against the spinning wheel, shown in the figure, the expected response is a slight increase in the chamber temperature after which the motor current should remain constant. This is the response for the lower three set-point temperatures, but not for the 200°C temperature. It starts with the same current flow, but after ~20 s, the motor current rises, then maintains a steady value between 2.0 – 2.2A, then after ~150 s, it falls to a lower steady value between 1.4 – 1.6 A, which it maintains until the end of the measurement. The principal difference here is that the 200°C trial exhibited smouldering and wear, whereas the lower temperatures did not. While the two changes in motor current are relatable to the properties of the wood undergoing pyrolysis (discussed in Section 5.5), the lack of any drift is the important result. Thus, it can be concluded that thermal effects do not influence the current readings for the duration of the trials conducted in this work.

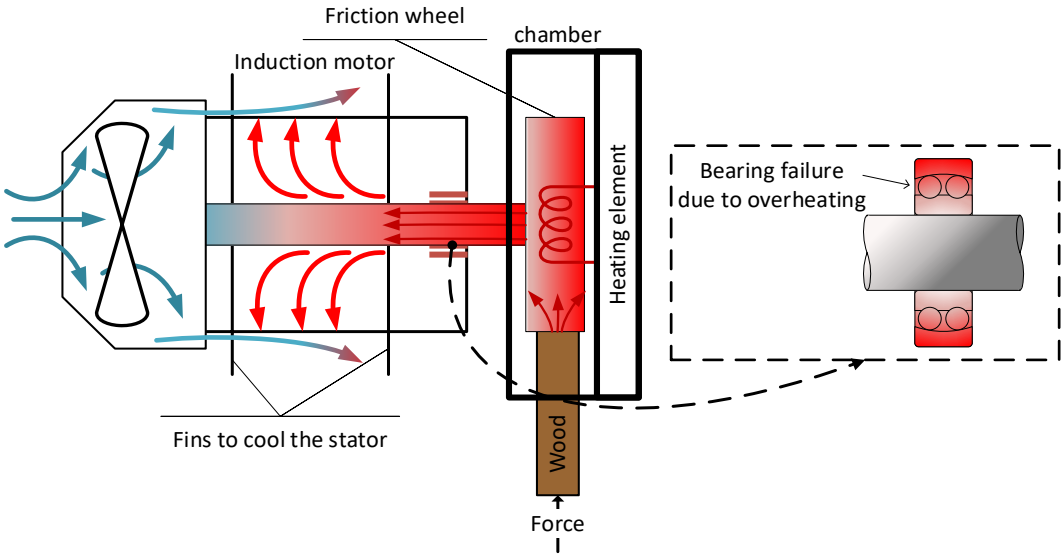

Figure 5.1: Schematic of the heat flow (→) that causes overheating to the front bearing. The fan is designed to cool the outer surface of the motor to maintain the stator operating temperature.
Picture of the induction motor parts is shown in (Appendix B.5).

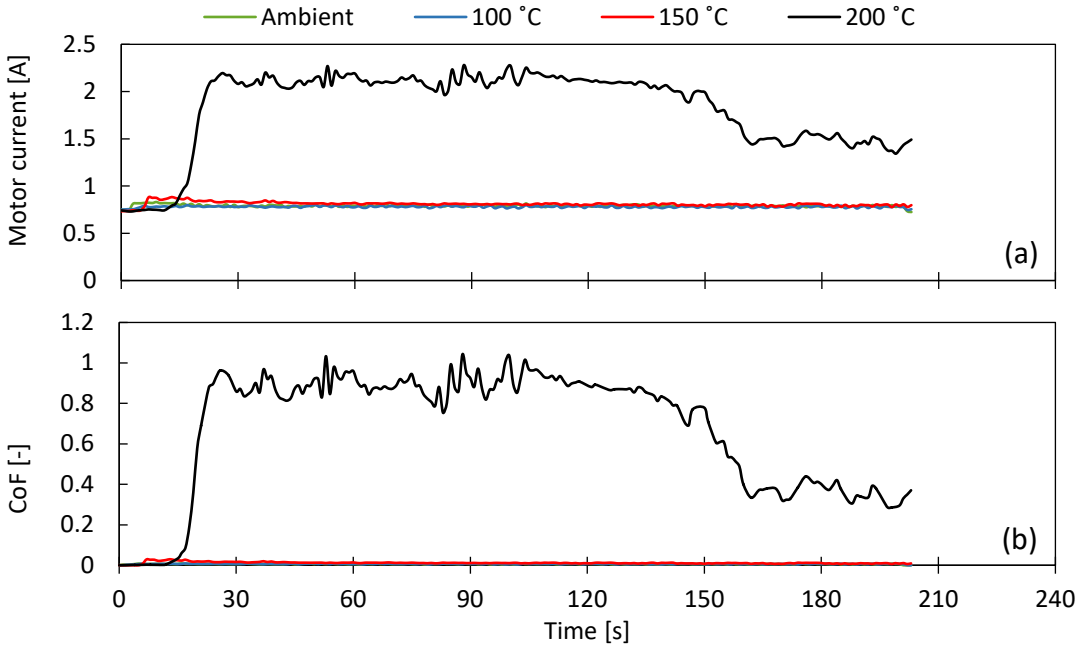

Figure 5.2: **(a)** The influence of temperature on motor current; **(b)** the influence of current on COF.
Conditions at 9.81 N pressing force and 3000 rpm wheel speed

A second limitation to consider is the upper limits of the pressing force and wheel speed before they overload the motor. Figure 5.3 shows the current consumption for various pressing forces in an ambient environment, for various speeds. It shows that the rated current is exceeded only when the lowest wheel speed, 1000 rpm, is used and at the higher pressing forces. This low speed did not result in smouldering of the wood at ambient conditions, which occurred for the higher wheel speeds: smouldering results in lower current because the frictional resistance is reduced. The experimental range of wheel

speeds was set to 2500 – 3500 rpm with pressing forces up to 70 N. At these conditions the motor did not become overloaded.

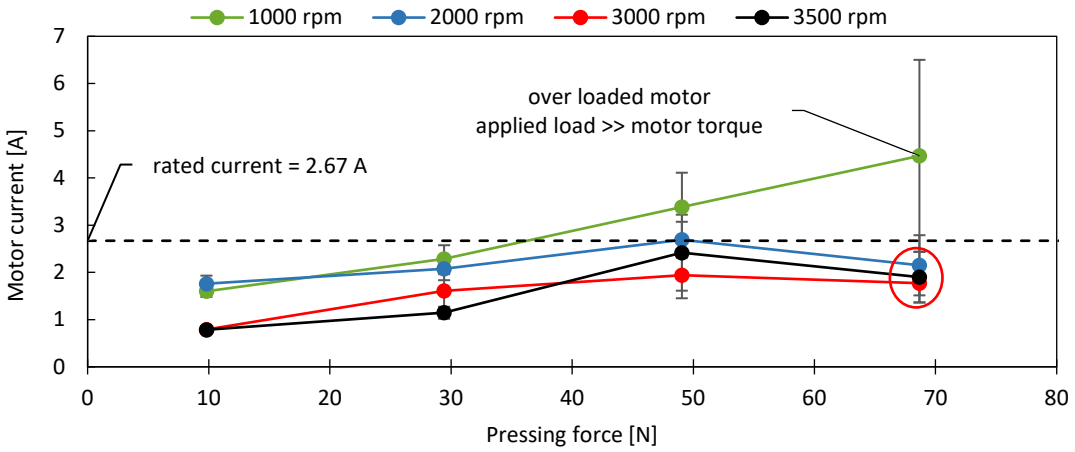

Figure 5.3: The effect of pressing force on current consumption for different speeds at ambient conditions. (◯) indicates the drop in current due to the lubrication at the interface by wood (*not necessary smouldering*)

A third limitation to consider is overheating of the ball bearings. According to Karmakar *et al.* (2016), overheating can cause ball bearing failures in induction motors, due to degradation of the lubricant around the ball bearings. Most ball bearing units are designed to withstand temperatures between – 20 to 100 ˚C (IEC standards). Here, in Figure 5.3 at 200 °C, the CoF is close to 1 and the motor made an abnormal rubbing noise during and after releasing the load. Thus, this indicates a significant combined effect of the thermal stress conducted through the shaft into the bearing and the eccentric mechanical load of the pressing force.

To further explore the thermal effect on the bearings, a transient thermal analysis on conduction along the shaft is shown in Figure 5.4. This was done in SolidWorks, with a number of simplifying assumptions, given in Table 5.1below. Figure 5.4 shows that as the temperature increases the bearing temperature increases dangerously beyond its normal operating range. The result highlights the importance of selecting bearings suitable to the conditions, or designing the system to avoid the problem.

Table 5.1: Assumptions used in the transient thermal analysis of heat flow from a hot friction wheel into and along a motor shaft.

Assumption	**Value**
The wheel temperature is constant at the set-point temperature	200 °C
Initially, the shaft temperature equals the ambient temperature	20 °C
Constant thermophysical properties	
Wheel and shaft made cold rolled steel	λ_s=51.9 W m^{-1} K^{-1}
Ball bearing made of chrome steel	λ_b=18 W m^{-1} K^{-1}
Estimated forced convection heat transfer coefficient for the motor fan cooling acting on the tail of the shaft and the outer case of the motor	h_F= 10 W m^{-2} K^{-1}
The air gap between the shaft and stator has a heat transfer coefficient at 30 °C (motor interior temperature is higher)	h_a=0.2 W m^{-2} K^{-1}
Radiation from the chamber back wall to the motor face is negligible	

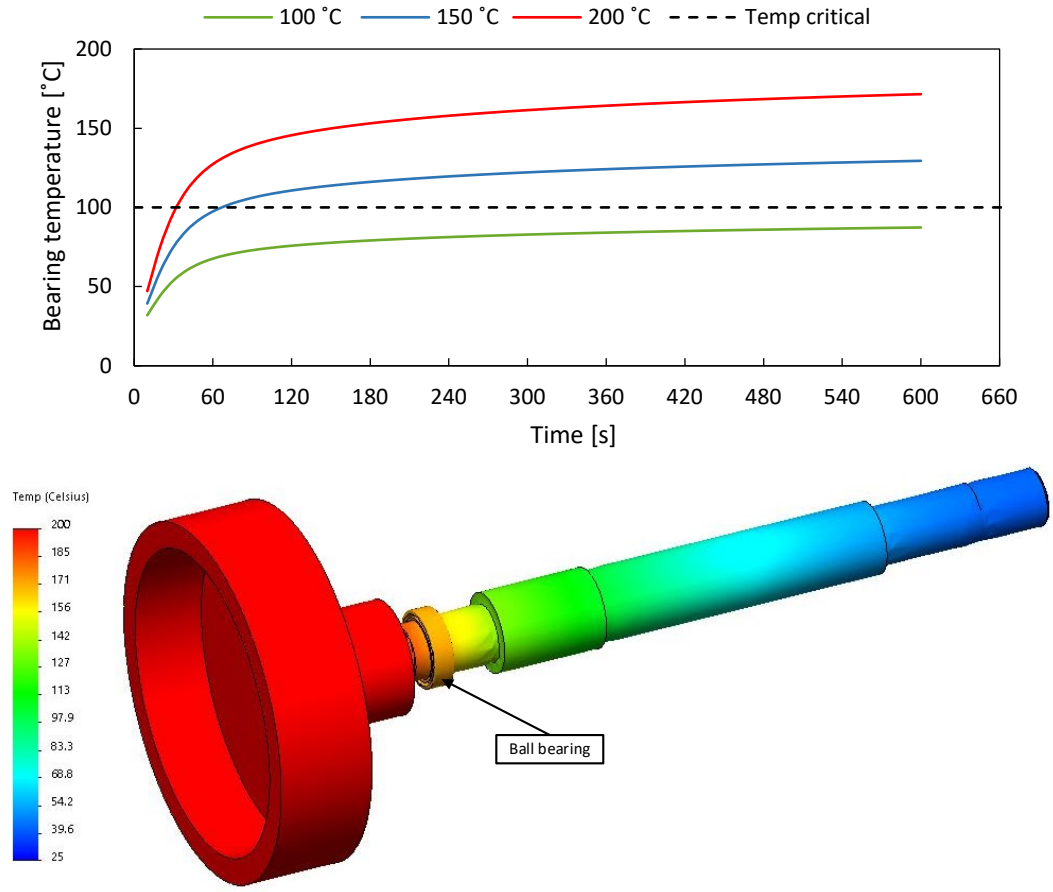

Figure 5.4: The ball bearing temperature profile for various temperatures (top). Heat conduction profile through the shaft at 200 °C after 600 s (bottom).

5.3 Smouldering limits without supplementary heating

This section details experiments conducted with the door open and without additional heating (see Figure 4.3). The temperatures were recorded using a thermal camera directed at the side view of the interface between the wood and the spinning wheel. The experimental results for the nine runs are presented in Figure 5.5, which are sorted according to their applied normal force. The forces (i.e. 29.4, 49.1 and 68.7 N) are referred to as low, middle and high, respectively.

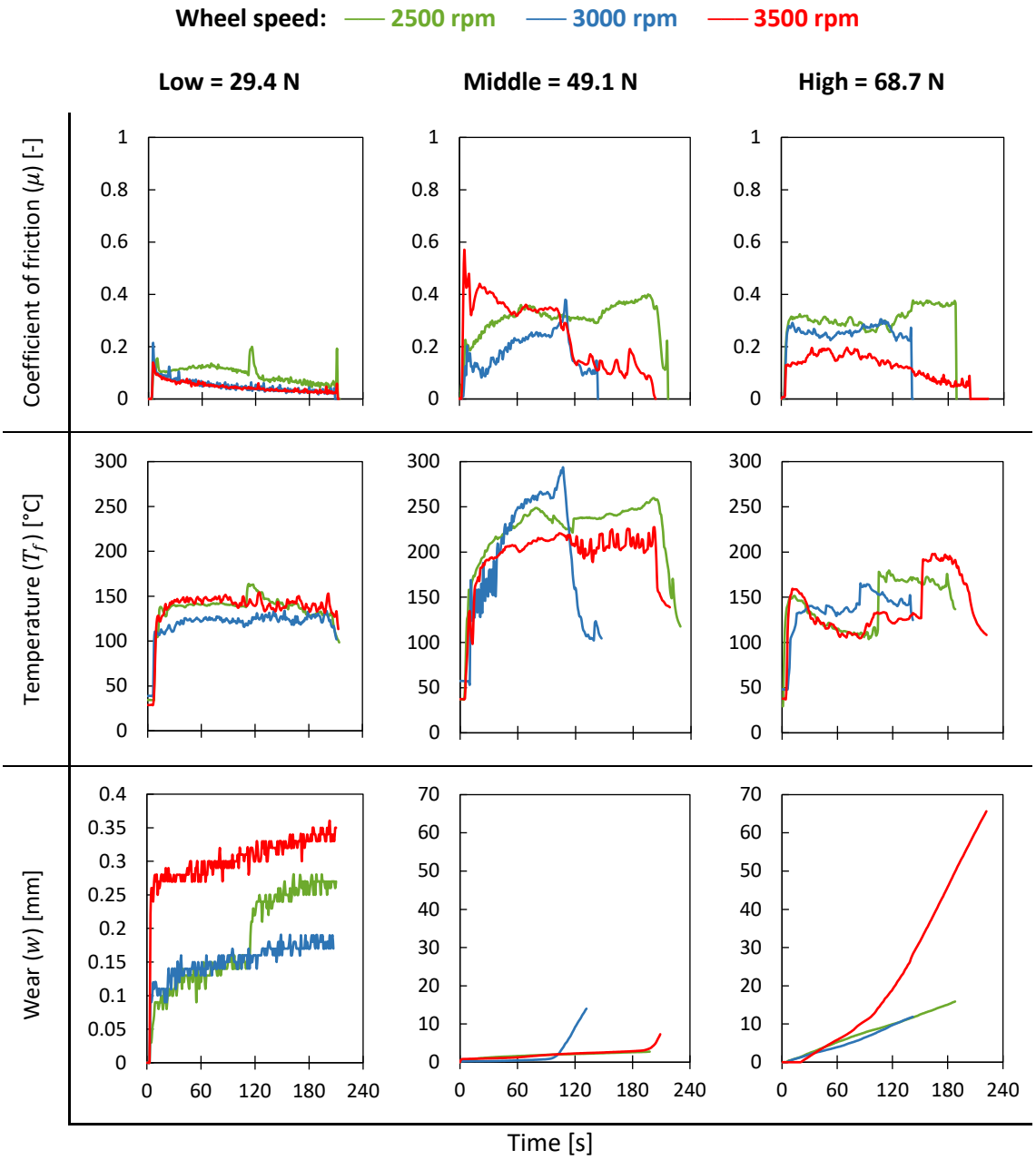

Figure 5.5: The variations in CoF, T_f and wear profiles of wood as a function of force and wheel speed.

The relationship between friction and smouldering is complicated. The lowest pressing force (29.4 N) has the least friction and almost non-existent wear for all wheel speeds. At these conditions, smouldering was not observed. Therefore, it can be concluded that the interface temperature, measured between 120 – 150 °C, was insufficient for pyrolysis to occur and that the frictional heat is dissipated into the surroundings.

Both the middle (49.1 N) and high (68.7 N) forces exhibited smouldering, where its onset is associated with a dramatic increase in wear rate ($\dot{w}$) and a reduction in coefficient of friction and a drop in temperature for the middle force. For the middle force, the 2500 rpm wheel speed did not promote smouldering, and so the wear rate was minimal. However, the 3000 and 3500 rpm speeds did promote smouldering after ~200 then ~75 seconds, respectively (Figure 5.6). The onset of smouldering was even faster for the highest force, occurring after ~23 seconds at 2500 rpm speed and almost instantaneously for the higher speeds.

After the onset of smouldering, the wear rates for the middle force were 0.4 – 0.55 mm s^{-1}. For the high force, the wear rates were lower at 0.1 – 0.15 mm s^{-1} until the 3500 rpm trial exhibited a runaway wear rate, increasing from ~90 seconds, and stabilising at ~0.45 mm s^{-1}, which is similar to the wear rates of the middle force trials at 3000 and 3500 rpm. The reason for this runaway is unknown. It could be due to the biological nature of wood, which varies, or it could be due to a transition in reaction kinetics, or due to a transition in the friction properties of the wear material.

The interface temperatures were higher for the middle force than the high force, reaching ~300 °C. However, it must be noted that these temperatures are indicative because the thermal imaging camera could only observe (in side-view) the temperature at the outer edge of the interface. Readings will depend on the local friction and on whether pyrolysis oils are present, and how they got there, and whether they accumulate here.

No damping mechanism was used when pushing the wood against the wheel, and so the wood plank sometimes vibrated in the sheath, which caused the apparent noise in some of the wear rate and temperature results. Also of interest, but unexplained, is the periodicity, ~20 seconds, that appears across many of the plots.

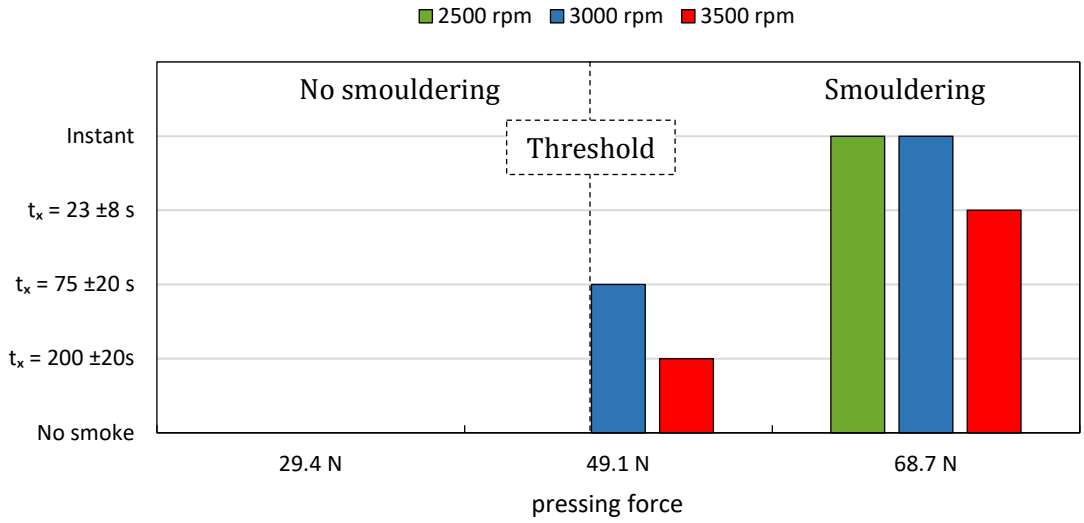

Figure 5.6: Onset volatilisation time (t_x) boundaries as a function of force and wheel speed. Volatilisation is the heavy intense smoke released by friction which indicates the start of the smouldering process.

5.4 Smouldering limits with supplementary heating

Supplementary heating was supplied by a heater to attain steady chamber temperatures of 100°C, 150°C and 200°C before the wood was pressed against the spinning wheel (per the method in Section 4.4). The experimental results for the 12 runs are presented in Figure 5.7, which are sorted according to their applied normal force. The forces (i.e. 9.8, 29.4, 49.1 and 68.7 N) are referred to as very low, low, middle and high, respectively. Wheel speed was fixed at 3000 rpm. Because the door was closed in these experiments (see Figure 4.4), it was difficult to measure the contact temperature between the wheel and the wood. Therefore, the wheel temperature is inferred from the heating element (T_E) and chamber (T_C) temperatures [˚C], where the heating element temperature is measured close to the inner rotating rim of the wheel. It is referred to as the average wheel temperature in the remainder of this discussion.

For all the results in Figure 5.7, the onset of smouldering is highly dependent on the wheel temperature (T_E). Only the lowest force (9.8 N) shows no wear or any sign of smouldering at wheel temperatures 100 and 150 ˚C and is accompanied by very low CoFs. This indicates that the friction was wood against metal and did not generate enough heat to initiate pyrolysis.

At 200°C and 9.8 N and for all other pressing forces, smouldering and wear occurred. Three interesting features can be seen in the wear plots; (i), wear appears to transition from a lower to a higher wear rate; (ii), the transition occurs more quickly for higher pressing forces and higher temperatures; and (iii), the higher wear rate (the slope in Figure 5.7) is

faster for higher pressing forces and higher temperatures. Effects (ii) and (iii) are shown in Figures 5.9 and 5.9. Both pressing force and temperature have a marked effect on transition time, which occurs instantaneously when the set-point temperature is 200°C for forces above 9.8 N. Effect (iii) appears to depend only on pressing force for set-points of 100°C and 150°C, but then appears independent of pressing force at a set-point of 200°C. Interestingly, the smoke density and smell intensity increased when the wear rate transitioned, which indicated a transition in reaction dynamics. Later, it will be explored whether this is a change from an endothermic to exothermic reaction.

The measured temperature (T_E), shown in Figure 5.7, rises in all cases where smouldering occurs when the set point is 100°C or 150°C. Very little, if any, temperature rise is observed when the set-point is 200°C.

The coefficient of friction, shown in Figure 5.7, is indicative of the mechanical power, additional to the free load condition, needed to maintain the wheel spinning when the wood is pressed against it. All results have periodicity of ~20 Hz, likely to relate to the vibration of the wood when pressed against the wheel, but otherwise not explored. Four trends can be seen; (i), the CoF transitions from a high value to a low value; (ii), the transitions occur at the same aforementioned wear rate transitions; (iii), before the transition, the CoF values are highest for the 200°C set point and lowest for the 100°C set point, but there is no apparent pattern with respect to the influence of pressing force; and (iv), after the transition, there is no apparent pattern with respect to the influence of either temperature or pressing force.

The mechanical power input is shown in Figure 5.10. Sharp decreases in power correspond to both the onset of smouldering and the lower-to-higher wear rate transition. This indicates a relationship between the magnitude of the mechanical power input and the start of the higher wear rate. For instantaneous smouldering at the higher wear rate, it appears that the minimum power requirement to promote the 2nd wear rate is ~700 W.

It is important to establish the role of the other heating elements in the controlled temperature set-point trials. In these the plane and tape elements were rated to 200 W and 600 W respectively. The fundamental control of the heating elements is ON/OFF control, the elements will always supply 800 watts in total to reach any set point temperature. However, the temperature gain is rather dictated by the oscillation rate between when the elements are ON or OFF (i.e. PWM control), the state of which is determined by the difference between the setpoint temperature and a temperature signal received from a thermocouple connected to a PID controller (i.e., feed-back loop). The element will always

be OFF when the chamber temperature ≥ than the setpoint temperature. It turns out that in these experiments, the friction always causes heating of the chamber; thus, these supplementary heating elements are always OFF once friction trials start. Therefore, during trials, the only energy input is the mechanical energy to overcome friction between the wood and the wheel.

The results are now discussed relative to the conditions required for pyrolysis and the energy flows needed. Extenuating factors are also discussed.

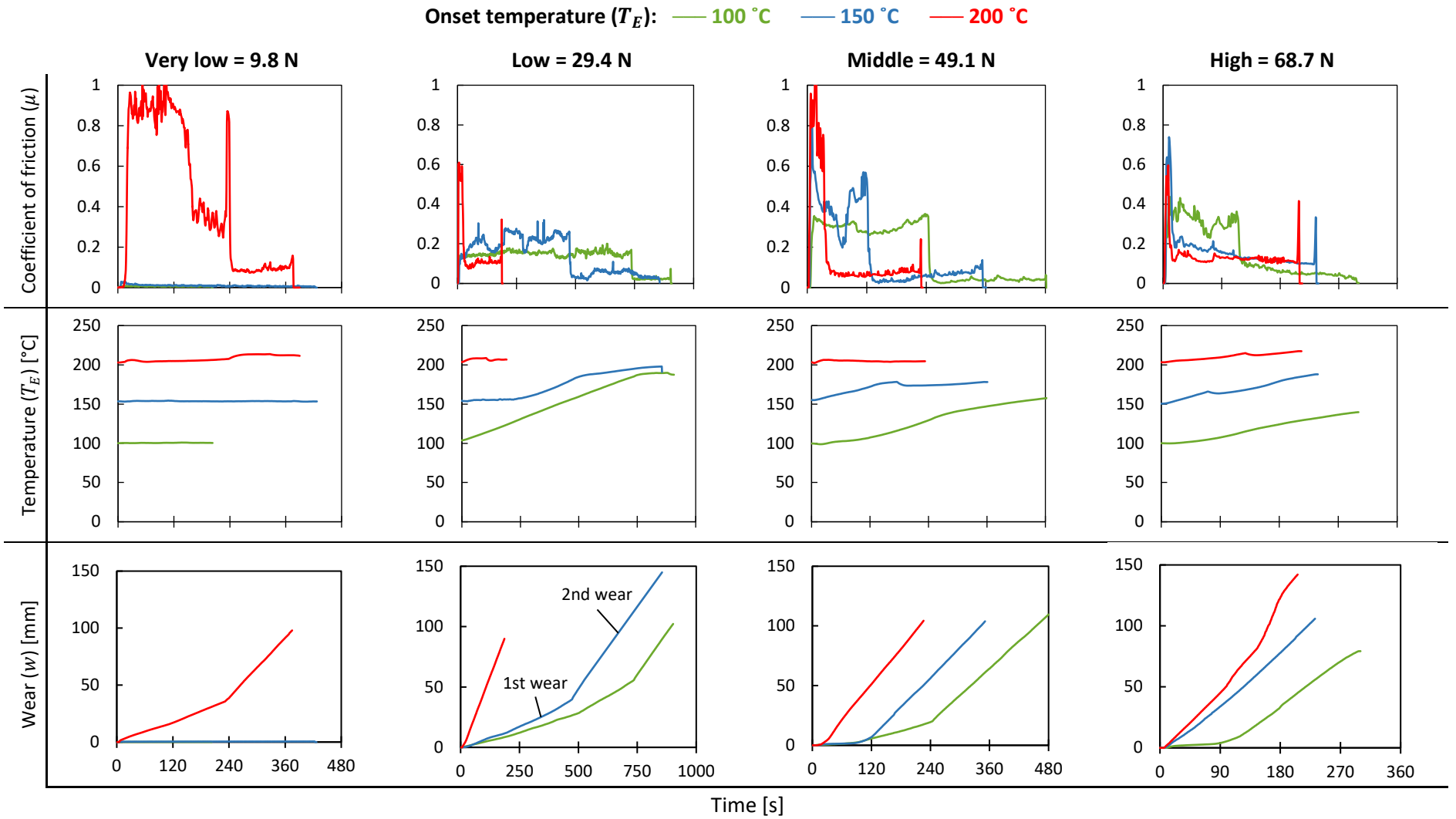

Figure 5.7: The influence of supplementary heat on CoF and wear of wood at wheel speed of 3000 rpm.

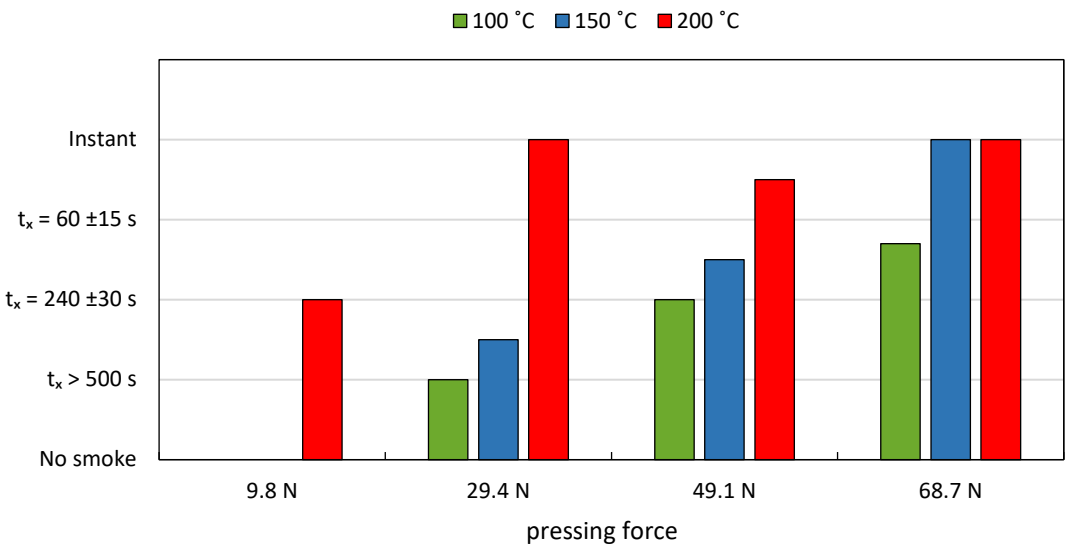

Figure 5.8: Onset volatilisation time (t_x) boundaries as a function of force and onset temperature at wheel speed of 3000 rpm. Volatilisation is the heavy intense smoke released by friction which indicates the start of the smouldering process.

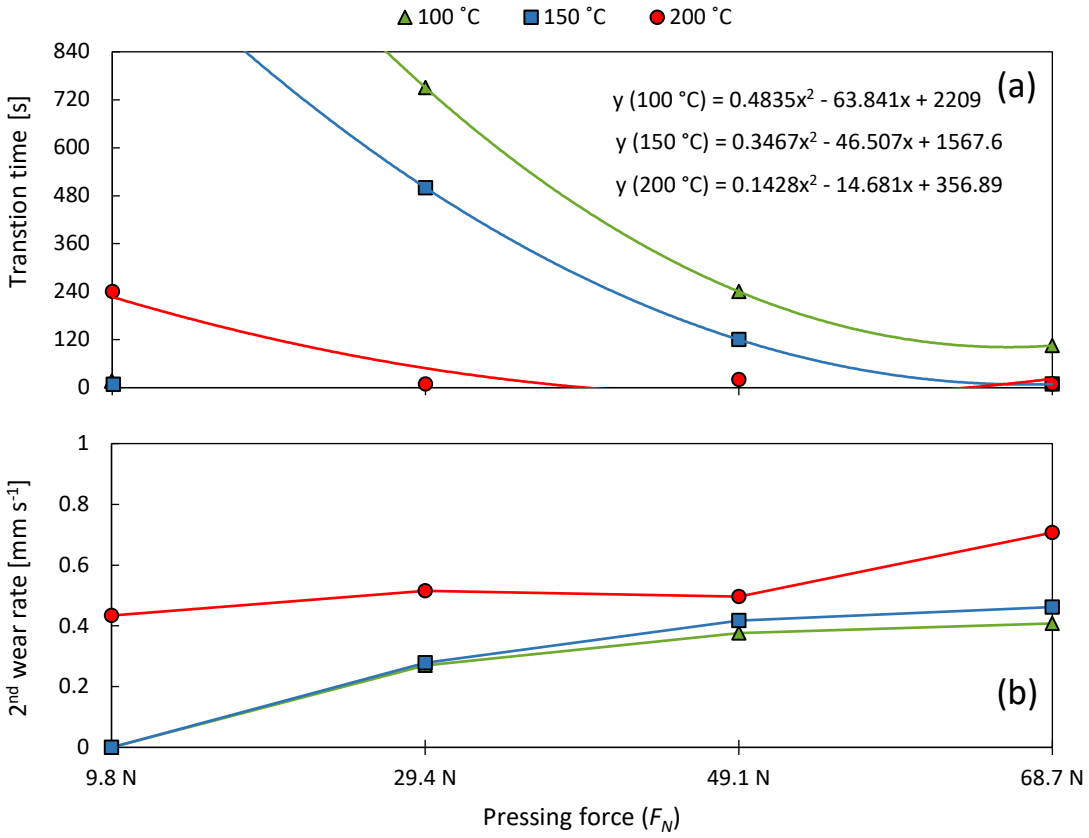

Figure 5.9: At 3000 rpm the effect of onset temperature (T_E) and pressing force (F_N) on:
(a) the transition time from 1st to 2nd wear rate ($t_{\dot{w}}$) [s] and **(b)** the magnitude of the 2nd wear rate ($\dot{w}^2$).
The results in (a) shows a trend that fits a quadratic form.

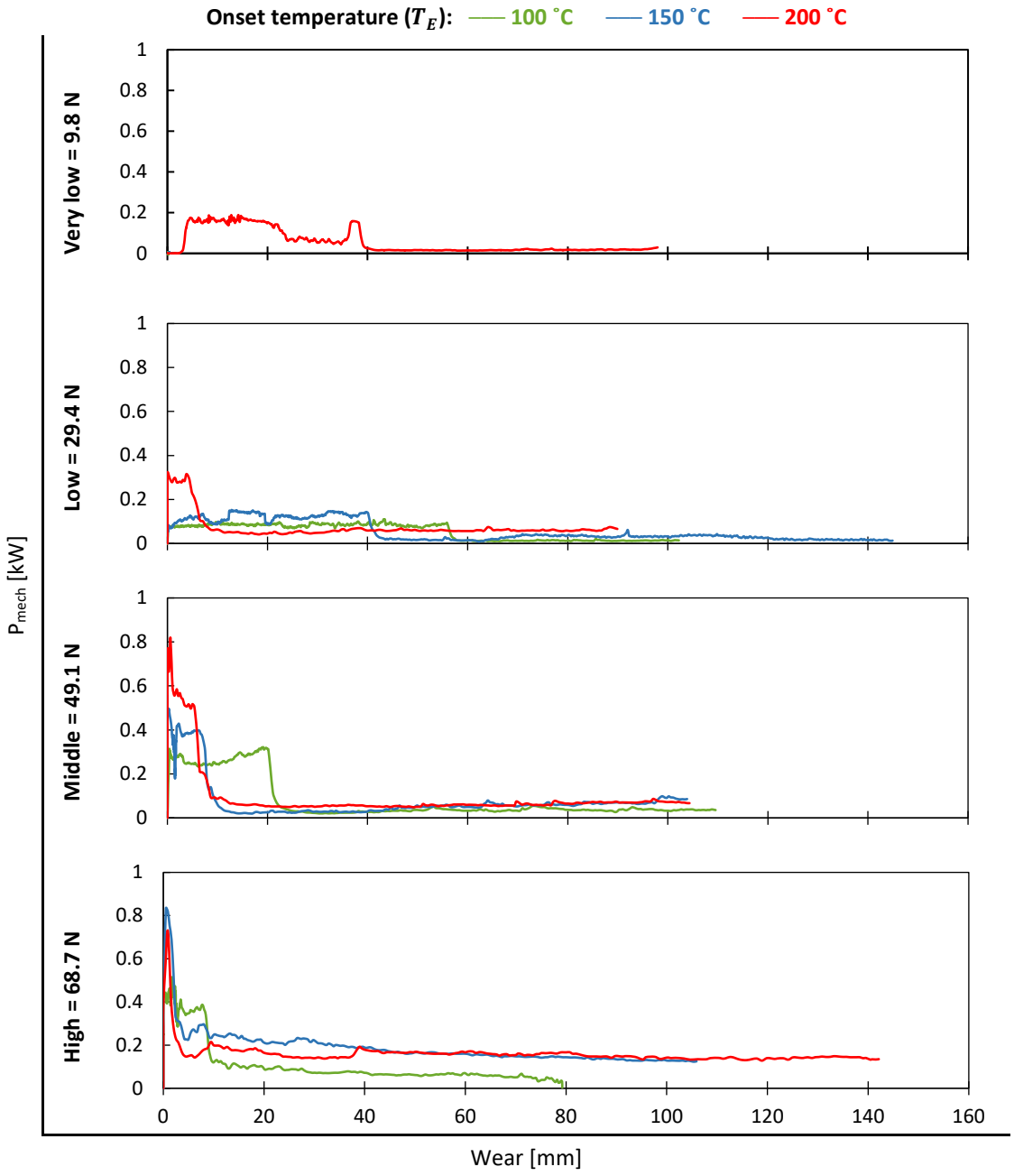

Figure 5.10: The mechanical power supplied for smouldering as a function of the amount of wear.

5.5 Discussion of friction results

It is important to determine whether the observed wear is due to pyrolysis, or whether it is mechanical refining of the wood. Smouldering occurs at the onset of pyrolysis between 250 – 300 °C when wood liquefies and volatilises. At this point, the sliding surface of the wheel removes the liquid and the gas from the pyrolysis zone. This wear is either by abrasion, cutting or viscous removal by the sliding surface (see Section 2.5). Abrasion or cutting are likely to be negligible, because the lowest force results do not show wear, which they would if the wheel surface asperities were sharp enough to cut the wood. Viscous shearing is more

likely, but may occur before pyrolysis starts if the frictional heating has softened the lignin, allowing the fibres to shear apart from one another. This mechanism is exploited in mechanical refining of pulp; if it were present here, smouldering would not occur, and the sheared wood would still appear brown in colour, rather than black as observed here. Therefore, wear can be attributed to pyrolysis.

It is also important to determine exactly where the pyrolysis occurs. Wood is a known insulator and so heat will not travel easily into the wood, which is made more difficult because the advancing wear front is in the opposite direction to heat transfer. Therefore, it is reasonable to assume that the frictional interface must be thin and must heat rapidly, raising its temperature from the ambient into the pyrolysis zone. In the limit, this thin zone is a plane.

The reaction kinetics of pyrolysis are complex and are best understood by the lumped models discussed in Section 2.9, using Arrhenius expressions. These show that the kinetics are temperature dependent. The balance between primary (endothermic) and secondary (exothermic) reactions depends also on the temperature. Therefore, the overall heat of reaction and whether the net effect is endothermic or exothermic will be dependent on the temperature attained at the frictional interface. In addition, secondary reactions are known to be enhanced where pressure is elevated (Mok *et al.*, 1983). If the force is distributed evenly across the 12×12 mm plank, the three forces correspond to pressures of 204, 340 and 477 kPa respectively, but this only applies if the interface contact is perfect or if it is filled with a liquid film.

Because the kinetics depend on the temperature attained, it is important to understand how heat accumulates at the frictional interface in the context of the observed results. Evidence of heat accumulation is in the two observations, of an onset time when pyrolysis and wear begin, and the later transition from a lower-to-higher wear rate. The open door experiments, at ambient temperature, had an onset from no wear to wear, but did not show a subsequent lower-to-higher transition in wear rate, except for the 68.7 N pressing force. This lag time to onset of pyrolysis indicated that it took some time for the frictional interface to reach a temperature sufficient for pyrolysis to begin. In the closed door experiments with supplementary heating, only the lowest pressing force, 9.8 N, at 100°C and 150°C, showed no wear at all. All other trials had almost instantaneous smouldering. Some trials did not exhibit a lower wear; instead, almost instantaneously starting at the higher wear rate. As indicated these were the trials with a mechanical power input of ~700 W. These observations support the above hypotheses that the frictional interface is a volume rather than a plane because it takes time to heat, and that the attainment of specific interfacial

temperatures are responsible for both the onset of wear and its transition from a lower to a higher wear rate.

In all experiments with a lag time before the onset of smouldering, the lag time decreases when the applied force increases and when the speed of the wheel is increased. The later transition time, from lower-to-higher wear rate ($t_{\dot{w}}$), has been more thoroughly studied. Transition times ($t_{\dot{w}}$) follow a trend when fitted to a quadratic of force (see Figure 5.9 a),

$$t_{\dot{w}} = a(T_E)\, F_N^2 - b(T_E)\, F_N + c(T_E) \tag{5.1}$$

with coefficients that are functions of the transition temperature, shown below and plotted in Figure 5.11.

$$\begin{bmatrix} a \\ b \\ c \end{bmatrix} = \begin{bmatrix} -0.0034\, T_E + 0.8354 \\ -0.4916\, T_E + 115.42 \\ -18.521\, T_E + 4156 \end{bmatrix} \tag{5.2}$$

The effect of temperature becomes less pronounced as force increases. Mechanistically, this must relate to the influence of force on the heat generation rate and the time it takes to elevate the interface temperature towards that required for pyrolysis at the higher wear rates. Clearly, because an initiation time exists, some local accumulation of heat is necessary, which again indicates that frictional interface is not planar, but must be a volume. The force also influences the pressure at the wheel which will enhance the secondary reactions, and therefore the heat of reaction will be less endothermic or even exothermic for pyrolysis at higher forces. For cellulose, increased pressure reduces the heat of pyrolysis and increases the char yield (Mok *et al.*, 1983).

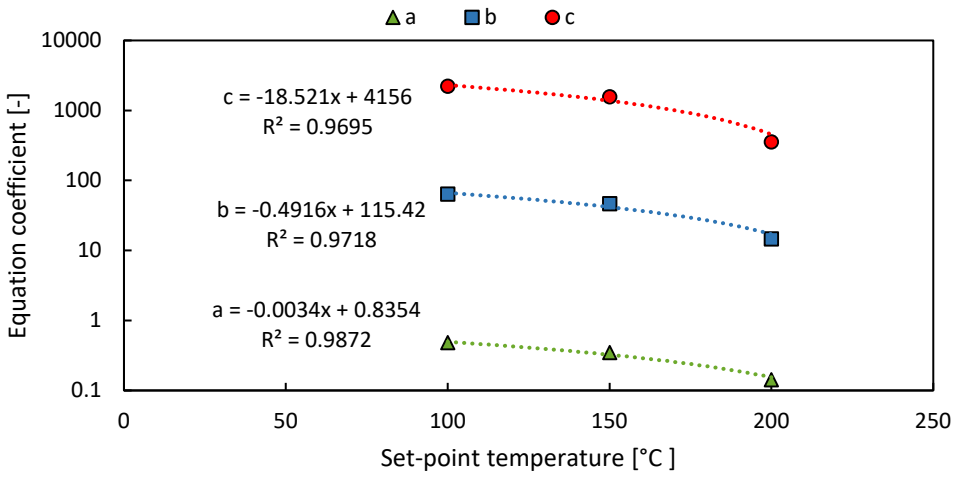

Figure 5.11: Equation coefficients for equation 5.2 as a function of the set-point temperature.

As deduced in the discussion above, prior to the onset of smouldering, the temperature is too low for pyrolysis. The exact temperature at which smouldering begins is unknown. In the open door experiments using the infrared camera, peak temperatures of 293, 259 and 220°C were obtained for the three trials at 49 N pressing force. While the first two are within the pyrolysis range, the other open door experiments never reached the pyrolysis onset range, expected to be between, 240 – 280°C. However, as highlighted (Section 4.3), the method recorded surface temperature, not the actual interface temperature. Accumulating tar will cool and give lower temperature readings. The closed door experiments, with supplementary heating, could only record the averaged temperatures, T_E and T_C (see Section 4.4). This lack of direct measurements indicates that it is important to understand how the mechanical power dissipates as heat within the system.

Heat flows from the frictional interface into the wheel or away with the products of pyrolysis: char, tar, tarry vapours and simple gases. The wheel, which is made of carbon steel, has a high thermal diffusivity compared to wood, and so draws heat far more quickly away from the interface. The heat entering the wheel is either conducted to the shaft and away, or lost by convection and radiation into the chamber environment as the wheel rotates. The wheel also acts as a heat sink and then a reservoir, absorbing sensible heat until an equilibrium is reached with the chamber environment. Thus, the observed rising T_E temperatures (Figure 5.7) at all set-points below 200°C, demonstrate that the interface temperature is elevated and driving the reaction. At 200°C, the value of T_E change little, generally rising only slightly over the experiment time.

After both the onset of pyrolysis and the later lower-to-higher wear rate transition, two significant changes occur, the coefficient of friction (CoF) decreases and the wear rate increases. Each will be discussed. While the CoF exhibited considerable variability, which made comparisons between trials hard to draw, within trials there are clear trends. At the start of each experiment and up to the onset to smouldering, the CoF is initially high (Figure 5.7). Then, after the onset of wear, all experiments showed a decrease in the CoF, which was followed by yet another decrease at the lower-to-higher wear rate transition. These sudden drops in CoF could be caused by a number of mechanisms, all relating to the changing properties of the pyrolysis products at the frictional interface. First, lubrication is the most obvious where, before the onset of smouldering the friction occurs between dry rough wood and the wheel, then after the onset of smouldering, pyrolysis liquids create a lubricating boundary layer between the wood and the wheel. The high force produced the greatest wear, and so more pyrolysis liquids are expected, leading to its observed lower coefficients of friction. This may also explain why the temperatures appear lower for the

high than for the middle force (49.1N) of the open door experiments, the rationale here being that the greater generation of pyrolysis liquids is unable to fully volatilise before the wheel does a full rotation, thus accumulating until sheared off the wheel as it rotates to again meet the wood plank. If accumulating, the longer residence time will allow more cooling, so explaining the lower observed interface temperature. A second mechanism that may cause the coefficient of friction to decrease is abrasion, where attrition particles are deformable and fill to pack the spaces between asperities in the wheel surface. This will result in a smoother contact surface and subsequently less friction. This is a possible fate for the solid char that forms during pyrolysis at the interface. A third mechanism is that the tar liquids bake onto the wheel surface forming char that packs into the spaces between wheel asperities, resulting also in a smoother contact surface. Observations of the wheel after each experiment (Figure 5.15) do show that fouling occurs by a black substance and is more pronounced at higher forces. This could be due either to the second or third mechanisms, and shows that changes in the coefficient of friction cannot be explained by lubrication alone. If fouling does occur, it will reduce the heat transfer between the hot friction zone and the wheel, because the char layer is insulating compared to the steel wheel. A fourth mechanism could be that the high wear cases are associated with higher interface temperatures which produce a higher fraction of vapour. By partially supporting the load with a vapour cushion, the net area of viscous contact is reduced, and so lowers the apparent friction. It is not at all clear which of these four mechanisms dominate or when, but they probably all occur at some stage.

The second significant change is the wear rate, being almost zero before the onset of smouldering, after which is rises to the so named "lower" wear rate, and later transitioning to a "higher" wear rate. These are also called the 1st and 2nd wear rate. At high pressures and temperature, the higher wear rate occurs almost instantaneously. This higher wear rate is dependent on temperature and pressure, but non-linearly (Figures 5.7 and 5.9). With the wheel and chamber temperature at the 200°C set-point, the higher wear rate is constant and independent of pressure. In contrast, at the 100°C and 150°C set points, it is dependent on pressure and independent of temperature. Also, the effect of force on wear rate decreases as the force increases, highlighted by the decreasing slope in Figure 5.9

Mechanical power input is shown in Figure 5.10. This power is dissipated as heat, which drives the smouldering and hence the wear of the wood plank. Therefore, it is useful to examine the relationship between them. Figures 5.12 and 5.13 plot the millimetres of wear per 1 kilojoule of mechanical energy input for the open door and closed door experiments. When no wear occurs, this number is zero. In all experiments, a sudden increase in mm/kJ

occurs at the transition from lower-to-higher wear rate. The results show both temporal variation and periodicity; the latter carried through from the earlier observed ~20 Hz seen in the CoF plots. Temporal variation is partly due to changing wood properties as the plank is consumed but, because it is significant, more likely reflects changing frictional resistance. Interestingly, even though variation occurs in mm/kJ, the wear rate was constant for each trial after the transition, except for one; the 200°C, 68.7 N trial, where yet another transition in rate was observed at 140 s. Table 5.2 compares the effect of temperature and pressing force on the millimetres of wear per kilojoule of mechanical energy input, noting the variation ranges as a higher range and a lower range. There are three features; (i), the higher range occurred before the lower range; (ii), the ranges tend to decrease as pressing force is increased; and (iii), the ranges tend to decrease as the temperature is increased. The first feature demonstrates that the frictional properties at the interface change during wear despite the fact that the wear rate remains constant. Possible causes of the change in frictional properties are discussed above, including fouling which was found to occur in many of the trials. Features (ii) and (iii) depend on the interplay between the interface temperature, the pressing force and the heat of pyrolysis, and tribology of the pyrolysis products. This interplay is complex and modelling is not possible because it relies on many unknowns, including the heat losses. Nevertheless, it is possible to demonstrate that the pyrolysis reaction must be exothermic at these higher wear rates. Take the open door experiment at 67.8 N, 3500 rpm, where 1 kJ of mechanical energy input produced wear ~6 mm of the wood plank. Using a density for Mānuka of 780 kg m^{-3} (Ripberger et al., in preparation) this represents ~1500 joules supplied per gram of wood pyrolysed. Heat losses here can be estimated from the open door trial, which had the greatest power input without smouldering (49.1 N, 2500 rpm). At a friction coefficient of ~0.4, this trial received 316 watts of mechanical power, which can all be assumed to be lost heat. Returning to the 67.8 N, 3500 rpm trial, at its maximum wear rate of ~0.5 mm s^{-1}, it will take 12 seconds to remove 6 mm of wood. The heat loss over this time is ~2800 joules. Therefore, the pyrolysis must be exothermic, generating ~1300 J g^{-1} to sustain itself. This result is far higher than the findings in Ripberger et al. (Ripberger *et al.*, 2018) when secondary reactions dominate the heat of pyrolysis. Notably, the pressure is 477 kPa at 67.8 N force, which will increase the secondary reactions and therefore the exothermicity to an unknown extent. For the closed door experiment, no wear occurred in the early stages of the 49.4 N trial at 100°C set-point temperature. Here the CoF was ~0.3, which represent heat losses of ~290 W, a similar value. After the transition from lower-to-higher wear rate, the wear rate is 0.38 mm s^{-1} (Figure 5.12) and ~10 mm of wear occurs per kilojoule of mechanical energy expended (Table 5.2). The heat loss during 10 mm of wear is therefore 10/0.38×290 =

7,600 J. Given that only 1000 J of mechanical energy input was expended, the net result is that 6,600 J of energy must have been supplied from the heat of reaction. This nominal heat of pyrolysis is far higher than any values in the literature (Ripberger *et al.*, 2018). Nevertheless, it is still far lower than the heating value of wood of ~20,000 J kg^{-1}. However, there are many unknowns and measurement uncertainties, including whether air ingress to the chamber and the rotating action of the wheel may cause some combustion. The unknowns are the heat transfer into the wood, the fouling resistance of the wheel and its effect on heat transfer, other heat losses through radiation and convection into the chamber environment and conduction through the wheel and to the shaft. Then there are other wood property variations such as the grain direction and cavity density in the Manuka planks (Figure 5.14). Measurement uncertainties relate to the assumptions needed to convert the current readings to mechanical energy input, the effect of vibration and hence periodicity, and the practical inability of measuring the interface temperature. Together these make it impossible to achieve a heat balance. Nevertheless, the results provide some insight into the conditions that cause pyrolysis and how pyrolysis changes with the operating variables of the friction smoker.

Table 5.2: Ranges of wear per kilojoule of mechanical energy input, at 3000 rpm wheel speed unless otherwise stated. Often two ranges were evident after the transition from lower-to-higher wear rate, an initial faster preceding a later slower wear peer kilojoule.

Set-point temperature (T_E)	**Pressing force (F_N)**			
	9.8 N [mm kJ^{-1}]	**29.4 N** [mm kJ^{-1}]	**49.1 N** [mm kJ^{-1}]	**68.7 N** [mm kJ^{-1}]
ambient	-	-	3.5→4.5	6 [3500 rpm]
100°C	-	26→18	14→18→10	4→6
150°C	-	15→20→7→15	18→13→8→6	2→4
200°C	30→24	12→9	10→7	4→8→4.5

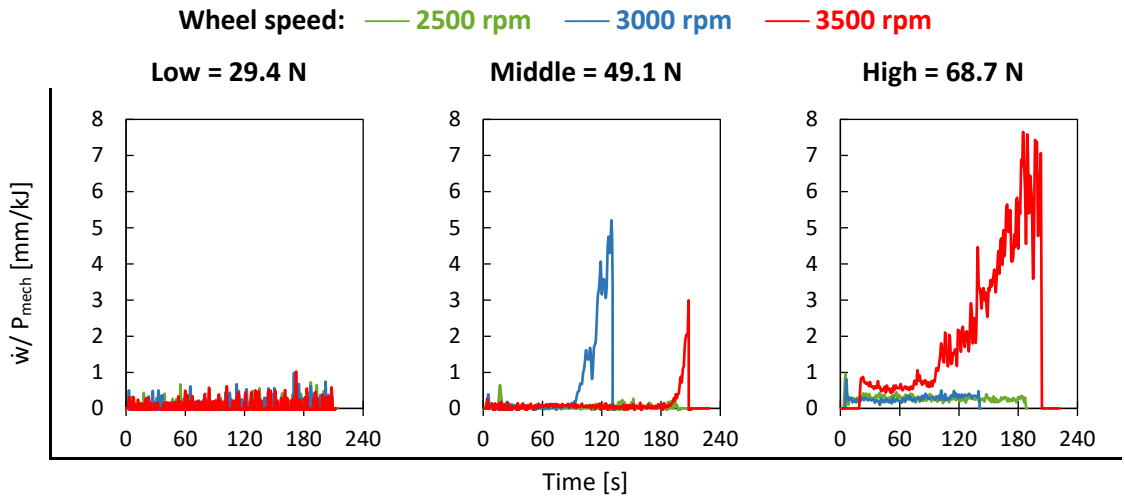

Figure 5.12: Ratio of mechanical power input to wear rate [mm/kJ] for open door experiment. The units describe the energy required to pyrolyse a millimetre length of wood.

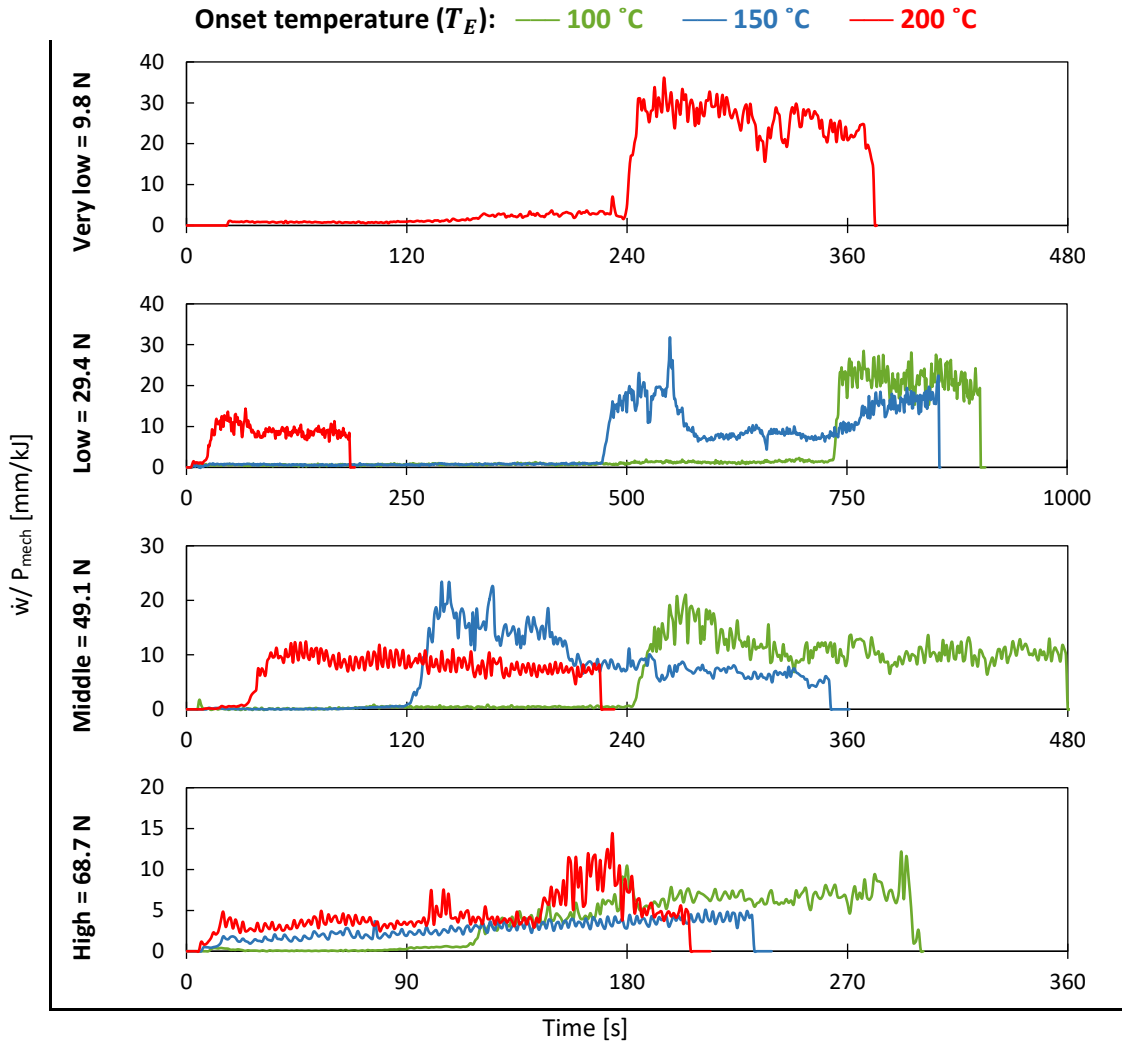

Figure 5.13: Ratio of mechanical power input to wear rate [mm/kJ] for closed door experiment during smouldering with supplementary heat.

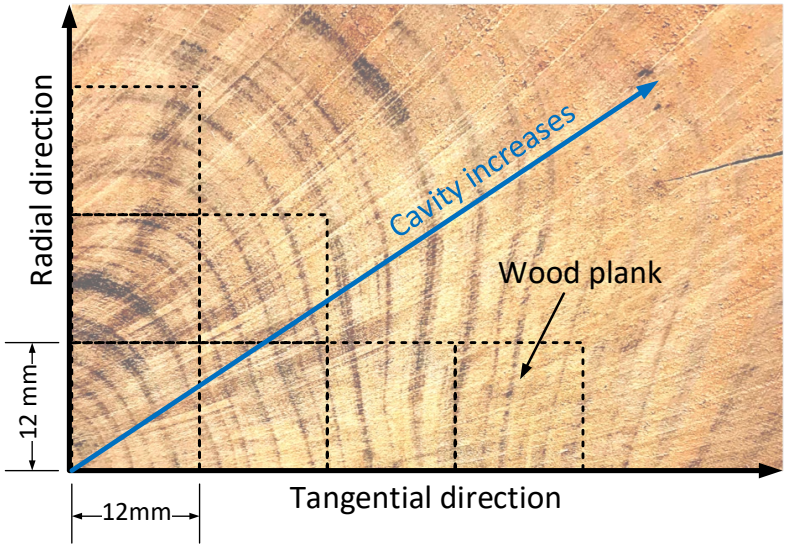

Figure 5.14: Cross-section of mānuka feedstock showing the cuts of the wood planks used for the experiment.

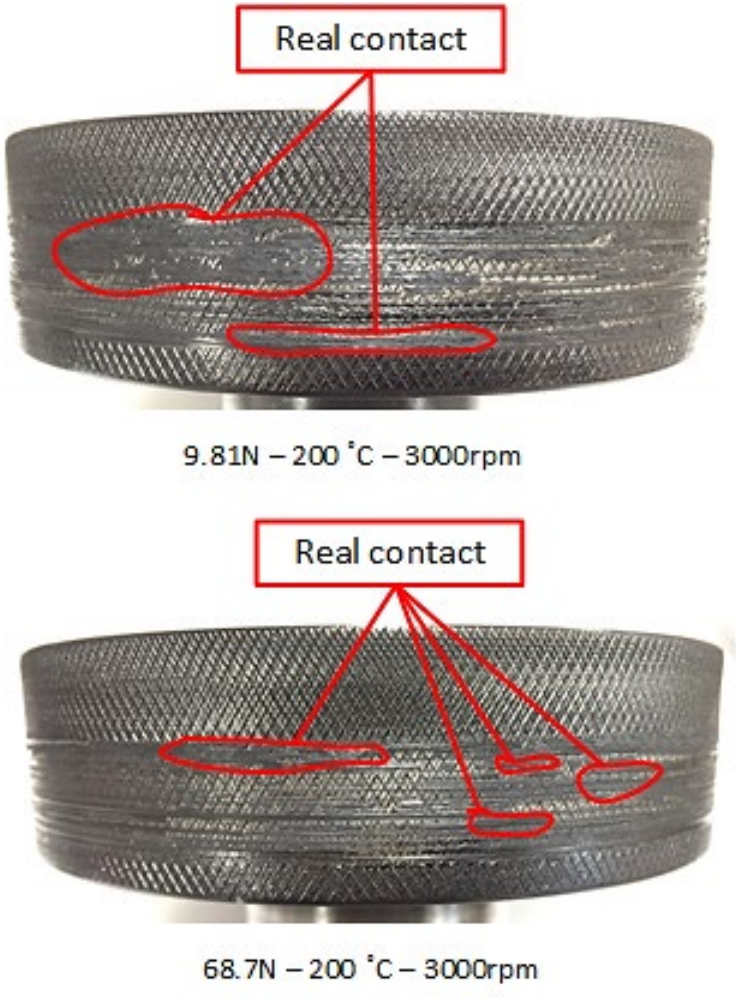

Figure 5.15: The change in the real contact area due to tar formation for the lowest and highest smouldering conditions. The rest of the trials are shown in Appendix A.1

One of the extenuating factors mentioned above is changing wood properties. These can result from the variation in the regional cuts in the experimental wood planks. Cuts made further from the pith (i.e. the centre of the wood) have decreasing density of annual rings per unit area as illustrated in Figure 5.14. These changes from one plank to another include the tendency for cavities to form inside the wood that can promote internal cracks which negatively affect the rigidity of the wood (Bjurhager, 2011; Winandy *et al.*, 1984). Such cavities will affect the dynamics of heat and mass transfer if they form, and may explain some of the variability seen in the transition times, for example, between the higher transition times for the 29.4 N, 200 ˚C trial compared to the 49.1 N, 200 ˚C trial.

As noted in the literature review, other work in tribology aims at understanding the frictional properties where, when the temperature is examined as an effect, the disc speed is reduced to a minimum to avoid the effect of frictional heating. Here, speed is essential to the generation of additional frictional heat to promote pyrolysis. However, wheel speed as a variable was only examined in the open door experiments. It appears to have less significance than the pressing force, although both are directly proportional to the mechanical power delivered to the frictional interface (per Eq.(4.6)). However, this appearance is a product of the experiments because the range of speeds, 2500 to 3500 rpm is much less than the range of pressing forces, 29.4 to 68.7 N in the open door trials where speed was varied. Because pyrolysis and heat loss occur simultaneously, it is not possible to isolate the effects of speed from force here, for example, in the manner of Archard (Basu, B. *et al.*, 2011) who compared contact temperature as a function of the applied pressure and sliding speed for composite materials under friction. No literature known to the author has been carried out where smouldering of wood for smoke generation is the objective. Thus, comparisons are not directly possible. However, extensive work has been done on the heat of pyrolysis, but again, not for friction systems that aim to smoulder (see Section 2.9). Some is done in ablation for fast pyrolysis, however smouldering is driven by the heat of a high temperature moving surface at low speed rather its being induced by friction (see Section 2.10). Again, this does not provide comparable materials that can be related to the friction system.

The closest comparison is with friction welding of wood (in Section 2.5.1). Although the Stamm *et al.* (2005) aim was to study the bonding properties between woods, their results reveal a comparable trend between the change in CoF as a function of interface temperature. When pyrolysis takes place, the CoF goes from a higher-to-lower value, then remains steady. This behaviour is similar to the findings in Figure 5.5 and more pronounced in Figure 5.7 for the smouldering cases. In addition, the temperature profiles of Stamm *et al*. (phase III

to V in Figure 2.14) and Figure 5.7 exhibit similar trends, where the temperature increases to reach a steady state. This trend was not observed during friction with the door open, due to the significance of the heat loss.

Despite the differences between contact bodies (i.e. wood-to-wood verses wood-to-steel), when the lubricating layer forms the contact body becomes wood-to-tarry char in both cases. Thus, the observation of Stamm *et al.* (2005), that the interface temperature increases as the thickness of the lubricating layer increase, is also most likely to be valid here. Both this work and that of Stamm *et al.* (2005), show that the applied pressure and sliding speed (delivered by the frequency and amplitude of oscillation in the work of Stamm *et al.* (2005)) are important to the rate of smouldering. One difference, however, is Stamm *et al.* (2005) claim that the reaction zone (phase V) is highly endothermic. Here, in this work, the analysis implies that the 2nd wear rate zone is exothermic. This needs further investigation.

5.6 Smoke analysis

This section presents a preliminary investigation on the smoke generated reflects what was able to be achieved at this late stage of the project. The objective here is to compare the effect of various operating conditions on the formation of six targeted aromatic compounds and PAHs, as recommended by Dr Graham Eyres of the University of Otago. The experimental runs for this section are included in Appendix A.3.

5.6.1 Formation of aromatic volatiles

Here, the six compounds selected for the study are shown in Figure 5.16. These were thoroughly discussed by Maga (1988) for his comparative analysis between different wood species. These compounds are most likely to significantly contribute to the aromatic profile of the smoke.

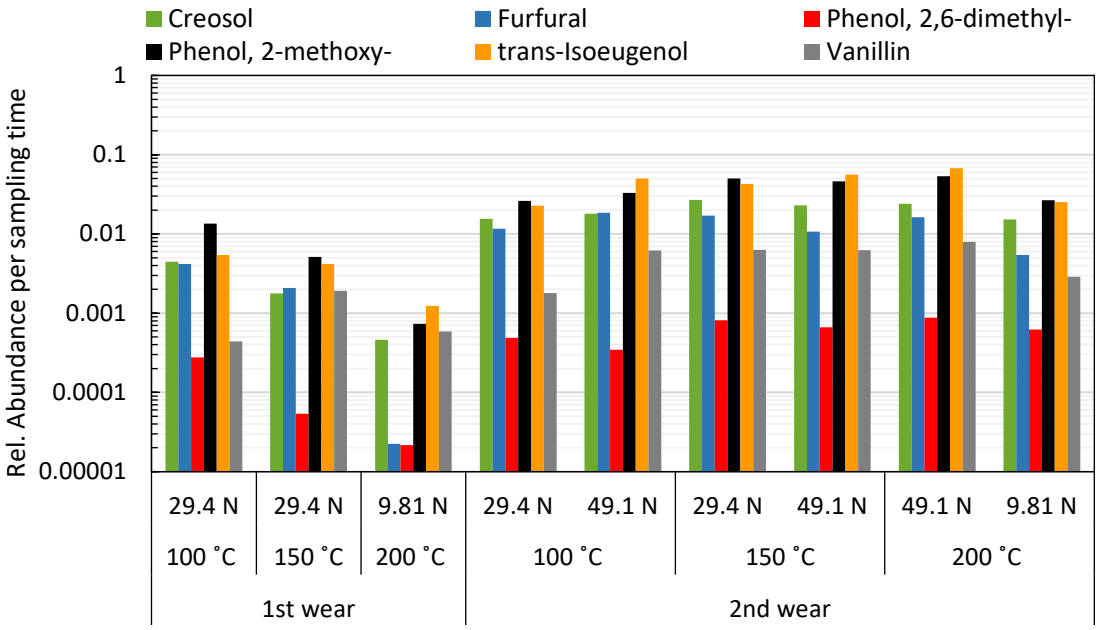

Figure 5.16: Aromatic compound profile at wheel speed of 3000 rpm with various applied forces and onset temperatures. 1st and 2nd wear are the nominal endothermic and exothermic wear regime seen in Fig.5.7.

Figure 5.16, shows the rate of volatiles formation adjusted for wear rate. Here the production rate for all the compounds at the 2nd wear rate seems unaffected by the change in operating conditions, where the compounds ratio across the conditions is relatively stable. However, deposition of condensable volatiles was significant on the holding tube walls for all the 2nd wear rate samples compared to the 1st wear rate. This indicates that the twisters were over saturated which may potentially mask out any differences between the operating conditions.

On the other hand, the samples with 1st wear rate were free of fouling. The formation of compounds shows a significant dependence on the onset temperature. At 29.4 N, the 2-methoxyphenol (Guaiacol) and 2, 6 dimethyl phenol show drastic depletions with increasing the onset temperature where, in contrast, they seem unaffected at the 2nd wear rate.

These results, although preliminary, do show that smoking conditions alter the volatiles formation, the most significant effect appears at the 1st wear rate region, where the production rate overall is higher in the 2nd wear rate, however does not reveal the changes in the compounds because of the oversaturation of the 2nd wear samples.

5.6.2 Formation of PAHs

The analysis results in Figure 5.17 covers PAHs with low molecular weight, which are able to be detected using the GC/MS method. These PAHs have a carcinogenic factor of 3 (a thousand times less carcinogenic than Benzo[a]pyrene) according to the International Agency of Research on Cancer (IARC).

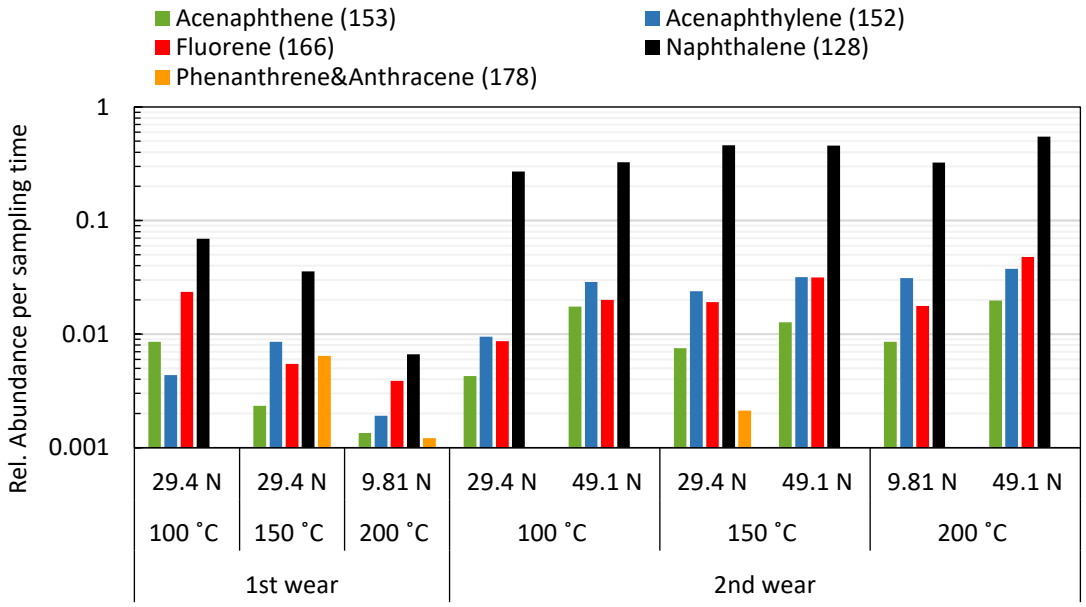

Figure 5.17: PAH profile at wheel speed of 3000 rpm with various applied forces and onset temperatures

The results show that PAH production increases when shifting from 1st to 2nd wear rate as the temperature is higher during 2nd wear, due to the exothermic reaction. At 1st wear rate the combination PAH release appears more influenced by force. At 2nd wear, it appears mildly influenced by force.

For this section the same conditions were replicated in addition to more, to estimate the volatile matter in the produced char in the following section.

5.7 Proximate analysis

One of the unknowns in friction smoking is the extent of the pyrolysis reaction. To ascertain this, a proximate analysis was performed on the char residue collected from the chamber. The volatile matter determination followed the ASTM-D1762-84 (2007) procedure and the results are presented in Figure 5.18.

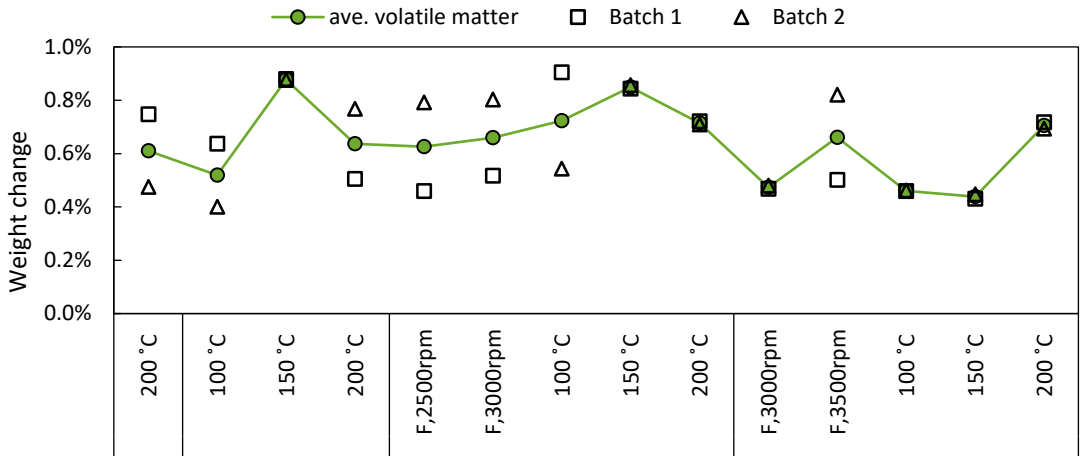

Figure 5.18: Proximate analysis of the char yield from various smoking conditions.
(F=ambient temperature with friction only, all the condition with supplementary heat @ 3000 rpm)

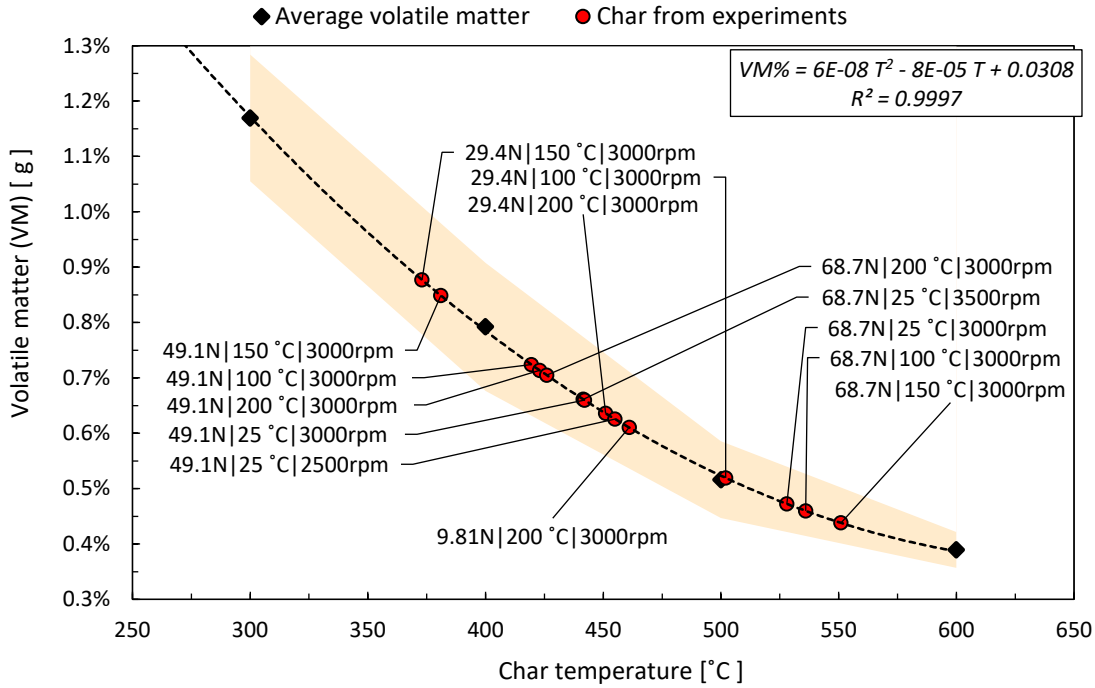

Figure 5.19: ♦ Char calibration curve (obtained by preparing char at different temperatures and following ASTM-D1762-84 protocols to determine the VM). ● Measured VM content of char residue collected from the chamber after experiment completion (experimental conditions noted). The points are located on the calibration curve in order to identify their formation temperature.

The volatile matter for all the experiments was found to be low, ranging from ~0.4% to 0.9%, which are indicative of high charring temperatures, shown in Figure 5.18. However, this is most likely because the char was exposed to some oxidation induced by air drawn into the chamber around the edges of the plank guide, due to the pumping action of the spinning wheel creating a low internal pressure. The deviation between replicates was noticed to be related to the amount of residual tar in the char samples. The samples with less tar content are more consistent between their replicates. For more accurate results, the char needs to be collected immediately after the start of the smouldering process to avoid the oxidation effect. According to Khavan *et al.* (1971) in section 2.4, this is a possible temperature for the char to reach when compared to the trials 49.1N and 68.7N at 25 ˚C, but not for the other cases where the temperature is higher.

Proximate analysis of the volatiles matter (VM) content of the char was used to estimate the formation temperature of the char. Char was pyrolysed directly in a furnace to obtain the calibration between formation temperature and VM content, labelled as (♦) (i.e. control sample) in Figure 5.19. The proximate analysis results for the char produced from the smoking experiments shown in (●) are placed on the calibration curve to indicate their temperature of formation. Clearly, they are higher than the chamber temperature (or the expected interface temperature). They do however show the char residue does undergoes secondary oxidation after formation.

5.8 Closure

This section highlights a number of conclusions:

- Conduction of heat along the shaft occurs, but does not cause electrical drift in the motor current. Nevertheless, it is a concern and so to avoid this, the shaft should contain a thermal break.
- Conduction along the shaft most likely raises the motor front bearing above its working temperature, thus indicating that care must be taken in selecting bearings for duty.
- Increasing the pressing force and system set-point temperature shortens the time to the onset of smouldering. At higher forces and temperatures, smouldering begins instantaneously.
- Smouldering shows two wear rates, a 'lower' and a 'higher' wear rate, with a sharp transition between them. Trials with a system set-point temperature of 200°C and pressing forces ≥29.4 N exhibited almost instantaneous smouldering at the 'higher' wear rate.
- The time taken to the 'lower-to-higher' transition in wear rate is non-linearly dependent on the pressing force and the system set-point temperature, being independent of pressing force at the 200°C set-point temperature. Sliding speed is of less significance.
- Instantaneous smouldering occurs at a mechanical power input of ~700 W.
- Wear and mechanical power input were related as millimetres of wear per kilojoule of power input. For the 'higher' wear rates, the ratio tended to decrease with increasing temperature and pressing force. However, there was significant variability. Nevertheless, approximate heat balances imply that pyrolysis must be exothermic.
- Many factors can influence the coefficient of friction: lubrication by tarry liquids, abrasion and packing of interstices, baking of tar onto the wheel, and further lubrication by partial volatilisation. It is not possible to isolate these, although baking of tar is present in all experiments where smouldering occurs.
- Wood properties also change. Among these are the grain direction and spacing of the annual growth rings, which affect the cavities inside the wood plank.
- The smouldering conditions influence the aromatic and PAHs constituents in the generated smoke.
- The proximate analysis does not provide any clues about the formation temperature due to the effect of oxidation inside the chamber.

These findings then allow the following two questions to be asked.

1. What are the optimal conditions for smoking?
2. Can the device be scaled-up in size while maintaining optimal conditions?

For the device developed here, smoking is consistent between a range of pressing foce29.4 – 68.7 N, and a range of temperature, 150 – 200 ˚C. The presence of two smoking regimes, described here as endothermic and exothermic is significant when scaled-up. The exothermic condition will become hotter when scaled-up because heat losses are proportional which then influence the PAH formation and other smoke compounds. This is most likely the reason why friction-type smoke generators are intermittently operated rather than continuously. Therefore, it is argued that the endothermic regime is favourable for this reason. Therefore, the optimal condition for this device are limited to those that exhibit endothermic smoking, 29.4 – 49.1 N and 100 – 150 ˚C

Conclusion and Recommendations

This project was conducted to understand the science behind friction smoke generators and the factors that influence smoke generation in order to propose how best to design and operate them. Here, a friction smoke generator was further improved from an early project by the author. The modifications made here were to improve control over the heating chamber temperature to ±2 – 4 ˚C, heat loss was minimised by adding an insulation layer between the inner and outer chambers, and the feeding mechanism was improved with tighter force control to within ±1.2 N. The coefficient of friction (CoF) was estimated using the known electrical power consumed by the induction motor and assuming an efficiency.

The smouldering limit from the experiments is driven by two factors, the pressing force and the set-point chamber temperature. These factors dictate the onset of smouldering, the rate of smouldering, and the time to the transition from the 'lower' to 'higher' wear rate. The 'higher' wear rate is constant at all pressing forces and independent of temperature when the chamber set-point temperature is maintained at 200°C. This demonstrates that smoke production can be well-controlled to an upper limit.

However, the wide range of consistent smoke seen in this device will not translate to a scale-up smoke generator because the exothermic regime at scale will operate at a significantly higher temperature this has implication for the PAH formation and other smoke compounds. It is the probable reason why friction-type smoke generators are intermittently operated.

It was difficult to account for all heat losses and so a crude energy balance was used to show that pyrolysis at the 'higher' wear rate is most likely to be exothermic and self-sustaining.

In later experiments, smoke from different conditions was collected for chemical composition analysis. This work was conducted by Dr Graham Eyres and co-workers at the University of Otago, New Zealand. The results show the pressing force and the chamber set-point temperature markedly influence the aromatic and PAH release. A total mass balance on the system was not possible, due to the difficulty in collecting the gas, tar and char residues, some of which deposits in the pipework. A proximate analysis was used to determine the volatile content of the char residue in order to estimate the interface temperature at which pyrolysis occurs. The results were not useful, due to the char being oxidised by external air entering the chamber.

From this work, a number of recommendations arise:

1. A torque transducer coupled to the motor shaft is required to eliminate the uncertainty caused by current measurement during motor overloading.
2. Air needs to be prevented from entering the chamber by use of a loose packing material around the wooden plank. This will reduce the opportunity for secondary oxidation of the volatiles and char.
3. Replace the solid friction wheel with a hollow steel wheel to reduce its weight and hence thermal mass. This will reduce the lag during frictional heating.
4. Further improve the smoke collection methodology to ensure experiments can be compared quantitatively.

References

Ahmad, J. I. (2003). SMOKED FOODS | Applications of Smoking A2 - Caballero, Benjamin *Encyclopedia of Food Sciences and Nutrition (Second Edition)* (pp. 5309-5316). Oxford: Academic Press.

Anderson, C. A., & McHenry. (1971). Smoke generator with automatic control system therefor: Google Patents.

ASTM-D1762-84. (2007). Standard Test Method for Chemical Analysis of Wood Charcoal *ASTM International*. West Conshohocken PA, United States.

Atack, D., & May, W. (1958). Frictional mechanisms in the grinding process. *Pulp and Paper Magazine of Canada, 58*(3).

Baltes, W. (1985). Application of pyrolytic methods in food chemistry. *Journal of Analytical and Applied Pyrolysis, 8*, 533-545. doi:http://dx.doi.org/10.1016/0165-2370(85)80050-4

Basu, B., & Kalin, M. (2011). *Frictional Heating and Contact Temperature Tribology of Ceramics and Composites: A Materials Science Perspective* (pp. 60-69).

Basu, P. (2013). *Biomass Gasification, Pyrolysis and Torrefaction : Practical Design and Theory* (Vol. 2nd edition). Amsterdam: Academic Press.

Bhushan, B. (2013). *Introduction to tribology* (2nd ed.). Oxford: Wiley-Blackwell.

Bjurhager, I. (2011). *Effects of cell wall structure on tensile properties of hardwood.* Doctoral thesis.

Blau, P. J. (2009). *Friction science and technology : from concepts to applications*: Boca Raton : CRC Press ; [Park Ridge, Ill.] : STLE, c2009

2nd ed.

Cardinal, M., Cornet, J., Sérot, T., & Baron, R. (2006). Effects of the smoking process on odour characteristics of smoked herring (Clupea harengus) and relationships with phenolic compound content. *Food Chemistry, 96*(1), 137-146. doi:http://dx.doi.org/10.1016/j.foodchem.2005.02.040

CGGlobal. (2018). Aluminium Enclosure Motors - Safe Area. Retrieved from http://www.cgglobal.com/

Chomanee, J., Tekasakul, S., Tekasakul, P., Furuuchi, M., & Otani, Y. (2009). Effects of moisture content and burning period on concentration of smoke particles and particle-bound polycyclic aromatic hydrocarbons from rubber wood combustion. *Aerosol and Air Quality Research, 9*(4), 404-411.

Coggins, P. C. (2012). Attributes of Muscle Foods: Color, Texture, Flavor *Handbook of Meat, Poultry and Seafood Quality* (pp. 35-44): Blackwell Publishing Ltd.

Commission, E. (2011). Commission Regulation (EU) No 835/2011 of 19 August 2011 amending Regulation (EC) No 1881/2006 as regards maximum levels for polycyclic aromatic hydrocarbons in foodstuffs. *Official Journal of the European Union, 20*(8), L215/216-L215/218.

Coriolis. (2013). *iFAB 2013 Seafood Review*. Retrieved from http://www.coriolisresearch.com/pdfs/coriolis_iFAB_2013_seafood.pdf

Coriolis. (2014). *IFAB 2013 F&B Industry Overview*. Retrieved from http://www.coriolisresearch.com/pdfs/coriolis_iFAB_2013_overview.pdf

Di Blasi, C. (1996). Kinetic and heat transfer control in the slow and flash pyrolysis of solids. *Industrial & Engineering Chemistry Research, 35*(1), 37-46.

Fastexlubes. Lubrication Terminology. Retrieved from http://www.fastexlubes.com/main.php?doc_id=469&cat_id=40

GERSTEL. (2017). Handling of GERSTEL Twister (01/2014 ed.). Germany: GERSTEL GmbH & Co. KG.

Gfeller, B., Zanetti, M., Properzi, M., Pizzi, A., Pichelin, F., Lehmann, M., & Delmotte, L. (2003). Wood bonding by vibrational welding. *Journal of Adhesion Science and Technology, 17*(11), 1573-1589.

Gilbert, J., & Knowles, M. E. (1975). The chemistry of smoked foods: a review. *International Journal of Food Science & Technology, 10*(3), 245-261. doi:10.1111/j.1365-2621.1975.tb00028.x

Gottlieb, I. M. (1997). 3 - Practical aspects of AC motors. In I. M. Gottlieb (Ed.), *Practical Electric Motor Handbook* (pp. 62-98). Oxford: Newnes.

Guan, N., Thunell, B., & Lyth, K. (1983). On the friction between steel and some common Swedish wood species. *Holz als Roh- und Werkstoff, 41*(2), 55-60. doi:10.1007/bf02612232

Guillén, M. D., & Manzanos, M. J. (2005). Characteristics of smoke flavourings obtained from mixtures of oak (Quercus sp.) wood and aromatic plants (Thymus vulgaris L. and Salvia lavandulifolia Vahl.). *Flavour and Fragrance Journal, 20*(6), 676-685. doi:10.1002/ffj.1599

Gupta, M., Yang, J., & Roy, C. (2003). Specific heat and thermal conductivity of softwood bark and softwood char particles☆. *Fuel, 82*(8), 919-927. doi:https://doi.org/10.1016/S0016-2361(02)00398-8

Havimo, M., & Hari, P. (2010). Temperature gradient in wood during grinding. *Applied Mathematical Modelling, 34*(10), 2872-2880. doi:https://doi.org/10.1016/j.apm.2009.12.021

Hsu, S. M., Zhang, J., & Yin, Z. (2002). The Nature and Origin of Tribochemistry. *Tribology Letters, 13*(2), 131-139. doi:10.1023/A:1020112901674

J, R. H., & R, R. H. (1961). Method and apparatus for the production of smoke for food-treating purposes: Google Patents.

Jankowska, A., & Kozakiewicz, P. (2013). Comparsion of thermal properties of selected wood species from Africa. *Annals of Warsaw University of Life Sciences-SGGW. Forestry and Wood Technology, 82*.

Karmakar, S., Chattopadhyay, S., Mitra, M., & Sengupta, S. (2016). *Induction motor fault diagnosis : approach through current signature analysis*: Singapore : Springer, 2016.

Kennedy, F. E. (2001). Frictional heating and contact temperatures. *Modern tribology handbook, 1*, 235-272.

Kostyra, E., & Baryłko-Pikielna, N. (2006). Volatiles composition and flavour profile identity of smoke flavourings. *Food Quality and Preference, 17*(1–2), 85-95. doi:http://dx.doi.org/10.1016/j.foodqual.2005.06.008

Lede, Panagopoulos, & Villermaux. (1983). Experimental Measurement of ablation rate of wood pieces, undergoing fast pyrolysis by contact with a heated wall. *Prepr. Pap., Am. Chem. Soc., Div. Fuel Chem.;(United States), 38*(CONF-830814-).

Lede, Panagopoulos, J., Li, H. Z., & Villermaux, J. (1985). Fast pyrolysis of wood: direct measurement and study of ablation rate. *Fuel, 64*(11), 1514-1520.

Lede, J., Li, H. Z., & Villermaux, J. (1988). Pyrolysis of Biomass: Evidence for a Fusionlike Phenomenon: ACS Publications.

Ledesma, E., Rendueles, M., & Díaz, M. (2016). Contamination of meat products during smoking by polycyclic aromatic hydrocarbons: Processes and prevention. *Food Control, 60*, 64-87. doi:http://dx.doi.org/10.1016/j.foodcont.2015.07.016

Maga, J. A. (1987). The flavor chemistry of wood smoke. *Food Reviews International, 3*(1-2), 139-183. doi:10.1080/87559128709540810

Maga, J. A. (1988). *Smoke in food processing*. Boca Raton, FL: CRC Press.

McGrath, T., Sharma, R., & Hajaligol, M. (2001). An experimental investigation into the formation of polycyclic-aromatic hydrocarbons (PAH) from pyrolysis of biomass materials. *Fuel, 80*(12), 1787-1797. doi:http://dx.doi.org/10.1016/S0016-2361(01)00062-X

McGrath, T. E., Chan, W. G., & Hajaligol, M. R. (2003). Low temperature mechanism for the formation of polycyclic aromatic hydrocarbons from the pyrolysis of cellulose. *Journal of Analytical and Applied Pyrolysis, 66*(1–2), 51-70. doi:http://dx.doi.org/10.1016/S0165-2370(02)00105-5

McKenzie, W., & Karpovich, H. (1968). The frictional behaviour of wood. *Wood science and technology, 2*(2), 139-152.

McNair, H. M., & Miller, J. M. (2009). *Basic gas chromatography. [electronic resource]*: Hoboken, N.J. : John Wiley & Sons, 2009

Second edition.

Mok, W. S.-L., & Antal Jr, M. J. (1983). Effects of pressure on biomass pyrolysis. II. Heats of reaction of cellulose pyrolysis. *Thermochimica Acta, 68*(2-3), 165-186.

Park, W. C., Atreya, A., & Baum, H. R. (2010). Experimental and theoretical investigation of heat and mass transfer processes during wood pyrolysis. *Combustion and Flame, 157*(3), 481-494. doi:http://dx.doi.org/10.1016/j.combustflame.2009.10.006

Peacocke. (1994). *Ablative pyrolysis of biomass.* (PhD Thesis), Aston University.

Peacocke, & Bridgwater. (1993). Design of a novel ablative pyrolysis reactor *Advances in Thermochemical Biomass Conversion* (pp. 1134-1150): Springer.

Pearson, A. M., & Gillett, T. A. (1996). *Processed meats*: New York : Chapman & Hall, c1996

3rd ed.

Pöhlmann, M., Hitzel, A., Schwägele, F., Speer, K., & Jira, W. (2013a). Influence of different smoke generation methods on the contents of polycyclic aromatic hydrocarbons (PAH) and phenolic substances in Frankfurter-type sausages. *Food Control, 34*(2), 347-355. doi:http://dx.doi.org/10.1016/j.foodcont.2013.05.005

Pöhlmann, M., Hitzel, A., Schwägele, F., Speer, K., & Jira, W. (2013b). Polycyclic aromatic hydrocarbons (PAH) and phenolic substances in smoked Frankfurter-type sausages depending on type of casing and fat content. *Food Control, 31*(1), 136-144. doi:https://doi.org/10.1016/j.foodcont.2012.09.030

Rabinowicz, E. (1995). *Friction and wear of materials* (2nd ed.). New York: Wiley.

Ripberger, G. D., Jones, J. R., Chen, Q., Caco, N., & Paterson, A. H. J. (2018). *Heat of Primary Pyrolysis for Wood*. Paper presented at the Chemeca, Queenstown, New Zealand.

Roberts, A. F. (1971). Problems associated with the theoretical analysis of the burning of wood. *Symposium (International) on Combustion, 13*(1), 893-903. doi:https://doi.org/10.1016/S0082-0784(71)80090-5

Rowe, K. G., Bennett, A. I., Krick, B. A., & Sawyer, W. G. (2013). In situ thermal measurements of sliding contacts. *Tribology International, 62*, 208-214.

Seraj, M. (2016). *Design of a food friction smoker with precise control : Engineering project submitted as part requirement for B.Eng (Hons), paper number 228.798*. Retrieved from Massey University: http://ezproxy.massey.ac.nz/login?url=http://search.ebscohost.com/login.aspx?direct=true&db=cat03987a&AN=massey.b3742136&site=eds-live&scope=site

http://libcontent.massey.ac.nz/handle/123456789/1525

Sérot, T., Baron, R., Cardinal, M., Cataneo, C., Knockaert, C., Le Bizec, B., . . . Varlet, V. (2008). *Assessment of the effects of the smoke generation processes and of smoking parameters on the organoleptic perception, the levels of the most odorant compounds and PAH content of smoked salmon fillets.* Paper presented at the Report and papers presented at the second workshop on fish technology, utilization and quality assurance in Africa. Agadir, Morocco.

Sérot, T., Baron, R., Knockaert, C., & Vallet, J. L. (2004). Effect of smoking processes on the contents of 10 major phenolic compounds in smoked fillets of herring (Cuplea harengus). *Food Chemistry, 85*(1), 111-120. doi:http://dx.doi.org/10.1016/j.foodchem.2003.06.011

Sharma, R. K., & Hajaligol, M. R. (2003). Effect of pyrolysis conditions on the formation of polycyclic aromatic hydrocarbons (PAHs) from polyphenolic compounds. *Journal of Analytical and Applied Pyrolysis, 66*(1–2), 123-144. doi:http://dx.doi.org/10.1016/S0165-2370(02)00109-2

Sikorski, Z. E., & Kołakowski, E. (2010). Smoking *Handbook of Meat Processing* (pp. 231-245): Wiley-Blackwell.

Smith, D., & Stratton, J. (2007). Food preservation, safety, and shelf life extension. *University of Nebraska-Lincoln Extension, Institute of Agriculture Natural Resources, Lincoln, NE*.

Spitzer, D. W. (2012). *Variable Speed Drives : Principles and Applications for Energy Cost Savings, Fourth Edition* (Vol. 4th ed). [New York, N.Y.] [222 East 46th Street, New York, NY 10017]: Momentum Press.

Stachowiak, G. W., & Batchelor, A. W. (2014). *Engineering Tribology* (Vol. Fourth edition). Oxford: Butterworth-Heinemann.

Stamm, B., Natterer, J., & Navi, P. (2005). Joining wood by friction welding. *Holz als Roh- und Werkstoff, 63*(5), 313-320. doi:10.1007/s00107-005-0007-6

Straffelini, G. (2015). *Friction and wear: methodologies for design and control*: Springer.

Svensson, B. (2007). *Frictional studies and high strain rate testing of wood under refining conditions.* (PhD Thesis), Mid Sweden Universuty.

Svensson, B. A., Holmgren, S.-E., Gradin, P. A., & Höglund, H. (2007). High strain rate compression and sliding friction of wood under refining conditions.

TenWolde, A., McNatt, J. D., & Krahn, L. (1988). *Thermal properties of wood and wood panel products for use in buildings*. Retrieved from

Toldrá, F. (2010). *Handbook of meat processing. [electronic resource]*: Ames, Iowa : Wiley-Blackwell, ©2010.

Tóth, L., & Potthast, K. (1984). Chemical Aspects of the Smoking of Meat and Meat Products. In E. M. M. C.O. Chichester & B. S. Schweigert (Eds.), *Advances in Food Research* (Vol. Volume 29, pp. 87-158): Academic Press.

Winandy, J. E., & Rowell, R. M. (1984). The Chemistry of Wood Strength *The Chemistry of Solid Wood* (Vol. 207, pp. 211-255): American Chemical Society.

Yu, A.-N., Sun, B.-G., Tian, D.-T., & Qu, W.-Y. (2008). Analysis of volatile compounds in traditional smoke-cured bacon(CSCB) with different fiber coatings using SPME. *Food Chemistry, 110*(1), 233-238. doi:http://dx.doi.org/10.1016/j.foodchem.2008.01.040

Appendix - A: Raw and supplementary data

This section presents the raw and supplementary data for the project.

A.1 Tar accumulation on the spinning wheel

Before reconditioning the wheel between experiments, photographs were taken to show the tar formation on the rim. Attempts were made to measure the mass of baked tar, but this was unsuccessful due to the low mass of the tar compared to the wheel (2.05 kg) and because the scale that was available has a resolution of ± 0.005 kg.

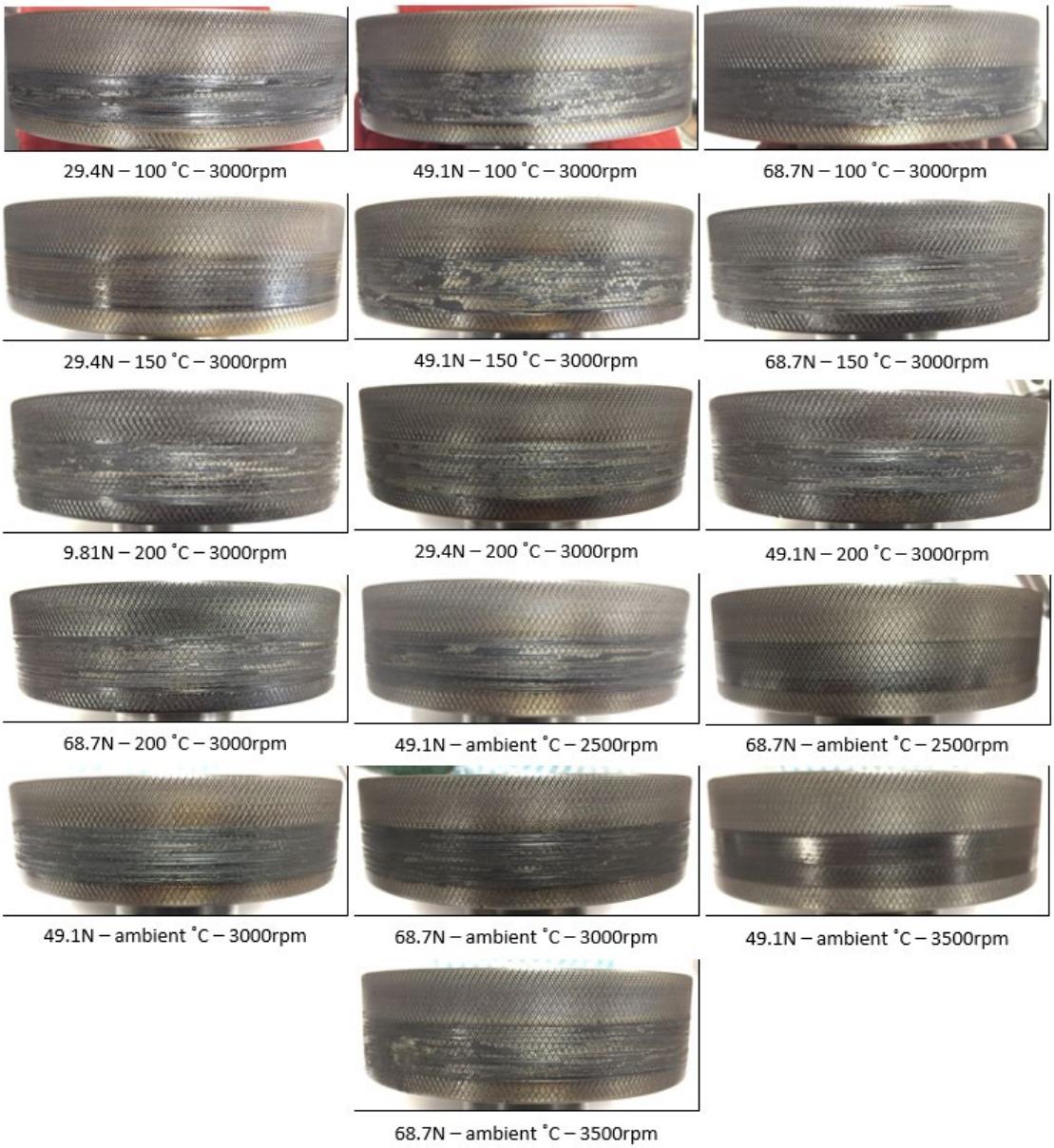

Figure A.1: Tar deposit on the friction wheel at various operating conditions.

A.2 Experimental condition screening

Slip between the actual motor speed and the set-point speed (synchronous speed) increases with load, until it falls outside the performance range for the motor. Experiments of slip used to determine the operating range for the experiments. The selected pressing forces and wheel speeds are based on the following plot. As can be seen, low speeds have too much slip and were avoided in the experimental design. Pressing forces ≥ 7 kgf, were found to have similar smoking behaviours.

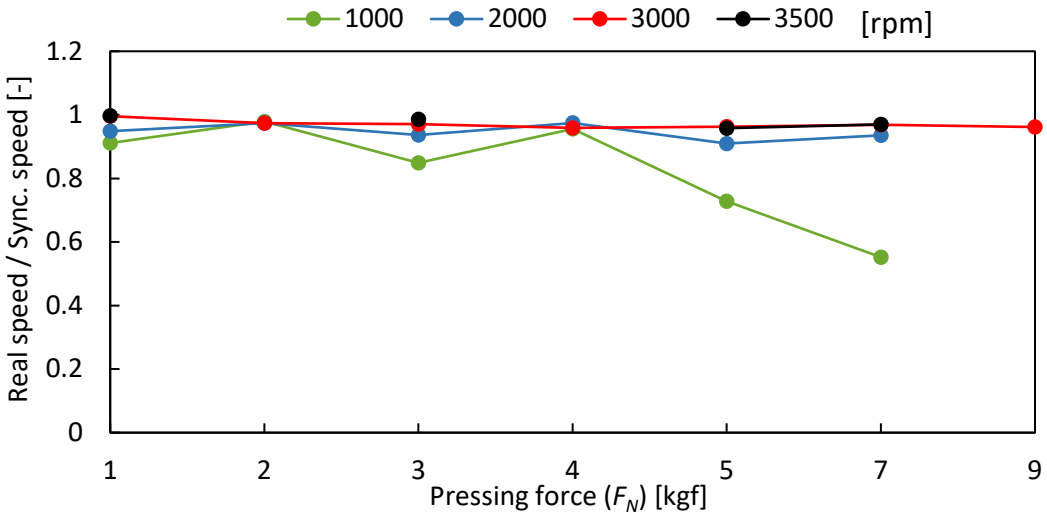

Figure A.2: The effect of pressing force on various motor speeds

A.3 Smoke samples

Wood conditions: air dried 12×12×150 mm, and bulk density of 785.32 kg m^{-3}

Disc conditions: surface roughness 200 µm, cleaned before each run.

Extraction conditions: the smoke flowrate passing the twister = 0.0216 L s^{-1}

Table A.1: Smoke sampling experimental data.

Sample	Sampling time [s]	Condition	Wear region	Wear rate	
				[mm/s]	[g/s]
S1	29	29.4N/100 °C	1st wear	0.11	0.0119
S2	132	29.4N/100 °C	2nd wear	0.29	0.0331
S3	46	29.4N/150 °C	1st wear	0.06	0.0066
S4	76	29.4N/150 °C	2nd wear	0.51	0.0581
S5	259	9.81N/200 °C	1st wear	0.01	0.0017
S6	146	9.81N/200 °C	2nd wear	0.38	0.0431
S7	131	49.1N/100 °C	2nd wear	0.39	0.0443
S8	118	49.1N/150 °C	2nd wear	0.53	0.0604
S9	118	49.1N/200 °C	2nd wear	0.65	0.0740

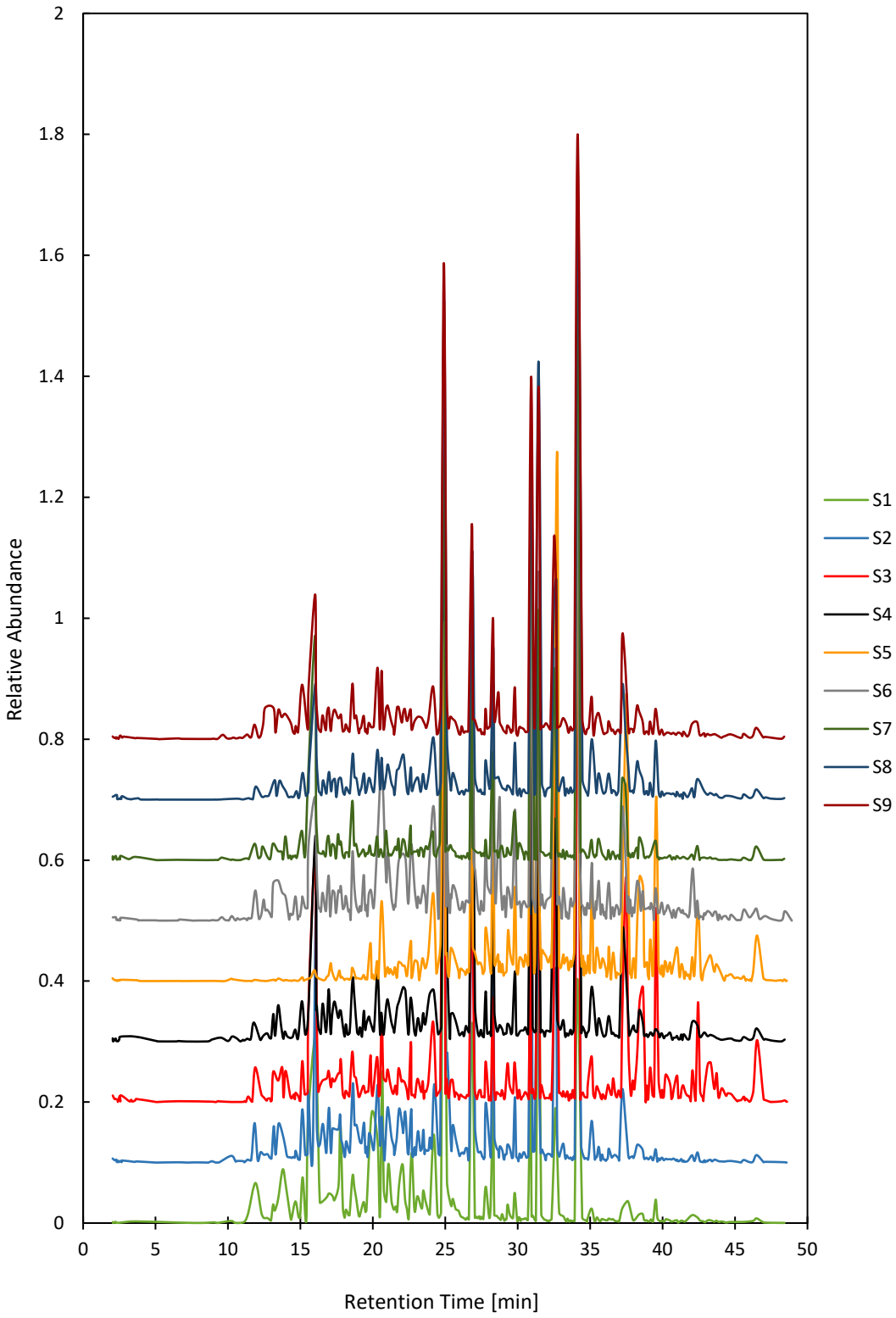

Figure A.3: GC - plot for mānuka smoke evolved during friction for conditions: (9.8 – 49.1N) and (100 – 200 °C) at 3000 rpm

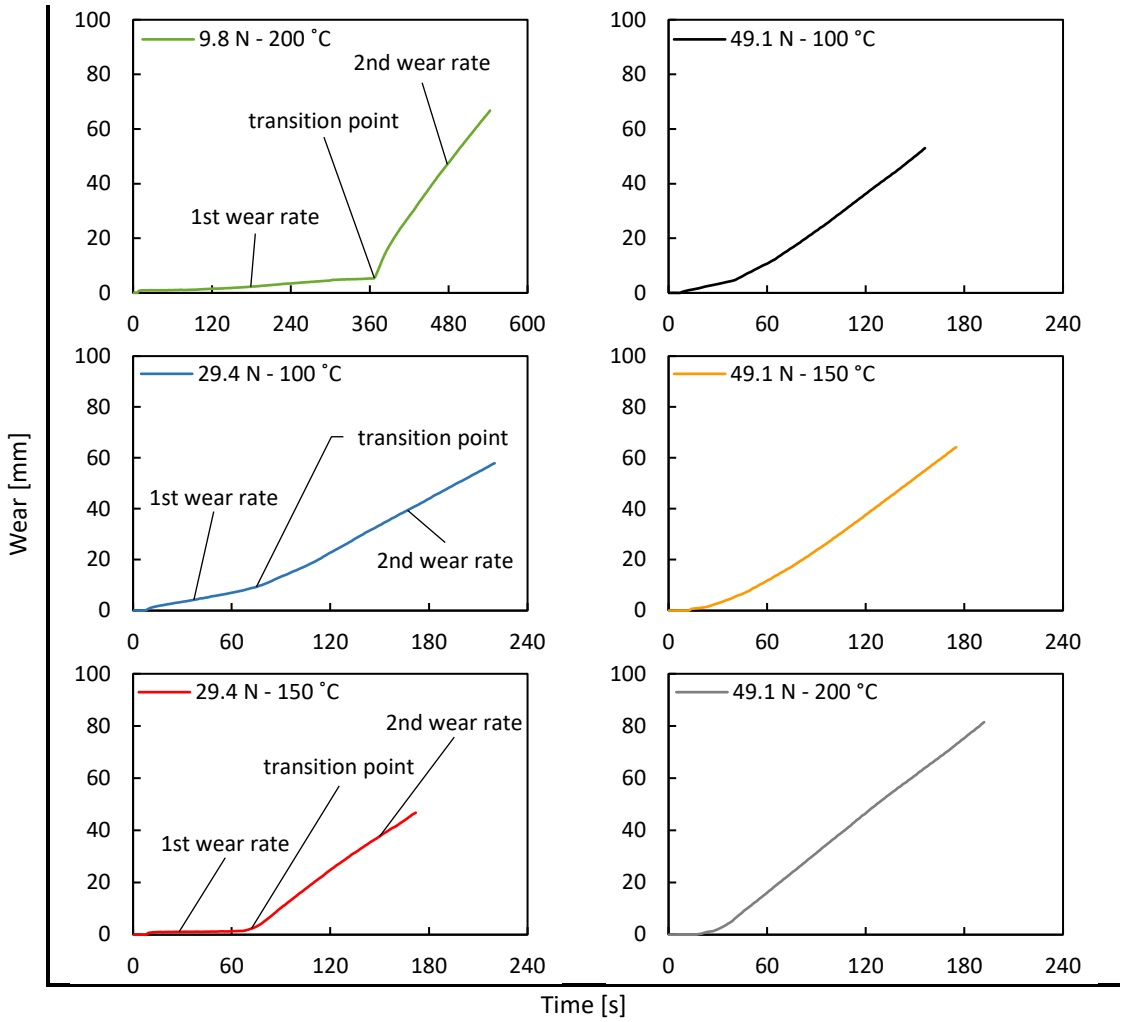

Figure A.4: Wear profile during smoke sampling for various applied forces and onset temperature at 3000 rpm wheel speed

Appendix - B: Auxiliary information

B.1 PDMS twister handling procedure

Note: The PDMS coating is temperature-sensitive, where the maximum temperature is dependent on the sampling environment.

Oxygen environment: **150 °C MAX.**
Inert environment: **300 °C MAX.**

1. Laboratory gloves must be worn to avoid PDMS contamination.
2. Use 70% ethanol solvent to clean the tubes ahead the sampling path.
3. Use a magnetic rod for picking the stir bar from the storage vial.
4. Insert the stir bar into a clean glass tube to start smoke sampling.
5. After sampling use the magnetic rod to transfer the stir bar back into the storage vial.

B.2 Smoke sampling flow rate calibration

The calibration curve shown in Figure B.5 was obtained to allow for controlling the smoke sampling rate by using a pressure regulator connected to a compressed air-line. The air flows through the glass tube with 5 mm ID, where the air velocity was measured using a digital anemometer.

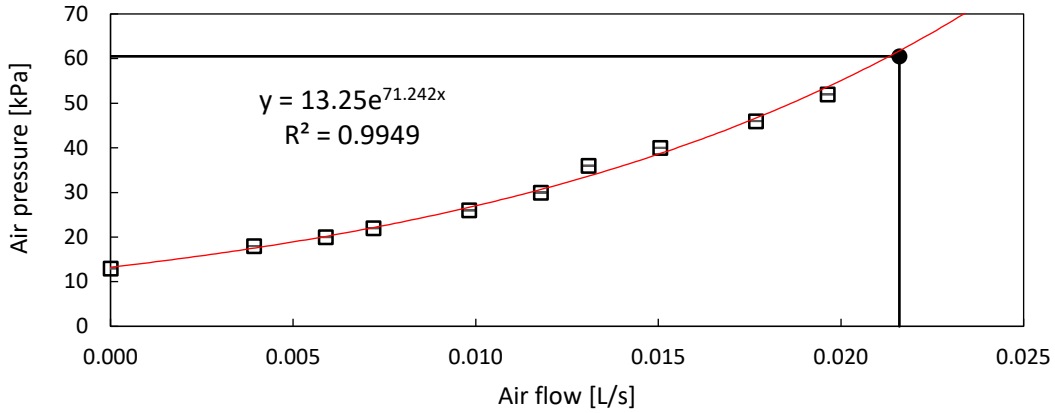

Figure B.5: Air pressure verses air flow calibration curve.

B.3 Wood preparation

Table B.2: Determining the moisture content (MC) of air-dried mānuka wood from randomly selected samples. Drying temperature at 105 °C for overnight

Weight before drying [g]	Weight after drying [g]	Weight difference [g]
23.219	20.817	0.115367
23.346	20.819	0.121339
23.508	21.017	0.118502
23.913	21.310	0.122148
22.654	20.147	0.124442
23.373	20.813	0.122971
	Mean MC	**12.1%**
	Relative error	**0.14%**

Table B.3: Selection of mānuka wood planks measurements

	Length [mm]	Width [mm]	Thickness [mm]
Wood plank dimensions	150.7	11.54	12.15
	150.84	12.84	12.14
	149.08	12.07	11.59
	150.21	12.11	11.84
	151.3	11.77	12.04
	150.21	11.83	12.2
	151.7	13.0	11.7
	148.49	10.6	12.02
	152.5	13.1	11.75
	150.3	12.67	12.99
	150.06	12.04	13.36
	149.06	11.71	12.96
Mean	**150.37**	**12.11**	**12.23**
σ	**1.102**	**0.682**	**0.544**

B.4 Mechanical actuator calibration

The mechanical actuator is used to press the wood onto the spinning wheel. The calibration curves below follows a linear trend, regular check for the calibration is required to ensure precision of control.

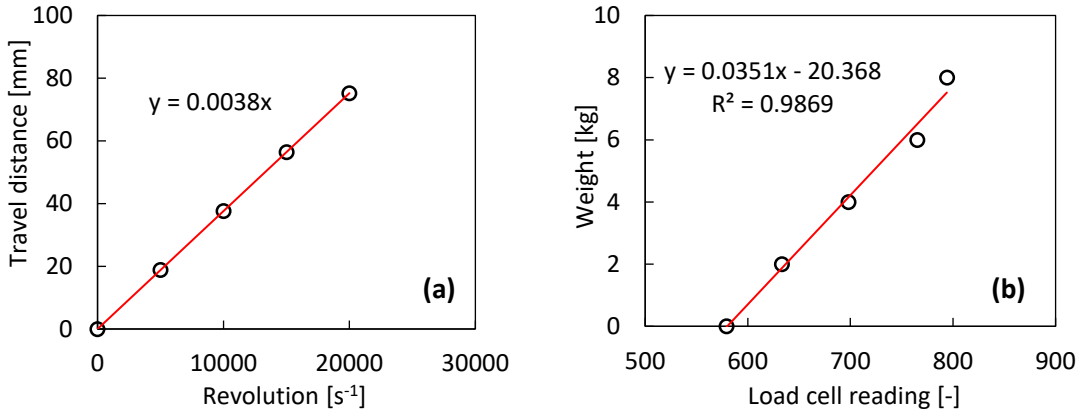

Figure B.6: Calibration curves (a) actuator travel distance (b) load cell for controlling the pressing force.

B.5 Induction motor components

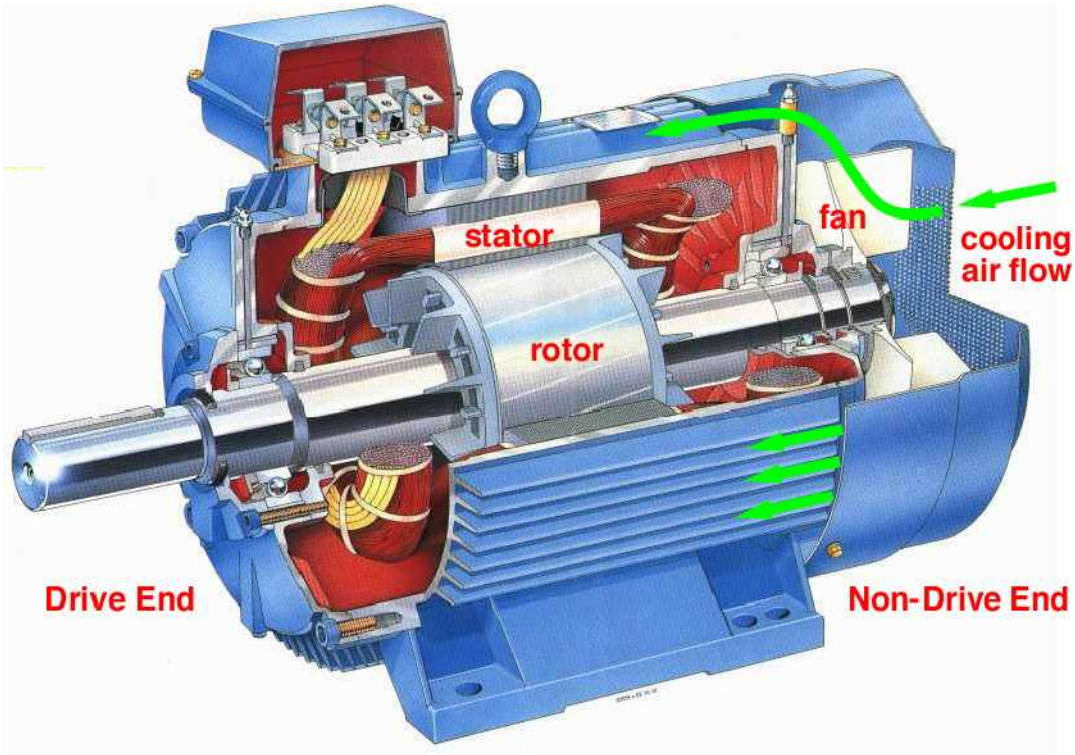

Figure B.7: Induction motor components. Adapted from (Polytechnic Hub)